Spring 5-6-2017

The Role of EHD2 in Triple-Negative Breast Cancer Tumorigenesis and Progression

Timothy A. Bielecki
University of Nebraska Medical Center

The Role of EHD2 in Triple-Negative Breast Cancer Tumorigenesis and Progression

By

Timothy Alan Bielecki

A DISSERTATION

Presented to the Faculty of

the University of Nebraska Graduate College

in Partial Fulfillment of the Requirements

for the Degree of Doctor of Philosophy

Cancer Research Graduate Program

Under the supervision of Professor Hamid Band

University of Nebraska Medical Center

Omaha, NE

April, 2017

Supervisory Committee:

Vimla Band, Ph.D.

Joyce Solheim, Ph.D

Jennifer Black, Ph.D.

Kay-Uwe Wagner, Ph.D.

.

Acknowledgements

First of all, I would like to thank my supervisor and mentor Dr. Hamid Band for his guidance, support, and motivation during the course of my PhD. I greatly appreciate his patience and mentorship. He has provided me with the freedom and encouragement to work and think independently. It has not only made me a better scientist, but it has also made me a better human being. I am indebted to him for giving me the opportunity to work in his lab and under his tutelage.

I would like to thank my supervisory committee members Dr. Vimla Band, Dr. Jenny Black, Dr. Joyce Solheim, and Dr. Kay-Uwe Wagner for their excellent supervision, suggestions, and constructive criticism throughout my graduate career. Without their extra guidance, I would have been unable to identify and overcome many significant obstacles throughout my studies.

I would also like thank all the current and former members of the Hamid Band lab for their help and support. The many characters and conversations have made my personal endeavor through graduate school an enlightening and entertaining time. Moreover, I learned more than I could have ever imagined from each and every one of them. Their kindness and generosity will always be cherished.

Finally, I would like to thank my family and friends for their unconditional love and support throughout my life and academic career. They have kept me focused and upbeat throughout the good times and the bad. Without their support and understanding, I would have never been able to complete this journey towards a PhD. I

would especially like to thank my mother, Valerie, for her constant guidance and for being my number one fan. I dedicate this thesis to her and my family.

The role of EHD2 in triple-negative breast cancer tumorigenesis and progression

Timothy Alan Bielecki, Ph.D.

University of Nebraska, 2017

Supervisor: Hamid Band, M.D., Ph.D.

Triple-negative breast cancer (TNBC) comprises 10%-15% of all breast cancer cases, yet is clinically challenging due to lack of targeted therapies which leads to higher mortality. Molecular subtyping has identified the most aggressive subclasses of breast cancer to be enriched in components of caveolae. While caveolae have been linked to many biological processes, their precise role in TNBC is still poorly understood. EHD2, a member of the C-terminal EPS15-Homology Domain-containing (EHD) protein family, has emerged as a new regulator of caveolae dynamics and is essential to maintain a stable membrane pool of caveolae. Studies in model cells demonstrate that caveolae facilitate repair of plasma membrane injuries incurred under stressful conditions. Importantly, new evidence suggests the invasiveness of tumor cells makes them vulnerable to plasma membrane injuries and hence a robust repair mechanism is essential to protect injured tumor cells from cell death.

EHD2 is found to be highly expressed within the basal myoepithelial layer throughout mammary gland development. High EHD2 mRNA and protein expression was observed in human TNBC cell lines and positively correlated with Caveolin-1 and Caveolin-2 expression. Furthermore, by analyzing publicly available gene expression databases, we found that high expression of EHD2 mRNA correlated with lower

probability of survival in TNBC patients. This led us to hypothesize that EHD2 is a marker and crucial regulator of tumorigenicity in TNBC. Using a cohort of 840 highly-annotated human breast cancer tissue samples, we discovered that high cytoplasmic expression of EHD2 marked TNBC cases, and served as a robust prognostic indicator of metastasis and lower patient survival. ShRNA-mediated knockdown of EHD2 in TNBC cell lines reduced invasiveness, growth under anchorage-independent conditions, and membrane repair ability *in vitro*. Using orthotopic implantation of human breast cancer cell lines in mouse mammary gland, we observed a dramatic abrogation of tumor growth and a reduction in metastasis of TNBC cell lines with EHD2 knockdown compared to their controls. These findings indicate that EHD2 is a novel clinical biomarker of poor prognosis in TNBC, and serves a novel role as a positive regulator of caveolae-dependent protection of plasma membrane against injury, enabling tumorigenicity and metastasis in TNBC. Our results support the potential of targeting EHD2 to develop therapeutic approaches against TNBC.

Chapter I: Introduction

I.1 Introduction

Breast cancer affects more women than any other type of cancer and is the second leading cause of cancer-related deaths among women (Figure 1.1) (Siegel, Miller, and Jemal 2017). The disease is generally classified into three main molecular subtypes: estrogen receptor (ER) and/or progesterone receptor (PR) enriched (or ER+/PR+), human epidermal growth factor receptor (HER2) enriched (HER2+), and tumors without ER, PR, or HER2 overexpression, typically referred to as triple-negative (Figure 1.2). This classification system typically dictates the course of treatment for patients, and targeted therapies have been developed to successfully treat tumors with elevated ER/PR, and HER2 expression (Malhotra et al. 2010). Although triple-negative breast cancer (TNBC) comprises only 10%-15% of all breast cancer cases, it is clinically challenging due to its aggressiveness and current lack of targeted therapies (Marmé and Schneeweiss 2015). TNBC itself is not a single disease. In fact, TNBC is comprised of 5 distinct subclasses based on gene expression: Basal-like 1, Basal-like 2, luminal androgen receptor+, mesenchymal, mesenchymal stem like, and immunomodulatory (Lehmann et al. 2011). These efforts to further characterize TNBC have yielded a better understanding of this heterogeneous disease and a large list of potential targets for therapy. One such target, commonly expressed in the most aggressive subclasses, are cellular structures called caveolae (Yadav, Chanana, and Jhamb 2015; Pinilla et al. 2006; Neve et al. 2006).

Caveolae, meaning “little caves” in Latin, are small (50-100 nm) plasma membrane-associated invaginations involved in endocytosis, lipid regulation, signaling

pathways, mechano-sensing, and membrane repair in many types of mammalian cells (Parton and del Pozo 2013; Martinez-Outschoorn, Sotgia, and Lisanti 2015; Lucas Pelkmans et al. 2004; L Pelkmans, Kartenbeck, and Helenius 2001; Okamoto et al. 1998; Blouin et al. 2010). While these caveolae-mediated processes are well understood in endothelial cells, adipocytes, and muscle cells, it's unclear what roles caveolae play in TNBC. Caveolin-1, an essential structural component and marker of caveolae, has both oncogenic and tumor suppressor functions in many tumor types, including breast cancer (Patani et al. 2012). Despite the considerable evidence that it serves as a tumor suppressor in ER+/PR+ and HER2+ breast cancers (Nawaz et al. 1999; Mercier et al. 2009; Thomas et al. 2010; Engelman et al. 1998), caveolin-1 functions mainly as a tumor promoter in TNBC. Immuno-histochemical analysis of a 900-patient cohort revealed that caveolin-1 protein expression is associated with TNBC (Elsheikh et al. 2008). In fact, roughly 90% of metaplastic breast cancers, a type of TNBC that is highly aggressive and difficult to treat, have been shown to express caveolin-1 (Savage et al. 2007). Interestingly, the TNBC cell lines MDAMB231, Hs578t, and BT549 require caveolin-1 for invadopodia formation and extracellular degradation *in vitro* (Yamaguchi et al. 2009). Caveolin-1 and caveolin-2 are also highly expressed within the myoepithelial/basal layer of the normal mammary duct (Figure 1.3) (Savage et al. 2008).

These findings suggest that caveolae are important for maintaining the aggressiveness of TNBC. However, more recent studies indicate that the central function of caveolae could be to protect the cell from plasma membrane stress and to repair membrane damage (Figure 1.4). Stretching of the plasma membrane from the

mechanical stress of osmotic shock causes caveolae to flatten and disassemble (Sinha et al. 2011). Furthermore, work in muscle cells has shown that caveolae cluster and regulate the repair of damaged regions of the plasma membrane (Corrotte et al. 2013). While much of this work has been based on *in vitro* experiments, there is also considerable evidence that the mechano-protective role of caveolae is physiologically relevant. In mouse endothelial, caveolae flatten and disassemble in response to increased membrane tension (Lo et al. 2015). The same study also found that vigorous muscle activity leads to cell damage in live zebrafish embryos lacking caveolae (Lo et al. 2015). Pharmacological stimulation of cardiac output increased mechanical stress, by increasing blood flow, on endothelial cells, resulting in the flattening of endothelial caveolae. Furthermore, depletion of caveolae made the endothelial cells more susceptible to acute plasma membrane damage (Cheng et al. 2015). Caveolin-1 has also been shown to be upregulated in TNBC cells subjected to fluid shear stress, indicating that caveolae serve a mechano-protective role during breast cancer metastasis (H. Yang et al. 2016).

Another ubiquitous component of caveolae and regulator of plasma membrane repair is the Eps15 homology domain-containing 2 protein (EHD2). EHD2 is a member of the EHD-containing protein family of ATPases that are endocytic trafficking regulators similar to the dynamin family of GTPases (Figure 1.5) (George et al. 2007). Our lab and others have found that EHD2 is also highly expressed in caveolae-rich endothelial cells, adipocytes, and muscle cells (Figure 1.6)(Doherty et al. 2008; Sohn, Brick, and Tuan 2016; Gudmundsson et al. 2010; Marg et al. 2012). In muscle, EHD2 and

caveolae are required components of the plasma membrane repair process (Marg et al. 2012; Lo et al. 2015). EHD2 dimerizes and forms oligomeric rings around lipids (Figure 1.7) (Daumke et al. 2007). Contrary to the conventional endocytic trafficking role of the EHD family, EHD2 is specifically localized to the necks of stable caveolae at the plasma membrane and not involved in endocytosis or endosomal recycling (Figure 1.8) (Moren et al. 2012; Stoeber et al. 2012; Ludwig et al. 2013). Although EHD2 is not required for caveolae formation, EHD2 depletion increases caveolae mobility and caveolae budding, resulting in more dynamic caveolae (Stoeber et al. 2012; Mohan et al. 2015; Shah et al. 2014).

Despite these recent advances in our understanding of how EHD2 regulates caveolae stability and dynamics, there is little known about the involvement of EHD2 in caveolae-mediated membrane repair and protection processes. In muscle cells, EHD2 binds to myoferlin and dysferlin, members of the ferlin family of proteins, which facilitate myoblast fusion and membrane repair, respectively (Doherty et al. 2008; Posey et al. 2011). The skeletal muscle membrane repair process has been even further characterized more recently and shown to involved annexins and EHD2 was shown to accumulate at the circumference of the repair patch (Figure 1.9) (Demonbreun et al. 2016). Ferlin-dependent membrane repair is a Ca^{2+}-dependent process that intimately involves caveolae (Cipta and Patel 2009). In endothelial cells, myoferlin binds to caveolin-1 during membrane fusion and fission events, and loss of caveolin-1 impairs membrane repair processes (Bernatchez et al. 2009). Recently, *in vivo* accelerated tumor

growth of human and murine carcinomas was found to rely on functional myoferlin-dependent membrane repair processes (Leung et al. 2013).

Recently, EHD2 has been implicated as a tumor suppressor in breast cancer (Yuhua Shi et al. 2015; X. Yang et al. 2015). Despite these findings, there is still no published literature on the role of EHD2 in TNBC, although previous studies have shown EHD2 mRNA expression to be significantly higher in caveolae-rich basal breast cancer cell lines and TNBC patient samples (Györffy et al. 2010; Neve et al. 2006). Understanding the regulatory role of EHD2 in caveolae-mediated membrane repair and protection processes in triple-negative breast cancer can provide a framework for potential new therapy targets that translate into novel treatment options for triple-negative breast cancer patients. Based on our findings here, and previous reports of caveolae expression in TNBC and the role of EHD2 in regulating caveolae dynamics, we hypothesize that EHD2 regulates the dynamics and stability of caveolae required for plasma membrane repair and protection in triple-negative breast cancer. We also hypothesize that EHD2-mediated regulation of caveolae is essential for the most aggressive and difficult to treat types of TNBC.

I.2 Figures

Figure 1.1

Figure 3. Leading Sites of New Cancer Cases and Deaths – 2017 Estimates

Estimated New Cases

Male			Female		
Prostate	161,360	19%	Breast	252,710	30%
Lung & bronchus	116,990	14%	Lung & bronchus	105,510	12%
Colon & rectum	71,420	9%	Colon & rectum	64,010	8%
Urinary bladder	60,490	7%	Uterine corpus	61,380	7%
Melanoma of the skin	52,170	6%	Thyroid	42,470	5%
Kidney & renal pelvis	40,610	5%	Melanoma of the skin	34,940	4%
Non-Hodgkin lymphoma	40,080	5%	Non-Hodgkin lymphoma	32,160	4%
Leukemia	36,290	4%	Leukemia	25,840	3%
Oral cavity & pharynx	35,720	4%	Pancreas	25,700	3%
Liver & intrahepatic bile duct	29,200	3%	Kidney & renal pelvis	23,380	3%
All sites	**836,150**	**100%**	**All sites**	**852,630**	**100%**

Estimated Deaths

Male			Female		
Lung & bronchus	84,590	27%	Lung & bronchus	71,280	25%
Colon & rectum	27,150	9%	Breast	40,610	14%
Prostate	26,730	8%	Colon & rectum	23,110	8%
Pancreas	22,300	7%	Pancreas	20,790	7%
Liver & intrahepatic bile duct	19,610	6%	Ovary	14,080	5%
Leukemia	14,300	4%	Uterine corpus	10,920	4%
Esophagus	12,720	4%	Leukemia	10,200	4%
Urinary bladder	12,240	4%	Liver & intrahepatic bile duct	9,310	3%
Non-Hodgkin lymphoma	11,450	4%	Non-Hodgkin lymphoma	8,690	3%
Brain & other nervous system	9,620	3%	Brain & other nervous system	7,080	3%
All sites	**318,420**	**100%**	**All sites**	**282,500**	**100%**

Estimates are rounded to the nearest 10, and cases exclude basal cell and squamous cell skin cancers and in situ carcinoma except urinary bladder.

Figure 1.1 Breast cancer is the most common cancer among women. Ten leading cancer types for the estimated new cancer cases and deaths by sex, United States, 2017, are shown on this table. Estimates are rounded to the nearest 10 and cases exclude basal cell and squamous cell skin cancers and *in situ* carcinoma except urinary bladder.

Used with permission from Siegel et al. (Siegel, Miller, and Jemal 2017)

Breast cancer pathogenesis and histologic vs. molecular subtypes

Eric Wong and Jenna Rebelo

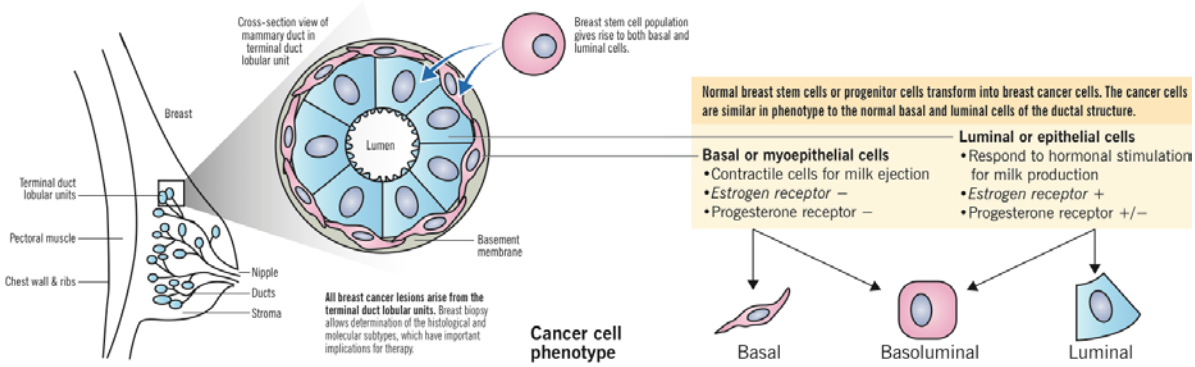

Histological subtypes	Ductal	Lobular
Preinvasive cancer 25% Cells limited to basement membrane	Ductal carcinoma in situ (DCIS) 80% May spread through ducts and distort duct architecture 1% progress to invasive cancer per year Usually unilateral	Lobular carcinoma in situ (LCIS) 20% Does not distort duct architecture Same genetic abnormality as ILC – E-cahderin loss 1% progress per year Can be bilateral
Invasive cancer 75% Extension beyond the basement membrane	Invasive ductal carcinoma (IDC) 79% Usually from DCIS precursor Cause fibrous response, producing a palpable mass on examination Metastasis through lymphatics and blood	Invasive lobular carcinoma (ILC) 10% Usually from LCIS precursor Minimal fibrous response, presents less often with palpable mass Metastasis through abdominal viscera to GI, ovaries, uterus Almost always ER+

Molecular subtypes	Triple negative (ER–, PR–, HER2–)	HER2+	Luminal B	Luminal A
% of breast cancers	15-20%	10-15%	20%	40%
Receptor expression		HER2		ER+/PR+
Histologic grade Level of cell differentiation	High (grade III)			Low (grade I)
Prognosis Correlates to histologic grade	Poor			Good
Response to medical therapy	Chemotherapy	Trastuzumab		Endocrine

Triple negative tumours respond best to chemotherapy, similar to other aggressive cancers.

Luminal A tumours respond best to endocrine therapy, e.g. antiestrogen or aromatase inhibitor.

Curr Treat Options Oncol. 2000 Aug;1(3):199-209.
Clin Transl Oncol. 2008 Dec;10(12):777-85.
Nat Clin Pract Oncol. 2007 Sep;4(9):516-25.
Robbins 8E

Figure 1.2 Breast cancer pathogenesis and histologic vs. molecular subtypes. The clinical breast cancer molecular subtypes (luminal A, luminal B, HER2+, and triple-negative) are defined by the phenotypes and gene expression patterns they share with normal epithelial cells in the mammary duct. Specifically, luminal subtypes share characteristics with luminal cells and the triple-negative subtype shares characteristics with basal/myoepithelial cells.

Used with permission from McMaster Pathophysiology Review, 2012

Figure 1.3

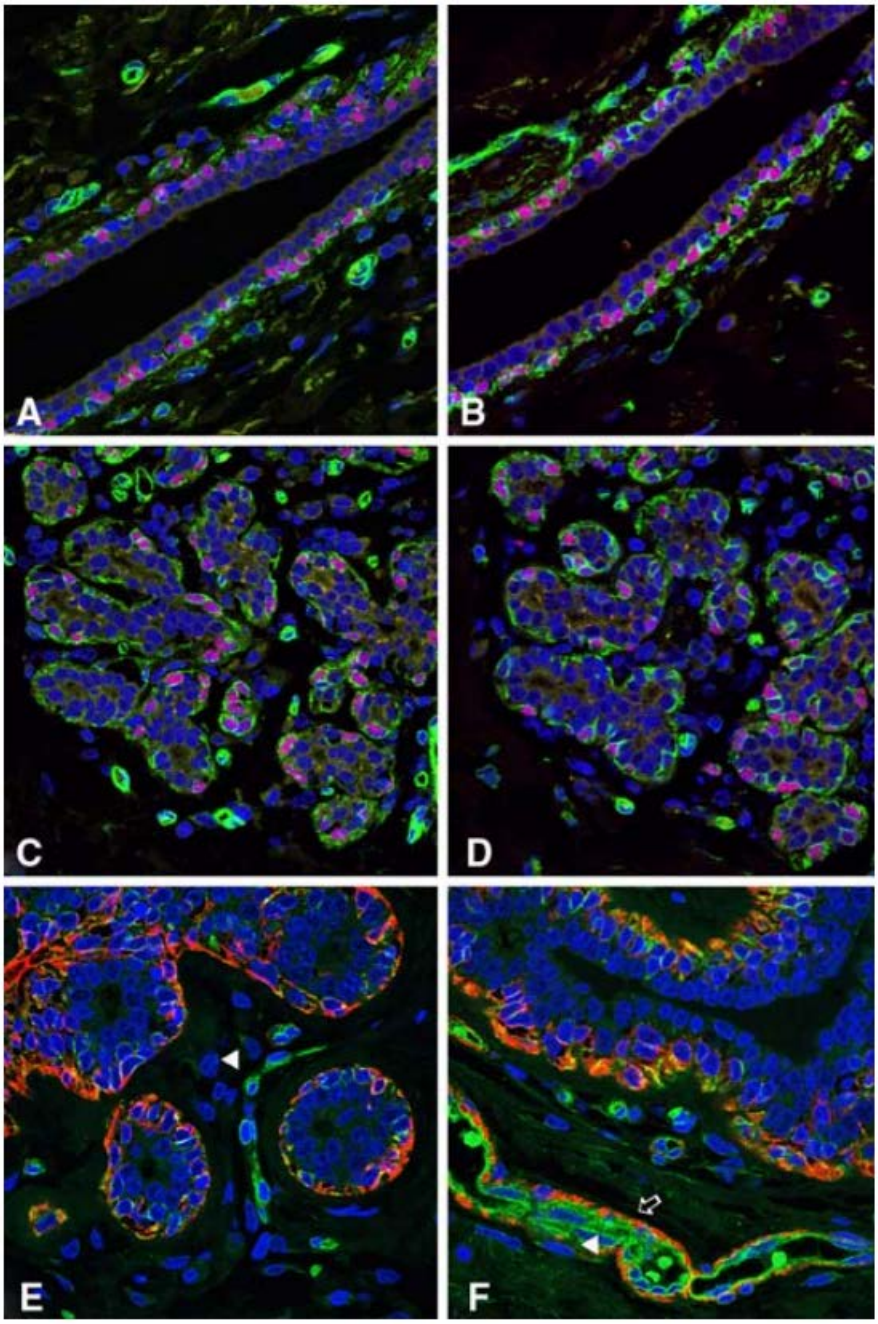

Figure 1.3. Analysis of caveolin 1 and 2 expression in normal breast by immunofluorescence. Normal breast ducts (A and B) and terminal duct-lobular units (C and D) display strong expression of caveolin 1 (A and C, green) and 2 (B and D, green) in myoepithelial cells, which also co-express p63 (A, B, C and D, red). Note that within breast ducts and lobules, caveolins 1 and 2 are expressed in similar cell populations (i.e., myoepithelial cells). In addition, caveolin are expressed in fibroblasts and endothelial cells. In E and F, please note the co-expression of caveolin 2 (E and F, green) and α-smooth muscle actin (E and F, red) in normal breast myoepithelial cells. In vessels, asmooth muscle actin is expressed in pericytes (E and F, red, arrow), whereas caveolin 2 is expressed in endothelial cells (E and F, green, arrowheads)

Used with permission from (Savage et al. 2008)

Figure 1.4

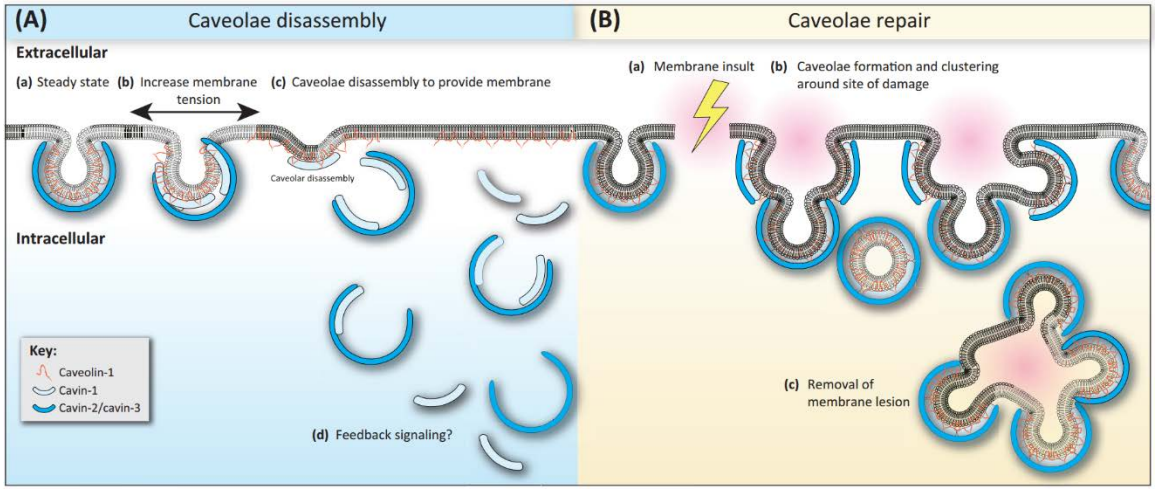
(A)
Caveolae disassembly
Extracellular
(a) Steady state
(b) Increase membrane tension
(c) Caveolae disassembly to provide membrane
Caveolar disassembly
Intracellular
Key:
Caveolin-1
Cavin-1
Cavin-2/cavin-3
(d) Feedback signaling?
(B)
Caveolae repair
(a) Membrane insult
(b) Caveolae formation and clustering around site of damage
(c) Removal of membrane lesion

Figure 1.4. Models of how caveolae may protect the plasma membrane from damage. (A) Increased membrane tension results in cavin 1-associated coats detaching from the membrane. Consequently, caveolae flatten, which increases the surface area and prevents membrane rupture. Disassembled complexes contain subpopulations of cavin 1 alone or bound to either cavin 2 or cavin 3. (B) Wounding of the membrane results in the formation and clustering of caveolae at the site of damage. The lesion is then removed by internalization of the caveolae, which reseals the membrane.

Used with permission from (Cheng and Nichols 2016).

Figure 1.5

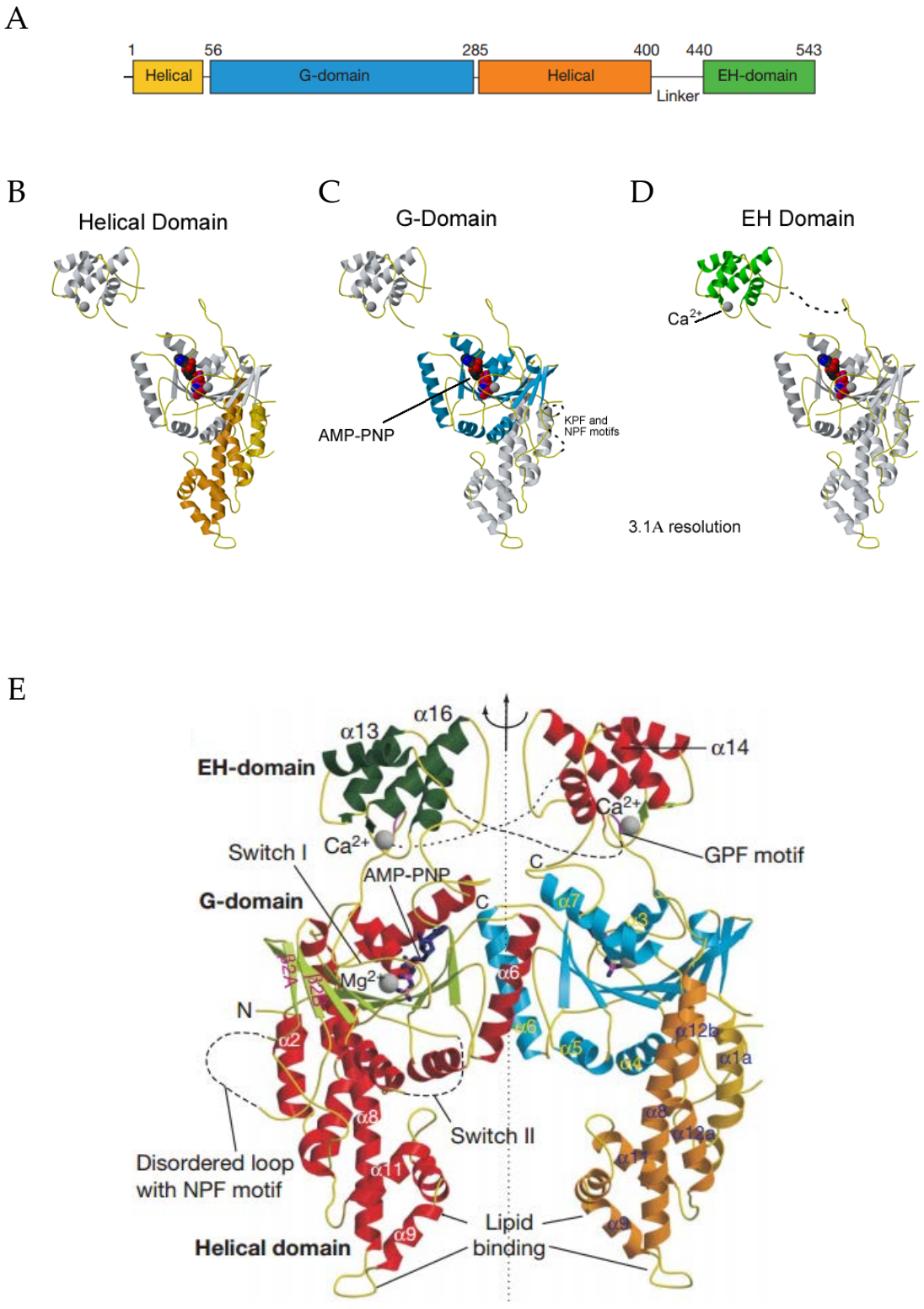
A
1
56
285
400
440
543
Helical
G-domain
Helical
Linker
EH-domain
B
Helical Domain
C
G-Domain
AMP-PNP
KPF and
NPF motifs
D
EH Domain
Ca2+
3.1A resolution
E
α16
α13
α14
EH-domain
Ca2+
Switch I
Ca2+
GPF motif
C
AMP-PNP
G-domain
C
α7
α3
β2A
β2B
Mg2+
α6
N
α2
α5
α4
α12b
α1a
α8
α12a
Switch II
Disordered loop
with NPF motif
α11
α1
α9
Lipid
binding
Helical domain

Figure 1.5. Structure and regions of EHD2. a, Domain structure of EHD proteins (numbering from mouse EHD2 amino acids). **b,** Helical domain. Organizes scaffolding with dimeric G-domain to help form scissor shape **c,** G-domain. Mediates oligomerization and contains nucleotide-binding site similar to the G-domain of dynamin. **d,** EH-domain. The EH-domain interacts with proteins containing Asn-Pro-Phe (NPF) motifs. **e,** Ribbon-type presentation of the EHD2 dimer (PDB code 2QPT). One molecule is colored according to the secondary structure (helices in red, β-strands in green) and the other according to the domain structure (see Fig. 1a). GPF and NPF motifs are indicated.

Adapted and used with permission from Daumke et al. (Daumke et al. 2007)

Figure 1.6

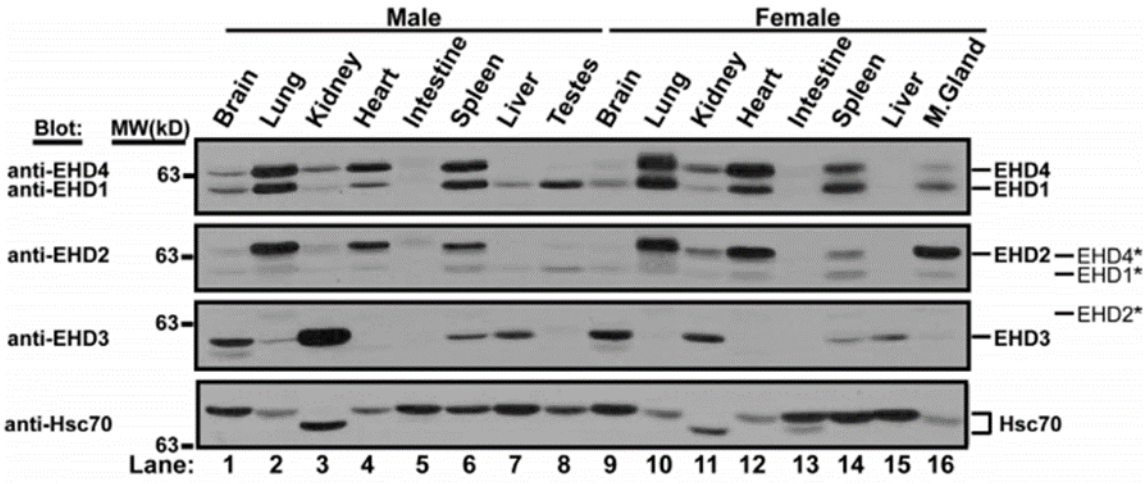
Male
Female
Brain
Lung
Kidney
Heart
Intestine
Spleen
Liver
Testes
Brain
Lung
Kidney
Heart
Intestine
Spleen
Liver
M.Gland
Blot:
MW(kD)
anti-EHD4
anti-EHD1
63
EHD4
EHD1
anti-EHD2
63
EHD2
EHD4*
EHD1*
63
EHD2*
anti-EHD3
EHD3
anti-Hsc70
Hsc70
63
Lane: 1 2 3 4 5 6 7 8 9 10 11 12 13 14 15 16

Figure 1.6. EHD protein expression in normal mouse tissues. An 18 week-old male and female C57BL/6 mouse were sacrificed and organs were removed and lysed in tissue lysis buffer. Aliquots of 100 μg tissue lysate were separated using 8% SDS-PAGE and a Western blot was performed using antibodies raised against human EHD proteins. The membrane was serially stripped and reprobed beginning with both EHD1 and EHD4, followed by EHD2, EHD3 and Hsc70 antibodies. The * denotes bands that bled through from the previous blot following stripping. Differential mobility of Hsc70 may represent tissue specific isoforms. Blots shown have exposure times of less than 10 seconds, upon longer exposures, most EHD proteins can be seen in each organ shown. Relative molecular weight (MW) markers are indicated in kiloDaltons (kD). As a loading control, Hsc70 was blotted. M. gland – mammary gland

Used with permission from (George et al. 2007)

Figure 1.7

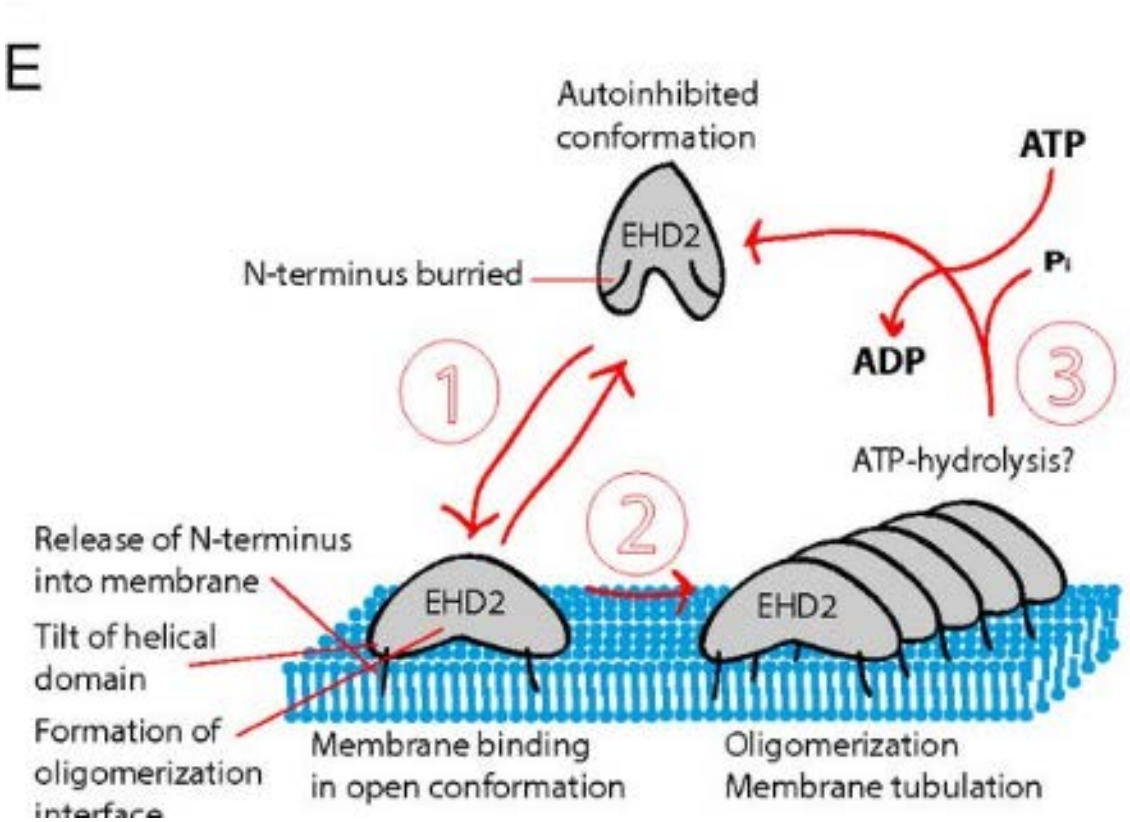
E
Autoinhibited conformation
ATP
EHD2
N-terminus burried
Pi
ADP
1
3
ATP-hydrolysis?
2
Release of N-terminus into membrane
Tilt of helical domain
Formation of oligomerization interface
EHD2
EHD2
Membrane binding in open conformation
Oligomerization Membrane tubulation

Figure 1.7. Schematic model illustrating the proposed steps involved in the mechanistic cycle of EHD2. Binding of ATP nucleotide enables membrane insertion in the open conformation. ATP hydrolysis enables detachment of the protein from the membrane. These two steps allow EHD2 to oligomerize when bound to the membranes, but not in solution. The energy that is necessary to deform the membrane is defined by the bending modulus (~12 kcal/mol for a typical lipid bilayer) (30). It is interesting to note that this energy appears to be drawn from the association of EHD2 into membrane-bound oligomers and not from ATP hydrolysis. Thus, the hydrolysis may primarily control the kinetics of the dissociation of the protein scaffold, which is important for a tight regulation of the process.

Used with permission from (Hoernke et al. 2017)

Figure 1.8

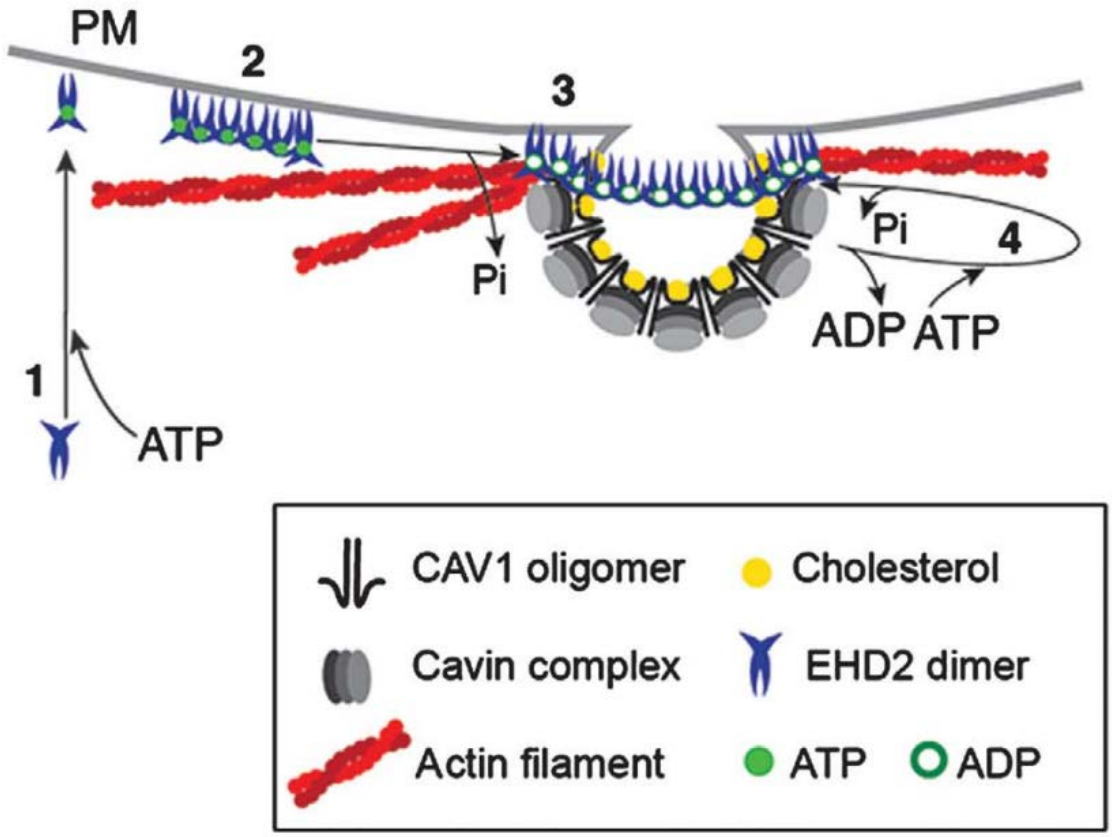
PM
2
3
Pi
Pi
4
ADP
ATP
1
ATP
CAV1 oligomer
Cholesterol
Cavin complex
EHD2 dimer
Actin filament
ATP
ADP

Figure 1.8. A model on the role of oligomer formation and the ATP cycle in EHD2 association with caveolae and dynamic exchange. (1) Newly synthesized EHD2 dimers bind ATP and are subsequently targeted to the plasma membrane via ionic interactions with negatively charged lipids. (2) Upon lipid binding, EHD2 dimers assemble into 60–75S oligomers via interactions of EH domain and KPF/NPF motifs in adjacent EHD2 dimers. (3) Association of EHD2 complexes with caveolae requires ATP hydrolysis, which may be stimulated at caveolae. (4) EHD2 proteins undergo dynamic exchange at caveolae, which requires a new cycle of ATP binding and hydrolysis. EHD2 mediates a link to actin fibers that run in close proximity to caveolae.

Used with permission from (Stoeber et al. 2012)

Figure 1.9

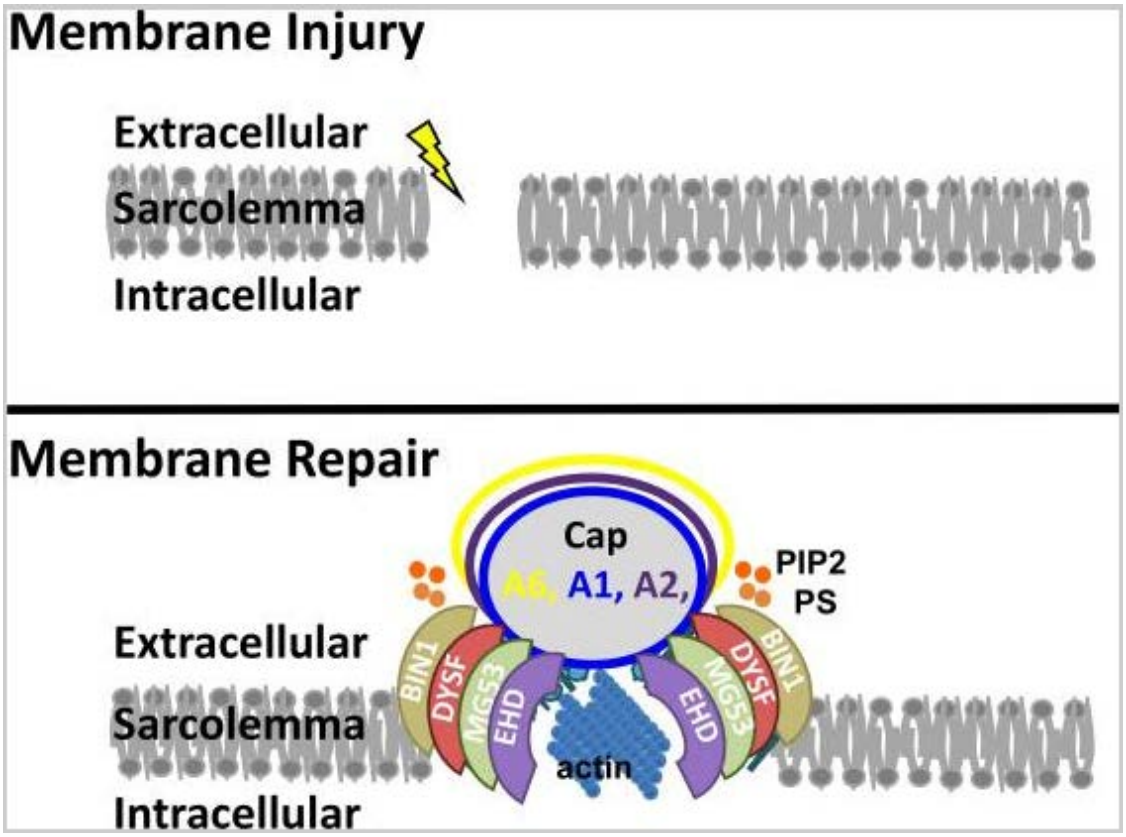
Membrane Injury
Extracellular
Sarcolemma
Intracellular
Membrane Repair
Cap
A6, A1, A2,
PIP2
PS
Extracellular
Sarcolemma
Intracellular
BIN1
DYSF
MG53
EHD
actin
EHD
MG53
DYSF
BIN1

Figure 1.9. Model of membrane repair. Upon plasma membrane injury, repair proteins localize to the site of damage and actin reorganizes, facilitating membrane repair. Annexins A1, A2, and A6 form a repair cap at the membrane lesion. Dysferlin (DYSF), MG53, BIN1, and EHD participate in forming a shoulder that abuts this repair cap. PIP2 and PS localize adjacent to the repair cap at the shoulder.

Used with permission from (Demonbreun et al. 2016)

Chapter II: Materials and Methods

II.1 Materials and Methods

Cell culture:

All breast cancer cell lines were obtained from ATCC and cultured in complete α-MEM medium with 10% fetal bovine serum, 10 mM HEPES, 1 mM each of sodium pyruvate, nonessential amino acids and L-glutamine, 50 μM 2-ME, and 1% penicillin/ streptomycin (Life Technologies, Carlsbad, CA). The TNBC cell lines BT549 and HS578t were cultured in α-MEM medium supplemented as above and with 1 μg/mL hydrocortisone and 12.5 ng/mL epidermal growth factor (Sigma-Aldrich, St. Louis, MO). For retroviral overexpression of control and EHD2 shRNA, HEK-293T cells were transfected with pQCXIX-RT3GEP vectors harboring control shRNA or EHD2 shRNAs (Fellmann et al. 2013) together with packaging vectors, and supernatants used to infect breast cancer cell lines followed by selection in puromycin. Cell lines were regularly tested for mycoplasma. Cell lines were not continuously cultured for >3 months.

Reagents

Bovine serum albumin (cat. # A7906-100G), paraformaldehyde (cat. # 158127-500G), sodium orthovanadate (Na_3VO_4, cat # S6508-50G), sodium deoxycholate (cat # D6750-100G), and Triton X-100 (cat. # 93418) were from Sigma-Aldrich (St. Louis, MO). Hema staining solutions (cat. # 23-123919), sodium fluoride (NaF, cat # S299-500), sodium chloride (NaCl, cat # S271-10), and Tris (cat BP152-5) were from Fisher Chemicals. EDTA-free protease inhibitor cocktail (cat. # 4693159001) was from Roche. ECL development reagent (cat. # 32106), BSA for bicinchoninic acid assay (cat # 23209), and PMSF (cat # 36978) were from Thermo-Scientific. Penicillin/streptomycin (cat. # 15140-

122) and fetal bovine serum (FBS) (cat. # 10427-028; lot # 1662765A120-01) were from Life Technologies. Alpha-MEM (cat. # SH30265.01) and DMEM/F12 (cat. # SHO30023.01) were from GE Life Sciences.

Antibodies for western blot

Anti-HSC70 (cat. #sc-7298) and anti-caveolin-1 (cat # sc-894) were from Santa Cruz Biotechnology. In-house generated Protein G-purified rabbit polyclonal anti-EHD1 antibody, and rabbit anti-EHD2, anti-EHD3 and anti-EHD4 antisera were used as described previously (Rainey et al., 2010). Secondary antibodies for immunoblotting included horseradish peroxidase (HRP)-conjugated Protein A or HRP-conjugated rabbit anti-mouse antibody (Invitrogen, Carlsbad, CA).

Antibodies for immunofluorescence (IF)

Anti-caveolin-1 (cat. # sc-53564) was from Santa Cruz Biotechnology; anti-EHD1 (cat. # ab109311) was from Abcam. Affinity-purified rabbit polyclonal rabbit anti-EHD2 was used as described previously (Rainey et al., 2010). Secondary fluorochrome-conjugated antibodies were from Life Technologies.

Mouse models

Ehd1-null mice were maintained on mixed 129; B6 background (Rainey et al. 2010). Single nucleotide polymorphism (SNP) analysis (DartMouse, Lebanon, NH) revealed these to have ~70% contribution from the C57BL/6 genome (Figure 2.1). Breeders were

maintained on high-fat chow (# 2019, Harlan Laboratories Inc., Madison, WI). Genomic DNA was extracted from adult tail tips with KAPA genotyping kits (KAPA Biosystems).

For the mammary gland developmental timepoint experiments, mating was set up in the evenings, and vaginal plugs were detected the following morning. The noon of the day of vaginal plug detection was considered Pregnancy day 0.5. Female mice were euthanized by CO_2 asphyxiation at the indicated time points followed by cervical dislocation, and whole inguinal mammary glands were harvested. Mammary glands were fixed at RT in 10% neutral-buffered formalin (NBF) for 48 hours, transferred to 70% ethanol prior to paraffin embedding, and sectioned at 4-6 μm. Sections were stained with hematoxylin and eosin (H&E). IHC for anti-EHD2 was performed according to the IHC protocol. Brightfield images were captured using an EVOS FL Auto microscope.

Cell Lysates: Cells were either lysed in RIPA lysis buffer (50 mM Tris pH 7.5, 150 mM NaCl, 1% Triton-X-100, 0.05% deoxycholate, 0.1% SDS, 1 mM phenylmethylsulfonyl fluoride (PMSF), 10 mM NaF, and 1 mM sodium orthovanadate) or Triton-X-100 lysis buffer (50 mM Tris pH 7.5, 150 mM NaCl, 0.5% Triton-X-100, 1 mM PMSF, 10 mM NaF, and 1 mM sodium orthovanadate)(2). Lysates were rocked at 4°C for at least 1 hour or frozen at -80°C and then centrifuged at 13,000 rpm for 20 minutes at 4°C and the supernatants assayed for protein concentration using the BCA assay kit (Thermo Fisher Scientific, Rockford, IL) or the Bradford assay (Bio-Rad Laboratories, Hercules, CA).

Immunoblotting

Immunoblotting/Western blotting was performed as described (Rainey et al. 2010). Briefly, cells were washed with ice-cold PBS and lysed in ice-cold RIPA lysis buffer or Triton X-100 lysis buffer. The lysates were vortexed, centrifuged at 13,000 rpm for 30 minutes at 4^{o} C, and supernatants collected. Protein quantification was done by using a Thermo Scientific-Pierce Bicinchoninic acid (BCA) assay (cat. # 23225). 40 μg of lysate protein per sample was resolved by SDS/PAGE and transferred to a PVDF membrane (Millipore, cat. # IPVH00010). The membranes were blocked in TBS-0.1% Tween 20 (BIO-RAD, cat. # 161-0781) with 5% Bovine Serum Albumin (BSA) with 0.05% sodium azide, incubated with the appropriate primary antibodies diluted in TBS-0.1% Tween 20 overnight at 4°C. Next, membranes were washed in TBS-0.1% Tween 20 (three times for ten minutes) followed by a one-hour incubation with HRP-conjugated secondary antibody at room temperature. The membrane was washed in TBS-0.1% Tween 20 (three times for ten minutes) and ECL-based detection performed.

Immunofluorescence (IF)

Cellular immunofluorescence was performed, as previously described (Bailey et al. 2014) with minor modifications. Cells were cultured on glass coverslips and fixed with 4% PFA/PBS for 10 minutes. The cells were then blocked with 5% BSA/PBS for 60 minutes and incubated with primary antibodies in 5% BSA/PBS overnight. Cells were then washed with PBS (three times), incubated with the appropriate fluorochrome-conjugated secondary antibody for 45 minutes at room temperature (RT), washed and

mounted using VECTASHEILD mounting medium (Vector Laboratories, Cat. # H-1400 and H-1500). Images were acquired using a Zeiss 710 Meta Confocal Laser Scanning microscope (Carl Zeiss) using a 4x, 10x, 20x, or 63× objective with a numerical aperture of 1.0 and appropriate filters. Merged fluorescence pictures were generated and analyzed using ZEN® 2012 software from Carl Zeiss.

For tissue staining, rehydrated tissue sections were boiled in antigen unmasking solution (H-3300, Vector Laboratories, Burlingame, CA) in a microwave for 20 min, slides were cooled, washed once in PBS, and blocked in heat-inactivated 10% FBS (SH30910.03, HyClone Laboratories, Logan, UT) for one hour at room temperature (RT). Primary antibodies diluted in blocking buffer were added overnight at 4°C (except EHD antibody staining, which was done at RT for an hour), slides were washed 3 times with PBS followed by incubation with Alexa Fluor 488 or 594-conjugated donkey anti-rabbit or anti-mouse secondary antibodies (1:200; Invitrogen, Carlsbad, CA) for one hour at RT in the dark. For negative controls, sections were incubated in the blocking buffer without the primary antibody. Nuclei were visualized with DAPI in antifade mounting medium (ProLong® Gold Antifade mountant, Invitrogen, Carlsbad, CA). Fluorescent images were captured on a Zeiss LSM-710 confocal microscope. Images were processed using Adobe Photoshop CC software. For presentation, signal intensities were adjusted equally for brightness and contrast between control and test images.

Transfection Reagents and Plasmids

XtremeGENE 9 transfection reagent was from Roche Applied Science (Indianapolis, IN). A pQCXIX-RT3GEP (Fellmann et al. 2013) shRNA construct for scrambled shRNA or EHD2-targeted shRNA was custom-made through a commercial vendor (Mirimus) (Figure 2.1).

Trans-well invasion assays

The cells were seeded in the top chamber of trans-well chambers with 8 μm pore size nitrocellulose filters (Corning) in serum-free medium. Medium containing 10% FBS served as a chemoattractant in the lower chamber. The membranes were coated with 1:2 diluted Matrigel (BD Biosciences) before seeding the cells. After 22 h, the cells on the upper side of the membrane were removed by scraping with cotton swabs, while those on the lower side were fixed with methanol, stained with HEMA solutions and cells were counted. The migrated cells from the whole well were enumerated using Image J (NIH, MD). All experiments were done in triplicates, and repeated three times.

Orthotopic xenograft tumorigenesis

5 x 10^6 cells mixed with 0.2 ml Matrigel (BD Biosciences) were implanted in the mammary fat pad of 4 to 6 week-old non-pregnant female nude mice (Figure 2.2) (The Jackson Laboratory). Three days prior to cell implantation, the mice were primed with a subcutaneous estrogen pellet (0.72 mg/ 60 day pellets; Innovative Research of America, Sarasota, FL) and tumor growth monitored weekly for 12 to 14 weeks. After euthanasia,

tumors were imaged, and formalin-fixed and paraffin-embedded for further analyses. Tumor dimensions were measured with Vernier calipers and tumor volume calculated as length x width x depth/2. Mice were euthanized when control tumors reached 2 cm^3 in volume or showed signs of ill health, as per institutional IACUC guidelines. At the end of the experiment, the tumor as well as liver and lung are resected, formalin-fixed and paraffin-embedded for further analyses.

Human and animal subjects

The procurement and use of human tissues were approved by the Ethics Committee of the University of Nottingham where the tissues are archived under the direction of our collaborator Dr. Emad Rakha (University of Nottigham Hospital, Department of Pathology, Breast Unit). Mouse studies were pre-approved by the UNMC Institutional Review Board (IRB) Committee, in compliance with Federal and State guidelines.

IHC analysis of breast cancer tissue microarrays

Tissue microarrays (TMAs) corresponding to a well-annotated 971 breast cancer patient cohort at the University of Nottingham Hospital Breast Unit were analyzed by IHC staining with a previously described anti-rabbit EHD2 antibody (Rainey et al., 2010) that was further validated (Figure 3.3). Of the whole series (840 cases), 759 were informative. The expression of EHD2 was detected in the cytoplasm and/or nucleus of the malignant cells while, in the normal parenchymal element its expression was noted in the nuclei of epithelial cells only. For statistical analysis, expression was dichotomized using cutoff points that were selected based on histogram distribution. The cutoff points were

selected using median and X-tile software as follows: a H-score of zero for nuclear EHD2 and H-score of 50 for cytoplasmic EHD2 expression. Statistical analysis was performed by using the SPSS IBM 22 statistical software. The relationship between nuclear and cytoplasmic EHD2 expression and different clinicopathological variables was assessed using Chi square-test. Survival curves were obtained using Kaplan–Meier method for outcome estimation and significance determined using the log-rank test. Two-tailed P-values less than 0.05 we re considered significant.

Anchorage-independent growth assay

Three thousand cells were seeded in 0.3% soft agar on top of 0.6% soft agar layer in 6-well plates. After two weeks, cells were stained with crystal violet and imaged under a phase contrast microscope. The colonies in the entire wells were enumerated using Image J (NIH, MD). All experiments were done in triplicates, and repeated three times.

Tumor-sphere assay

Cells were re-suspended in DMEM/F12 (cat. # SH30023.01, GE Lifesciences) media supplemented with 2mM L-glutamine, 100U/ml penicillin/streptomycin, 20ng/ml EGF (sigma), 10 ng/ml FGF (R&D Systems) and 1x B27 supplement (Gibco), and seeded at 100,000 cells/well into poly-HEMA coated 6-well plates. After one week, tumor-spheres were imaged under a phase contrast microscope. Tumorspheres greater than 40 μm in diameter were quantified as previously described (Shaw et al. 2012), using Image J (NIH, MD). All experiments were done in triplicates, and repeated three times.

Membrane repair assay

Cells were grown on coverslips and washed with PBS + 2mM Ca^{2+} before transferring to phenol red free HBSS + 2mM Ca^{2+} containing 2 mg/ml lysine fixable 10-kDa CascadeBlue dextran. Glass beads of about 20 mg (425-600 μm, Sigma) were sprinkled onto the cells and the beads were rolled gently 10-12 times over the cells to induce plasma membrane wounds. After wounding the coverslips were incubated as such at 37°C for 5 min. Following one wash with PBS + 2mM Ca^{2+} buffer, cells were incubated with prewarmed phenol red-free HBSS + 2 mM Ca^{2+} containing 2 mg/ml lysine fixable 10-kDA TRITC dextran at 37°C for 5 min. The coverslips were then washed in PBS twice and fixed in 4% PFA. The number of CascadeBlue-positive (total wounded cells) and TRITC-positive (wounded cells which have not resealed) were counted in 20 fields in duplicate. Cells were imaged using an EVOS FL Auto inverted microscope with 10x objective, using DAPI and TexasRed lightcubes. The number of wounded cells that failed to reseal were expressed as a percentage of the total wounded cells, as previously described (Defour, Sreetama, and Jaiswal 2014).

Matrigel spheroid assay

Cells were re-suspended as a single cell suspension in media containing 50% Matrigel and seeded at 2,000 cells/well on top of a base layer of Matrigel in an 8-well chamber slide. TNBC cell spheroids were allowed to grow for 7 days and then imaged and quantified. Quantification of invasive spheroids was performed by comparing the number of spheroids with invadopodia to the total number of spheroids. Over 100 total

spheroids were counted per well and all experiments were done in triplicates and repeated three times.

Statistics

P-values were calculated by using an unpaired Student's t-test and the threshold of significance was $p<0.05$. Data is shown graphically as mean ± SEM (error bars).

II.2 Figures

Figure 2.1


RT3GEP (pQCXIX)
T3G
tGFP
X
E
PGK
Puro

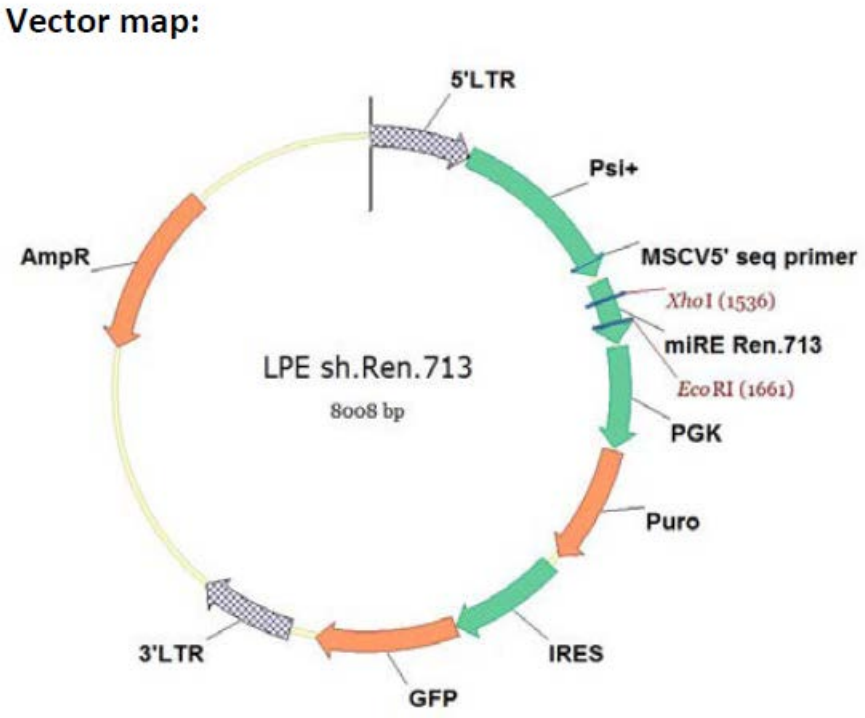
Vector map:
5'LTR
Psi+
MSCV5' seq primer
Xho1 (1536)
miRE Ren.713
EcoRI (1661)
PGK
Puro
IRES
GFP
3'LTR
AmpR
LPE sh.Ren.713
8008 bp

Figure 2.1 Retroviral plasmid for EHD2 shRNA. a, Retroviral vector used to form EHD2 shRNA. **b,** Constitutive shRNA expression vector obtained from Mirimus, Inc. The shRNA is embedded in an enhanced miR-30 backbone termed miR-E.

Figure 2.2

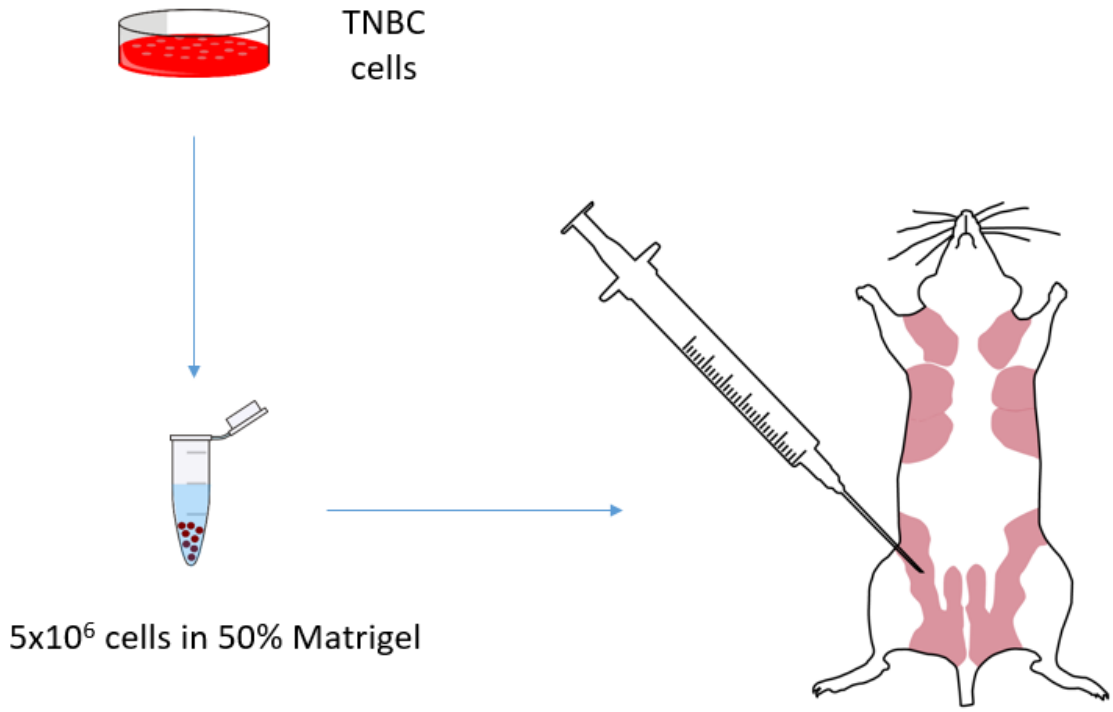

Figure 2.2 Orthotopic injection of breast cancer cells. TNBC cell lines (MDA-MB-231, BT549, or HS578T) with EHD2 or control shRNA were concentrated into 5 x 10^6 cells per 100uL suspensions of 50% Matrigel. Cell suspensions were implanted into the inguinal mammary gland of 4 to 6-week old non-pregnant female nude mice. Tumors were detected 3 weeks after implantation and followed for 11-13 weeks.

Chapter III: Results

III.1 Results

A. EHD2 and caveolin-1 are expressed within the myoepithelial/basal layer of the mammary duct

As described previously (George et al. 2007), EHD protein expression is differential throughout many murine tissues (Figure 1). Although EHD2 protein expression is high in western blots of total murine mammary gland lysates, we sought to further characterize the exact the expression and location of EHDs within this tissue. We initiated studies by first reconfirming the expression pattern of EHDs within total mammary gland lysate of wild type female C57BL/6 mice (Figure 3.1 A). Our results showed that EHD2 was indeed the highest expressed member of the EHD family of proteins within the murine mammary gland. Consistent with previous analysis (George et al. 2007), EHD 1 and EHD4 were both expressed while EHD3 was not observed.

We next sought to determine the localization of the EHDs expressed within the mammary gland. To accomplish this, we performed confocal immunofluoresence on formalin-fixed, paraffin-embedded (FFPE) mammary gland sections from twelve-week-old female C57BL/6 mice. Due to issues with antibody specificity, the localization of EHD4 could not be accurately observed. However, we found that EHD2 was specifically and consistently expressed in the myoepithelial/basal layer of the mammary duct and the adipocytes of the surrounding stroma (Figure 3.1 B). EHD1, on the other hand, was barely detectable within the mammary duct and surrounding stroma, except for the subcapsular sinus region of the mammary lymph node (Figure 3.2 A, Figure 3.2 B). Although striking,

these findings make sense given that the subcapsular sinus region contains CD-169^{+} macrophages with high expression of CSF-1 receptor(Shiota et al. 2016), and that EHD1 plays a crucial role in regulating the endocytic trafficking of CSF-1 receptor within macrophages(Cypher et al. 2016).

To confirm the specificity of our EHD2 antibody, we compared the wild type mammary gland expression with a newly developed *EHD2*$^{-/-}$ C57BL/6 mouse developed by GenOway. Western blot and confocal immunofluoresence confirmed that our EHD2 antibody was indeed specific (Figure 3.3 A, Figure 3.3 B). Interestingly, knockout of EHD2 in the *EHD2*$^{-/-}$ female mice led to an increase in EHD1 expression within compartments typically expressing EHD2 (Figure 3.3 C). This suggests that EHD1 serves a functionally redundant role to EHD2 in these specific mammary ductal compartments, consistent with previous literature regarding the functionally redundant roles of EHDs in other tissues (Rainey et al. 2010; Sengupta et al. 2009; George et al. 2011). Additionally, the upregulation of EHD1 in response to EHD2 knockout may explain why *EHD2*$^{-/-}$ mice do not exhibit any overt phenotype (data not shown). Despite these EHD1 findings, we elected to focus on EHD2 expression within the mammary gland.

While EHD2 was highly expressed within the myoepithelial/basal layer of 12-week old mice, we sought to confirm its localization in human tissue. Using human breast tissue sections, we performed immunohistochemical staining to confirm EHD2 localization in human mammary ducts is consistent with what we observed in mice. We found that EHD2 was indeed localized to the myoepithelial/basal layer in the mammary duct of human breast tissue (Figure 3.4 A).

Considering the highly dynamic nature of the mammary gland (Inman et al. 2015), we decided to investigate the consistency of EHD2 expression and localization during different points of mammary gland development. Using immunohistochemical staining, we found that EHD2 was consistently localized to the myoepithelial/basal layer of the murine mammary duct throughout puberty, adulthood, pregnancy, lactation, and involution (Figure 3.4 B).

Given the established role of EHD2 in caveolar dynamics (Stoeber et al. 2012; Moren et al. 2012), we suspected that the specific and consistent expression of EHD2 within the myoepithelial/basal layer of the mammary duct is relevant to caveolae function within these compartments. Accordingly, we found that caveolin-1 expression is also high within these same compartments (Figure 3.5 A) but knockout of EHD2 did not alter caveolin-1 levels (Figure 3.5 B), consistent with previous literature (Mercier et al. 2009; Aoki et al. 2011; Pinilla et al. 2006; Stoeber et al. 2012).

B. EHD2 and caveolin-1 are co-expressed in Basal B and Triple-Negative breast cancer cell lines

We then selected a large panel of human breast cancer cells and performed biochemical analysis to determine the protein expression of EHD2. We found that EHD2 was mainly expressed in TNBC cell lines and largely absent from the ER^+/PR^+ and HER2+ cell lines (Figure 3.6 A). EHD2 expression was also observed in the basal non-malignant mammary epithelial cell lines, 76Ntert and MCF10a.

Using the online database Gene expression-based Outcome for Breast cancer Online (GOBO) (Ringnér et al. 2011), we found that EHD2 mRNA expression was significantly higher in Basal B breast cancer lines compared to the Basal A and HER2+ cell lines in the panel (Figure 3.6 B). Moreover, caveolin-1 mRNA expression was also significantly higher in the Basal B cell lines (Figure 3.6 C). The Basal B subtype is the most invasive breast cancer subtype and is are considered to be triple-negative (Neve et al. 2006). When analyzing individual cell lines by the same method, we identified cell lines with high EHD2 mRNA expression (Figure 3.7 A) and high co-expression of EHD2 and caveolin-1 mRNA within the Basal B subtype (Figure 3.7 B).

Next, we selected a few cell lines to determine if EHD2 mRNA levels correlate with EHD2 protein levels. We found that EHD2 mRNA correlates with protein levels in our selected breast cancer cell lines (Figure 3.8 A), and EHD2 protein was high in our selected Basal B cell lines (Figure 3.8 B). Since we are studying the role of EHD2 in regulating plasma membrane associated caveolae, we used confocal microscopy to determine in our selected breast cancer cell lines expressed EHD2 at the cell membrane. We observed the majority of EHD2 localized at the plasma membrane in our EHD2 positive cell lines (Figure 3.8 C). To confirm the *in vitro* expression of EHD2 in our selected TNBC cell lines, we injected MDAMB468, Hs578t, or MCF7 cells into the inguinal mammary glands of NSG mice and harvested the tumors after 6 weeks. We then used immunohistochemical analysis to confirm that EHD2 was expressed in the tumors generated from the Basal B cell line (Hs578t) and not in the basal A (MDAMB468) or luminal cell line (MCF7) (Figure 3.8 D).

Once we determined the extent of EHD2 expression within our selection of human breast cancer cell lines, we sought to determine the extent of EHD2 co-expression and co-localization with caveolin-1. Although the regulation of caveolae via EHD2 is well established in the literature (Briand et al. 2014; Stoeber et al. 2012; Morén et al. 2012; Hansen, Howard, and Nichols 2011; Simone, Naslavsky, and Caplan 2014), there is nothing published that demonstrates the relationship between EHD2 and caveolae in breast cancer or the mammary gland. Moreover, the role of caveolae in breast cancer is unclear and seems to function as a tumor promoter in some subtypes while serving as a tumor suppressor in others (Feldman et al. 2015; Savage et al. 2008; Mercier and Lisanti 2012). Since caveolin-1 is the essential structural protein of caveolae, we used a large panel of breast cancer cell lines to ascertain the level of EHD2 and caveolin-1 co-expression. We found EHD2 and caveolin-1 protein expression to be mutually exclusive throughout our selected cell lines (Figure 3.9 A), indicating that EHD2 serves an important role for caveolae in breast cancer. Since EHD2 tends to be more highly expressed in TNBC and caveolae expression is believed to serve as a tumor promoter in TNBC (Elsheikh et al. 2008), we performed confocal immunofluorescence on EHD2-expressing TNBC cell lines to determine the extent of co-localization. We observed near perfect co-localization of EHD2 and caveolin-1 in MDA-MB-231, BT549, and Hs578t cell lines (Figure 3.9 B), showing that EHD2 is localizing to caveolae in breast cancer cell lines for the first time.

C. EHD2 and caveolin expression is associated with lower survival in patients with triple-negative breast cancer

After we determined that mRNA expression of EHD2 and caveolin-1 correlates to protein expression in human breast cancer cell lines, we sought to analyze co-expression of EHD2 mRNA with caveolin-1 (CAV1) and caveolin-2 (CAV2) mRNA in human breast cancer samples. We used bc-GenExMiner (Jézéquel et al. 2013; Jézéquel et al. 2012), an online database of mRNA expression from over 5,000 breast cancer samples, to determine the Pearson's pairwise correlation for EHD2 mRNA in relation to CAV1 and CAV2 expression across all tumor samples (Figure 3.10 A). We found EHD2 mRNA expression to be significantly positively correlated with CAV1 (Figure 3.10 B) and CAV2 (Figure 3.10 C).

Since we observed that EHD2 mRNA is positively correlated with CAV1 and CAV2 mRNA in breast cancer cases, we next examined the effect of EHD2, CAV1, and CAV2 mRNA expression in relation to survival of human breast cancer patients. Using KM-plotter (Győrffy et al. 2010), an online database of mRNA expression levels in relation to survival in breast cancer patients, we found that high EHD2 mRNA expression was significantly associated with lower probability of survival in patients with basal tumors, but not across all breast cancer cases (Figure 3.11 A). Interestingly, the same pattern in survival was seen for CAV1 (Figure 3.11 B) and CAV2 (Figure 3.11 C) mRNA expression. Using GOBO (Ringnér et al. 2011), we were able to screen for probability of survival for breast cancer patients with either combined low or combined high mRNA expression for EHD2, CAV1, and CAV2. Once again, we found that high combined EHD2, CAV1, and

CAV2 mRNA expression was significantly associated with lower probability of distant metastasis-free survival (DMFS) in patients with basal tumors, but not in across all patient tumor samples (Figure 3.12 A and Figure 3.12 B).

Although we determined mRNA expression to be a good indication of EHD2 protein expression in breast cancer cell lines, we wanted to determine if EHD2 protein expression was in fact associated with TNBC and caveolin expression in patient cases. In a blind study, we performed immunohistochemical staining using an anti-EHD2 on a tumor microarray (TMA) of a well-characterized cohort of 880 breast cancer patient samples that had previously been assessed for caveolin-1 and caveolin-2 protein expression(Elsheikh et al. 2008). The stained slides were then scored by pathologists and categorized for expression levels of nuclear and cytoplasmic EHD2 (Figure 3.13 A). The protein expression and localization scores were then compared to breast cancer specific survival (BCSS) for the patient cohort (Figure 3.13 B). High cytoplasmic expression was significantly associated with lower probability of survival for all cases and markers for poorer prognosis (Table 3.1). Interestingly, high nuclear expression was significantly associated with higher probability of survival and markers for better prognosis (Table 3.1). The unexpected nuclear expression of EHD2 and its association with higher survival could explain the previously observed discrepancy in survival probability between all tumor cases and basal tumors with regards to mRNA expression. In fact, when the samples are scored for only high or low/negative cytoplasmic EHD2 expression (Figure 3.14 A), high EHD2 expression is significantly associated with TNBC (Figure 3.14 B) and lower survival (Figure 3.14 C). Conversely, nuclear expression is associated with luminal

markers (Table 3.1). Consistent with our previous findings in breast cancer cell lines and mRNA expression data of human breast cancer patients, high EHD2 cytoplasmic expression is associated with Caveolin-2 expression (Table 3.2). Despite the interesting finding regarding EHD2 expression within the nucleus, we decided to focus on cytoplasmic EHD2 expression and its association with TNBC.

D. shRNA-mediated knockdown of EHD2 leads to reduced tumorigenicity and invasiveness of Triple-negative breast cancer *in vitro* and *in vivo*

Using retroviral transduction, we generated three TNBC cell lines (MDA-MB-231, BT549, and Hs578t) with stable EHD2 shRNA and control shRNA (Figure 3.15 A). We did not find any significant change in proliferation in TNBC cells with EHD2 shRNA (Figure 3.15 B). However, we found significant reduction in invasion in TNBC cells with EHD2 shRNA compared to controls (Figure 3.15 C). Additionally, cells with EHD2 shRNA had lower tumorigenicity, as indicated by fewer soft-agar colonies (Figure 3.16) and fewer tumorspheres in non-adherent conditions (Figure 3.17).

Next, we sought to examine the effect of EHD2 depletion in TNBC tumors *in vivo.* We performed xenograft injections into the inguinal mammary gland of 4-week-old nude mice. After two weeks, palpable tumors were observed in all mice. The tumor volume of each mouse was measure every week until the study was terminated in week eleven. We found that EHD2 knockdown dramatically halted tumor volume and progression, compared to mice with control shRNA in BT549 (Figure 3.18 A and Figure 3.18 B) and HS578t tumors (Figure 3.19 A and Figure 3.19 B). Additionally, EHD2 knockdown tumors

had a decrease in proliferation, per immunohistochemical staining of proliferative marker Ki-67 (Figure 3.20). We then performed confocal microscopy to verify the knockdown of EHD2 in the tumors with EHD2 shRNA (Figure 3.21).

Following the observation of the dramatic reduction in tumor, we set forth to determine the extent of metastasis associated with EHD2 knockdown in TNBC cells. Unfortunately, BT549 and HS578t cells are not reliably capable of metastasis. Instead, we performed xenograft injections of MDA-MB-231 cells as described above. We found that EHD2 knockdown in MDA-MB-231 cells led to a dramatic decrease in final tumor volume and a decrease in lung metastasis (Figure 3.22)

E. Triple-negative breast cancer cells require EHD2 for growth in extracellular matrix and plasma membrane repair

Although a decrease in tumor growth and metastasis was expected in TNBC tumors with EHD2 shRNA, the dramatic decrease in tumor volume across all TNBC cell lines led us to believe that EHD2 was necessary to an essential function for tumor cells *in vivo.* This lead us to once again investigate bc-GenExMiner to determine what other proteins EHD2 was correlated with in breast cancer patient samples and the functions those proteins may serve. By investigating gene ontology correlations, we found that EHD2 expression was tightly correlated with cellular components associated with the extracellular matrix, extracellular region, basement membrane, focal adhesion, and other functions associated with the plasma membrane (Table 3.3). This finding led us to next examine the growth of EHD2-knockdown TNBC cells within a basement membrane extract. To examine this, we used Matrigel, a commercially available mixture of various

extracellular matrix components. Matrigel is commonly used to mimic the ECM that tumors grow in *in vivo* (Ortega-Cava et al. 2011; Dimri et al. 2007). We found that EHD2 knockdown led to dramatic reduction in invasive morphology in MDA-MB-231 (Figure 3.23 A) and BT549 (Figure 3.24 A) cells grown in Matrigel. The EHD2 knockdown cells had fewer invasive projections, often referred to as invadopodia (Hashimoto et al. 2004), in both MDA-MB-231 (Figure 3.23 B) and BT549 cells (Figure 3.24 B).

Given the well-established role of EHD2 in regulating the dynamics of caveolae and the more recent discoveries that caveolae play an important role in membrane repair and invadopodia formation in cancer (Yamaguchi et al. 2009; H. Yang et al. 2016; Stoeber et al. 2012), we sought to determine the effect of EHD2 knockdown on membrane repair in TNBC cells. To examine membrane repair, we used a bulk wounding assay with glass beads and various cytoplasm staining dyes. Briefly, cells were plated on coverslips and then wounded via glass bead rolling. They were then incubated with a CascadeBlue-conjugated dextran to label cells with damaged membranes. Cells were then allowed to reseal their membranes and then incubated with a TRITC-conjugated dextran to label cells that failed to repair (Figure 3.25 A). Using this assay, we found that EHD2 knockdown resulted in a significantly higher percentage of cells with failed membrane repair in MDA-MB-231, BT549, and HS578t cells (Figure 3.25 B). These findings suggest that EHD2 regulation of caveolae is essential to membrane repair processes in TNBC cells.

III.2 Tables

Table 3.1

	EHD2 Subgroups				
	Double negative (nuclear -/cytoplasmic-) N (%)	**Nuclear +/cytoplasmic – N (%)**	**Nuclear-/cytoplasmic + N (%)**	**Double positive (nuclear+/cytoplasmic+) N (%)**	**P value**
ER					
Negative	94(28)	34(22)	51(44)	33(24)	<0.0001
Positive	241(72)	122(78)	66(56)	107(76)	
PR					
Negative	143(45)	51(34)	66(57)	50(37)	0.001
Positive	177(55)	100(66)	49(43)	85(63)	
HER2					
Negative	272(85)	135(88)	89(77)	109(84)	0.136
Positive	43(15)	19(12)	26(23)	21(16)	
Triple Negative					
Non triple negative	259(80)	137(90)	79(68)	117(84)	**<0.0001**
Triple negative	65(20)	16(10)	37(32)	22(16)	

Table 3.1. Table showing the relationship between EHD2 subgroups and the other markers. Of the whole series (840 cases), 759 were informative. The expression of EHD2 is detected in the cytoplasm and/or nucleus of the malignant cells while, in the normal parenchymal element its expression is noted in the nuclei of epithelial cells only. For statistical analysis, expression was dichotomized using cutoff points that were selected based on histogram distribution. The cutoff points were selected using median and X-tile software as follows: an H-score of zero for nuclear EHD2 and H-score of 50 for cytoplasmic EHD2 expression.

Table 3.2

	EHD2 Nuclear Expression			EHD2 Cytoplasmic Expression		
	Negative (=0)	Positive (>0)	*p*-value (χ^2)	Negative (<50)	Positive (≥50)	*p*-value (χ^2)
Age						
<50	163(36)	100(33)	0.449	123(34)	140(35)	0.796
≥50	288(64)	199(67)		234(66)	256(65)	
Menopausal Status						
Pre-	180(40)	111(37)	0.539	143(40)	149(37)	0.463
Post-	276(61)	187(63)		215(60)	250(63)	
Tumour Size (cm)						
< 2.0	185(41)	165(56)	**<0.001**	172(49)	179(46)	0.422
≥2.0	262(59)	129(44)		181(51)	212(54)	
Stage						
1	272(60)	185(63)	0.303	221(63)	238(61)	0.847
2	140(31)	92(31)		107(30)	126(32)	
3	38(9)	16(6)		25(7)	29(7)	
Grade						
1	45(10)	62(21)	**<0.001**	58(17)	49(12)	**0.012**
2	119(27)	103(35)		118(33)	105(27)	
3	285(64)	128(44)		176(50)	239(61)	
Mitosis						
1	101(23)	111(39)	**<0.001**	120(35)	92(24)	**0.006**
2	81(18)	59(21)		63(18)	78(20)	
3	261(59)	114(40)		163(47)	214(56)	
Vascular Invasion						
Probable/Negative	263(59)	208(71)	**0.001**	225(64)	248(64)	0.925
Definite	183(41)	85(29)		127(36)	142(36)	
ER						
Negative	145(32)	67(23)	**0.005**	92(26)	122(31)	0.151
Positive	307(68)	229(77)		262(74)	275(69)	
PgR						
Negative	209(48)	101(35)	**0.001**	142(42)	170(45)	0.419
Positive	226(52)	185(65)		200(58)	212(55)	
HER2 Status						
Negative	361(83)	244(86)	0.294	304(87)	304(82)	0.039
Positive	74(17)	40(14)		45(13)	69(18)	
AR						
Negative	195(49)	88(34)	**<0.001**	146(46)	139(41)	0.196
Positive	206(51)	170(66)		174(54)	203(59)	
Her3						
Negative	29(7)	25(10)	0.204	28(9)	26(7)	0.555
Positive	386(93)	232(90)		296(91)	325(93)	
Her4						
Negative	42(10)	36(13)	0.177	41(12)	37(10)	0.391
Positive	394(90)	244(87)		304(88)	337(90)	

Table 3.2 continued

Ck5						
Negative	278(79)	192(88)	**0.008**	240(87)	230(79)	**0.011**
Positive	72(21)	26(12)		37(13)	63(21)	
Ck7/8						
Negative	10(2)	5(2)	0.622	5(1)	11(3)	
Positive	425(98)	279(98)		340(99)	366(97)	0.181
Ck14						
Negative	378(91)	239(89)	0.444	297(90)	322(90)	0.925
Positive	39(9)	30(11)		34(10)	36(10)	
Ck17						
Negative	269(82)	170(89)	**0.039**	221(87)	219(82)	0.116
Positive	58(18)	21(11)		33(13)	48(18)	
HER1						
Negative	338(77)	227(79)	0.451	280(81)	287(75)	0.060
Positive	101(23)	59(21)		66(19)	95(25)	
Mucin1						
Negative	50(12)	15(6)	**0.005**	28(9)	39(11)	0.367
Positive	355(88)	245(94)		286(91)	315(89)	
P53						
Negative	292(68	207(74)	0.073	245(72)	255(68)	0.255
Positive	138(32)	72(26)		94(28)	118(32)	
Mdm2						
Negative	264(82)	152(71)	**0.003**	199(76)	219(78)	0.531
Positive	60(19)	63(29)		63(24)	61(22)	
Ki67						
Negative	99(29)	106(45)	**<0.001**	105(38)	101(33)	0.157
Positive	245(71)	132(56)		170(62)	209(67)	
ADA3						
Negative	201(53)	93(40)	**0.002**	149(52)	147(44)	0.058
Positive	181(47)	141(60)		138(48)	185(56)	
TN Status						
Non-TN	338(77)	254(87)	**0.001**	288(82)	305(79)	0.293
TN	102(23)	38(13)		62(18)	80(21)	
N cadherin						
Negative						
Positive	79(23)	64(31)	**0.047**	97(27)	47(25)	0.650
	261(77)	143(69)		265(73)	14(75)	
E cadherin						
Negative	173(41)	84(31)	**0.008**	170(37)	89(37)	0.957
Positive	247(59)	186(69)		284(63)	150(63)	
P cadherin						
Negative	171(46)	104(45)	0.881	182(47)	94(44)	
Positive	202(54)	126(55)		208(53)	122(56)	0.456

Table 3.2. Association with clinicopathological parameters. Of the whole series (840 cases), 759 were informative. The expression of EHD2 is detected in the cytoplasm and/or nucleus of the malignant cells while, in the normal parenchymal element its expression is noted in the nuclei of epithelial cells only. For statistical analysis, expression was dichotomized using cutoff points that were selected based on histogram distribution. The cutoff points were selected using median and X-tile software as follows: an H-score of zero for nuclear EHD2 and H-score of 50 for cytoplasmic EHD2 expression. Nuclear and cytoplasmic EHD2 expression showed contrasting associations with other variables with loss of nuclear expression and or cytoplasmic expression associated with variables characteristic of poor prognosis and shorter survival (tumor suppressor gene-like effect). There were associations between loss of nuclear EHD2 expression and poor prognostic variables including large tumour size, high tumour grade with frequent mitoses and high Ki-67, positive vascular invasion and high Nottingham Prognostic Index (NPI) scores. Nuclear EHD2 showed positive associations with good prognostic biomarkers including hormone receptors (ER, PR, AR) and other markers characteristics of the luminal class such as muc1, BEX1, nuclear BRCA1 and RAD51, FHIT, FOXA1 and E-cadherin. Loss of nuclear EHD2 expression was associated with basal-like molecular class biomarkers including CK5, CK 17 and Ki-67, and with triple negative phenotype and biomarkers associated with EMT including loss of E-cadherin and expression of N-cadherin. Nuclear EHD2 was associated with AKT and PI3K and with ERK (pan-ERK, phospho-ERK and p38). On the other hand, cytoplasmic

EHD2 expression showed positive association with poor prognostic markers including high grade, high mitotic rate and with basal-like biomarker (CK5) and the apoptosis marker Bcl2.

Table 3.3

CAVEOLIN1_STATUS

Count

		EHD2_CYTO_NUC_COEXPRESSION		Total
		EHD2 CYTO and NUC Negative	EHD2 CYTO Positive NUC Negative	
CAVEOLIN1_STATUS	.00	70	37	107
	1.00	4	5	9
Total		74	42	116

Chi-Square Tests

	Value	df	Asymp. Sig. (2-sided)	Exact Sig. (2-sided)	Exact Sig. (1-sided)
Pearson Chi-Square	1.581[a]	1	.209		
Continuity Correction[b]	.804	1	.370		
Likelihood Ratio	1.514	1	.219		
Fisher's Exact Test				.281	.184
Linear-by-Linear Association	1.568	1	.211		
N of Valid Cases	116				

a. 1 cells (25.0%) have expected count less than 5. The minimum expected count is 3.26.

b. Computed only for a 2x2 table

Table 3.3. EHD2 association with caveolin-1 status. Cases were defined based on the dual expression (CYTO and NUC). Then cases with any nuclear staining were excluded (Double CYT and NUC positive as well as the NUC positive CYTO Negative) cases.

Table 3.4

CAVEOLIN2_STATUS

Count

		EHD2_CYTO_NUC_COEXPRESSION		Total
		EHD2 CYTO and NUC Negative	EHD2 CYTO Positive NUC Negative	
CAVEOLIN2_STATUS	.00	67	30	97
	1.00	9	15	24
Total		76	45	121

Chi-Square Tests

	Value	df	Asymp. Sig. (2-sided)	Exact Sig. (2-sided)	Exact Sig. (1-sided)
Pearson Chi-Square	8.210[a]	1	.004		
Continuity Correction[b]	6.914	1	.009		
Likelihood Ratio	7.962	1	.005		
Fisher's Exact Test				.008	.005
Linear-by-Linear Association	8.142	1	.004		
N of Valid Cases	121				

a. 0 cells (0.0%) have expected count less than 5. The minimum expected count is 8.93.

b. Computed only for a 2x2 table

Table 3.4. EHD2 association with caveolin-2 status. Cases were defined based on the dual expression (CYTO and NUC). Then cases with any nuclear staining were excluded (Double CYT and NUC positive as well as the NUC positive CYTO Negative) cases.

Table 3.5

Cellular component

Total number of genes with annotations: 17 014

Best positive correlations with *EHD2*

Number of genes in target list: 226, with annotations: 195

Significant terms	Description	p-value	% target list	% universe	Associated genes
GO:GO:0031012	extracellular matrix	4.32e-47	23.08	1.11	*COL5A1, TGFB1I1, COL6A2, HTRA1, AEBP1, LTBP2, OLFML2A, PCOLCE, COL6A3, LAMB2, ECM1, BGN, COL1A1, EMILIN1, COL5A2, COL1A2, TIMP3, COL18A1, FBN1, MMP2, COL3A1, NID2, NID1, VCAN, CYR61, LOXL1, COL15A1, FBLN1, CRISPLD2, TGFB3, THBS2, MMP14, IGFBP7, DCN, OLFML2B, HSPG2, COL12A1, MFAP4, TNC, FN1, TPSAB1, COL7A1, COL8A2, THBS1, SERPINE1*
GO:GO:0005576	extracellular region	1.75e-26	34.87	8.09	*COL5A1, FAM180A, PAPL, COL6A2, EFEMP2, OLFML2A, COL6A3, LAMB2, COL5A3, BGN, IGFBP4, COL1A1, EMILIN1, SPARC, COL5A2, COL1A2, PRSS57, PLXDC1, SLIT3, BMP1, COL18A1, FBN1, C1QTNF8, CLEC11A, IGF2, MMP2, COL3A1, NID2, IGFBP5, DKK3, NID1, VCAN, OLFML1, LOXL1, ADAMTS2, COL15A1, FNDC1, FBLN1, HEG1, TIMP2, CRISPLD2, ADAM12, DHRS4L2, TGFB3, THBS2, FSTL1, ITGBL1, IGFBP7, DCN, OLFML2B, HSPG2, ACTN1, COL12A1, PDGFB, MFAP4, TNC, FN1, TPSAB1, COL7A1, COL8A2, THBS1, C5orf38, SERPINE1, FSTL3, CXCL12, CTSK, PSG8, GRP*
GO:GO:0005615	extracellular space	4.61e-21	28.72	6.80	*GDF6, COL6A2, HTRA1, AEBP1, LTBP2, ANGPTL2, PCOLCE, COL6A3, ECM1, IGFBP4, COL1A1, SPARC, COL1A2, PLXDC1, TIMP3, SLIT3, BMP1, COL18A1, FBN1, CLEC11A, IGF2, MMP2, COL3A1, SRPX2, MMRN2, IGFBP5, DKK3, VCAN, LOXL1, SPOCK1, COL15A1, C1QTNF6, ACTA2, AXL, FBLN1, TIMP2, TGFB3, FSTL1, IGFBP7, DCN, HSPG2, ACTN1, COL12A1, PDGFB, THBD, TNC, FN1, FAP, TPSAB1, COL7A1, THBS1, SERPINE1, FSTL3, CXCL12, CTSK, GRP*
GO:GO:0005604	basement membrane	1.71e-17	8.72	0.46	*COL5A1, EFEMP2, LAMB2, SPARC, TIMP3, COL18A1, FBN1, NID2, MMRN2, NID1, LOXL1, FBLN1, TIMP2, THBS2, TNC, COL7A1, COL8A2*
GO:GO:0005925	focal adhesion	1.40e-11	12.31	2.25	*PDGFRB, TGFB1I1, THY1, LRP1, MRC2, TNS1, ITGA5, ITGB5, PDLIM7, CNN1, MMP14, CNN2, HSPG2, ACTN1, LIMS2, TNC, CAV1, FAP, FERMT2, SPRY4, TENC1, LIMA1, AKAP12, CD99*
GO:GO:0005578	proteinaceous extracellular matrix	3.01e-11	9.74	1.39	*COL6A2, LTBP2, CD248, COL6A3, ECM1, BGN, EMILIN1, SPARC, TIMP3, BMP1, FBN1, MMP2, VCAN, CYR61, SPOCK1, ADAMTS2, FBLN1, TIMP2, COL8A2*
GO:GO:0005788	endoplasmic reticulum lumen	3.62e-11	8.72	1.08	*COL5A1, COL6A2, COL6A3, COL5A3, COL1A1, COL5A2, COL1A2, COL18A1, COL3A1, COL15A1, COL12A1, PDGFB, RCN3, COL7A1, COL8A2, THBS1, CERCAM*
GO:GO:0070062	extracellular exosome	9.69e-10	33.33	15.71	*EHD2, COL5A1, PDGFRB, COL6A2, MXRA8, HTRA1, AEBP1, LTBP2, CD248, ANGPTL2, EFEMP2, THY1, PCOLCE, COL6A3, LAMB2, COL5A3, ECM1, BGN, SEMA5A, EMILIN1, SNED1, PLVAP, CDH11, COL1A2, TIMP3, COL18A1, FBN1, ITGB5, IGF2, MYH11, NID2, MMRN2, MYOF, ESAM, NID1, COL15A1, LRRC15, ACTA2, AXL, MXRA5, FBLN1, TIMP2, CRISPLD2, FAM26E, FSTL1, PCDH12, TNXA, MYLK, PPAP2A, IGFBP7, FUT11, PRSS23, CNN2, HSPG2, ACTN1, COL12A1, MRGPRF, MFAP4, MYADM, CPE, FN1, THBS1, NEDD4, SERPINE1, CXCL12*
GO:GO:0005581	collagen trimer	4.37e-09	5.13	0.39	*COL5A1, COL6A2, EMILIN1, COL5A2, COL1A2, COL18A1, C1QTNF8, COL15A1, C1QTNF6, COL8A2*
GO:GO:0009986	cell surface	4.95e-08	11.28	2.88	*PDGFRB, MXRA8, BGN, SPARC, PLVAP, TNS1, ITGA5, CD93, ITGB5, GPR124, NID2, SRPX, SRPX2, AXL, TIMP2, TGFB3, PDGFB, THBD, GPR116, FAP, FERMT2, THBS1*
GO:GO:0031093	platelet alpha granule lumen	6.57e-08	4.10	0.28	*SPARC, IGF2, TGFB3, ACTN1, PDGFB, FN1, THBS1, SERPINE1*
GO:GO:0005588	collagen type V trimer	1.48e-06	1.54	0.02	*COL5A1, COL5A3, COL5A2*
GO:GO:0005634	nucleus	2.21e-06	14.36	28.88	*EHD2, PDGFRB, SSX7, AEBP1, PTRF, ZNF774, TIMP3, TSHZ3, NUAK1, TMEM89, MMP2, PDLIM7, TGFB3, PRSS23, MEIS3, EPAS1, APBB2, FILIP1L, ACTN1, ELK3, ZNF423, RUNX1T1, CPE, LIMS2, FERMT2, BNC2, ID3, FSTL3*
GO:GO:0001725	stress fiber	3.36e-06	3.59	0.33	*MYH11, PDLIM7, MYLK, CNN2, ACTN1, FERMT2, LIMA1*
GO:GO:0005911	cell-cell junction	1.87e-05	5.13	0.96	*ITGA5, CDH5, KIAA1462, FNDC1, HEG1, PCDH12, MYLK, CNN2, ACTN1, MYADM*
GO:GO:0005605	basal lamina	3.54e-05	2.05	0.10	*LAMB2, NID1, HSPG2, FN1*
GO:GO:0005577	fibrinogen complex	1.18e-04	1.54	0.05	*FBLN1, FN1, THBS1*
GO:GO:0005584	collagen type I trimer	1.31e-04	1.03	0.01	*COL1A1, COL1A2*
GO:GO:1903561	extracellular vesicle	2.62e-04	2.56	0.29	*COL6A2, EFEMP2, COL6A3, COL12A1, OLFML3*
GO:GO:0005589	collagen type VI trimer	3.89e-04	1.03	0.02	*COL6A3, DCN*
GO:GO:0031091	platelet alpha granule	4.92e-04	1.54	0.08	*SPARC, THBS2, THBS1*
GO:GO:0005654	nucleoplasm	5.38e-04	6.67	14.90	*PTRF, TSHZ3, DACT1, FNDC1, ADAM12, EPAS1, HOXC6, ELK3, RUNX1T1, FERMT2, BNC2, ID3, FSTL3*
GO:GO:0005829	cytosol	6.04e-04	8.72	17.58	*HTRA1, THY1, PTRF, SYDE1, EDNRA, DACT1, MYH11, ACTA2, MYLK, EPAS1, LMOD1, ACTN1, LIMS2, CAV1, PLEKHG2, FERMT2, NEDD4*
GO:GO:0071953	elastic fiber	7.72e-04	1.03	0.02	*FBLN1, MFAP4*
GO:GO:0005901	caveola	8.89e-04	2.56	0.38	*EHD2, PTRF, PLVAP, MYOF, CAV1*
GO:GO:0030485	smooth muscle contractile fiber	1.28e-03	1.03	0.03	*MYH11, ACTA2*
GO:GO:0043202	lysosomal lumen	2.02e-03	2.56	0.46	*PDGFRB, BGN, VCAN, DCN, HSPG2*
GO:GO:0005789	endoplasmic reticulum membrane	2.51e-03	0.51	4.47	*CAV1*
GO:GO:0005796	Golgi lumen	3.41e-03	2.56	0.52	*BGN, VCAN, MMP14, DCN, HSPG2*
GO:GO:0005886	plasma membrane	5.17e-03	30.26	21.79	*EHD2, PDGFRB, OR6M1, OR10AD1, PCDHGA1, THY1, LRP1, OR5AU1, OR1K1, PTRF, OR52N5, SEMA5A, OR5B17, CDH11, ITGA5, PLXDC1, EDNRA, OR5M11, CD93, CDH5, ITGB5, GPR124, IGF2, MMP2, MYOF, ESAM, APLNR, AXL, FNDC1, PCDH7, OR4D6, OR5D16, OR10G3, ADAM12, TGFB3, PCDH12, MMP14, PPAP2A, OR2Z1, HSPG2, ACTN1, THBD, GPR116, MYADM, CPE, LIMS2, CD34, CAV1, FAP, BNC2, OR5B3, NEDD4, TENC1, LIMA1, SERPINE1, AKAP12, CD99, OR4K1, CERCAM*

Table 3.5. EHD2 mRNA aassociation with extracellular-mediated cellular processes in TNBC patients. Using bc-GenExMiner v 4.0 (Jézéquel et al. 2013; Jézéquel et al. 2012), we performed gene correlation exhaustive analysis to identify genes best correlating positively to EHD2 in over 700 TNBC patient samples. We then sorted the results into their associated Gene Ontology term enrichments.

III.3 Figures

Figure 3.1

A

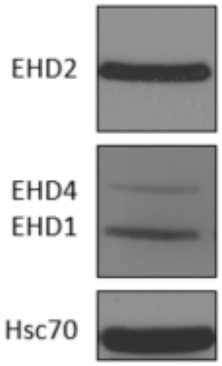
EHD2
EHD4
EHD1
Hsc70

B

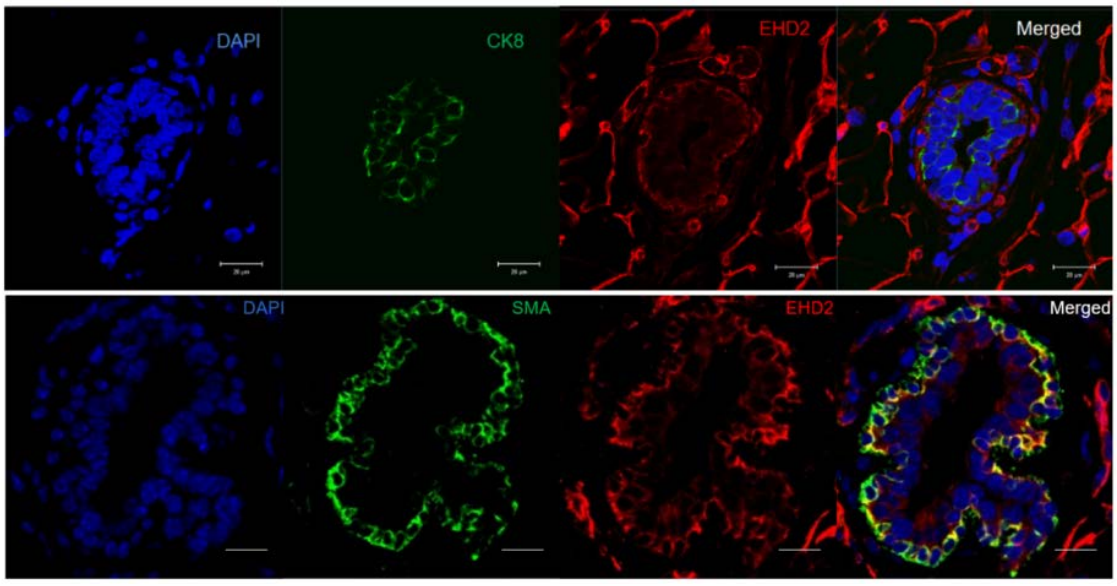
DAPI
CK8
EHD2
Merged
DAPI
SMA
EHD2
Merged

Figure 3.1. EHD2 expression in the mammary duct is localized to the myoeptheilium. **a,** Immunoblot analysis of EHD levels in normal murine mammary gland; Hsc70 loading control is shown on the bottom panel. **b,** Immunofluorescence images of normal mouse mammary gland. Top row is stained with anti-cytokeratin 8 (CK8) (green) and anti-EHD2 (red) antibodies. Bottom row is stained with anti-alpha smooth muscle actin (SMA) (green) and anti-EHD2 (red). Both rows were counterstained with 4,6-diamidino-2-phenylindole (DAPI, to stain DNA; blue). Scale bars, 20μm.

Figure 3.2

A

EHD1

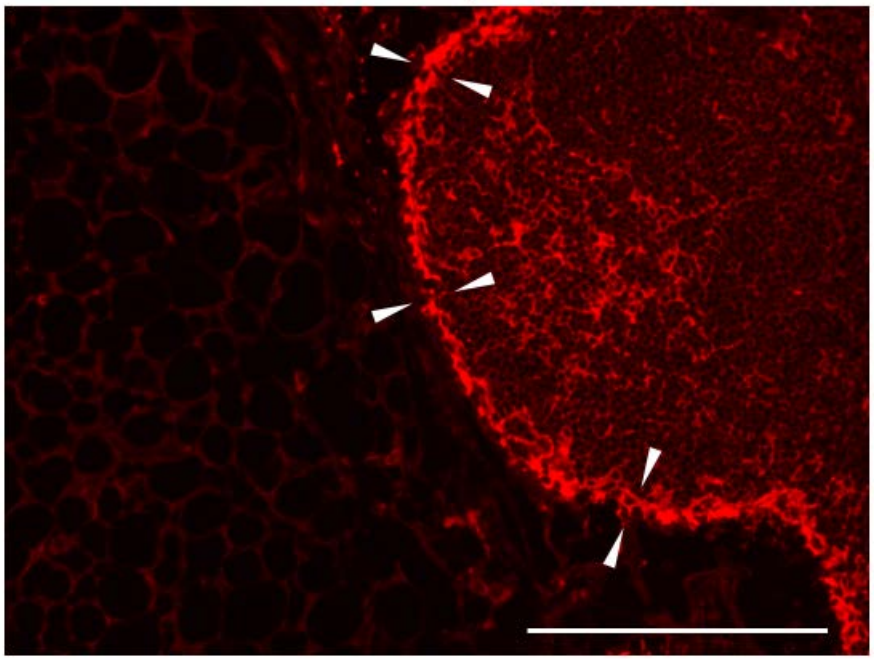

B

EHD1

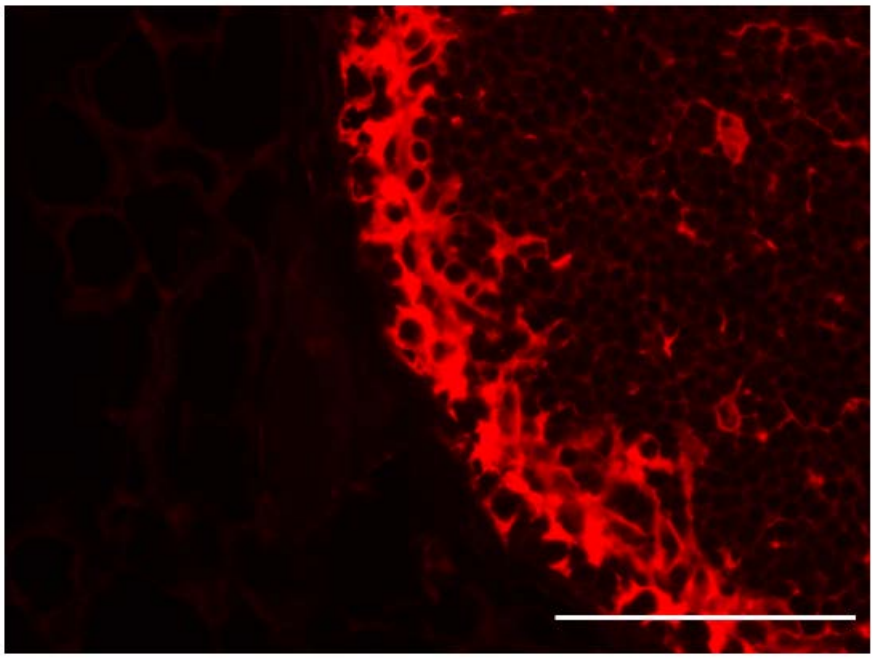

Figure 3.2. EHD1 expression in the mammary gland is primarily localized to the subcapsular sinus of the mammary lymphnode. a, Immunofluorescence images of normal mouse mammary gland stained with anti-EHD1. White arrows indicate subscapular sinus region of mammary lymph node. Scale bar: 200 μm. **b,** Immunofluorescence images of normal mouse mammary gland stained with anti-EHD1. Scale bar: 100 μm.

Figure 3.3

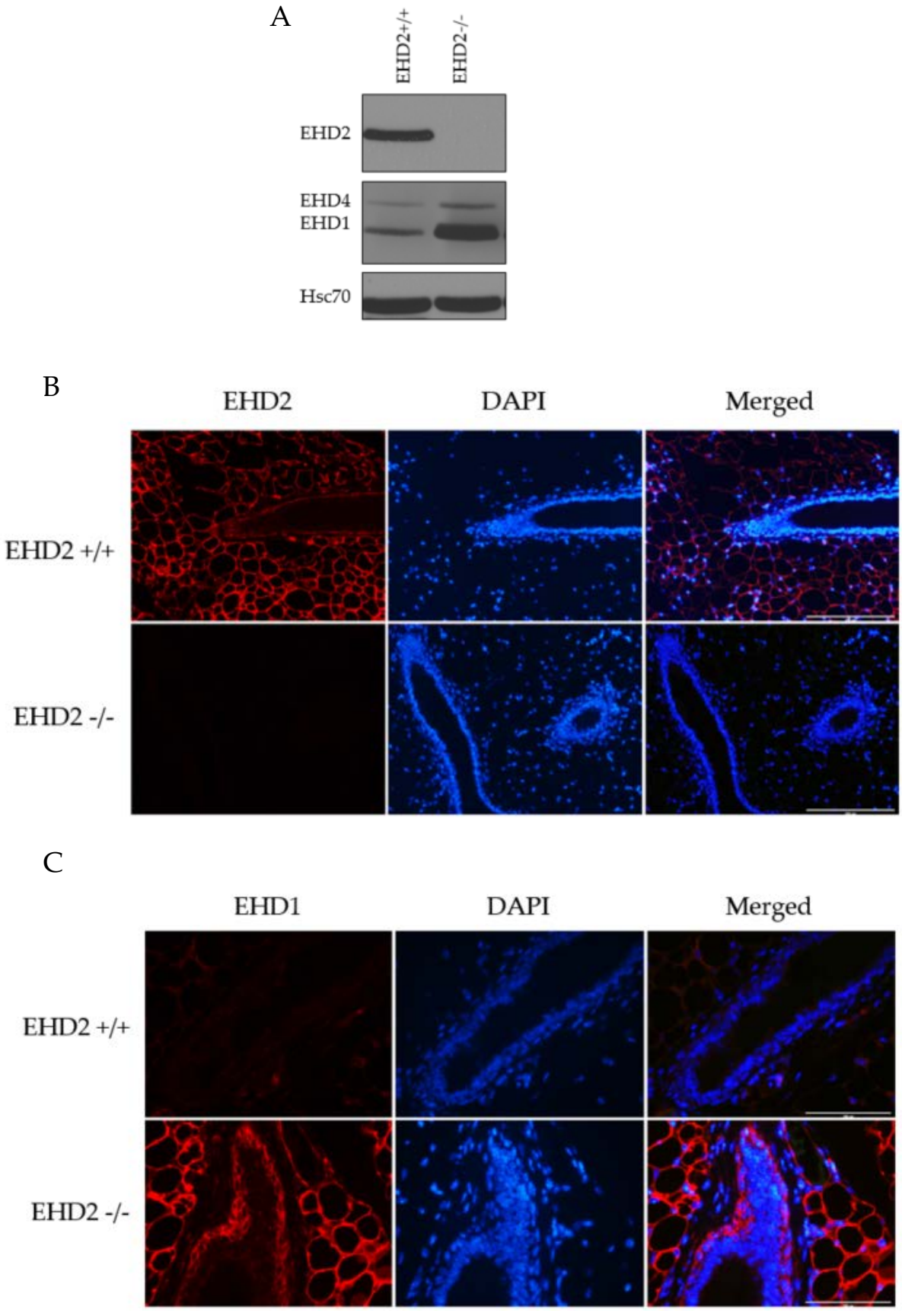
A
EHD2+/+
EHD2-/-
EHD2
EHD4
EHD1
Hsc70
B
EHD2
DAPI
Merged
EHD2 +/+
EHD2 -/-
C
EHD1
DAPI
Merged
EHD2 +/+
EHD2 -/-

Figure 3.3. Confirmation of EHD2 knockout and increased EHD1 expression in the mammary gland of EHD2 $^{-/-}$ mice. a, Immunoblot analysis of EHD levels in normal murine mammary gland and EHD2 null mammary gland; Hsc70 loading control is shown on the bottom panel. **b,** Immunofluorescence images of 12-week old female inguinal mammary glands of EHD2+/+ mice (top row) or EHD2 -/- mice (bottom row) stained with anti-EHD2 (left panel) and DAPI (middle panel). Merged images of EHD2 and DAPI show lack of EHD2 expression in EHD2 -/- mice. (right panel). Scale bars, 200 μm. **b,** Immunofluorescence images of 12-week old female inguinal mammary glands of EHD2+/+ mice (top row) or EHD2 -/- mice (bottom row) stained with anti-EHD1 (left panel) and DAPI (middle panel). Merged images of EHD2 and DAPI show lack of EHD2 expression in EHD2 -/- mice. (right panel). Scale bars, 100 μm.

Figure 3.4

A

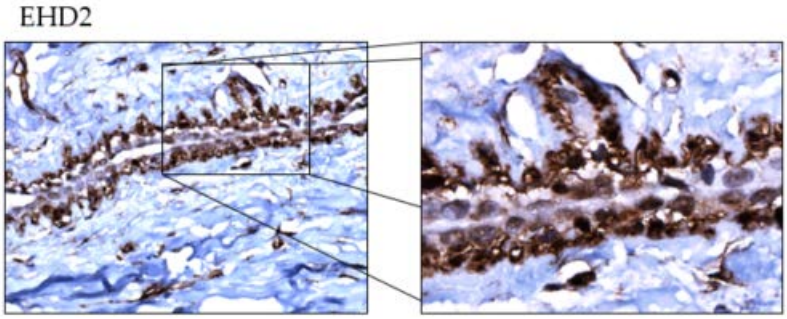
EHD2

B

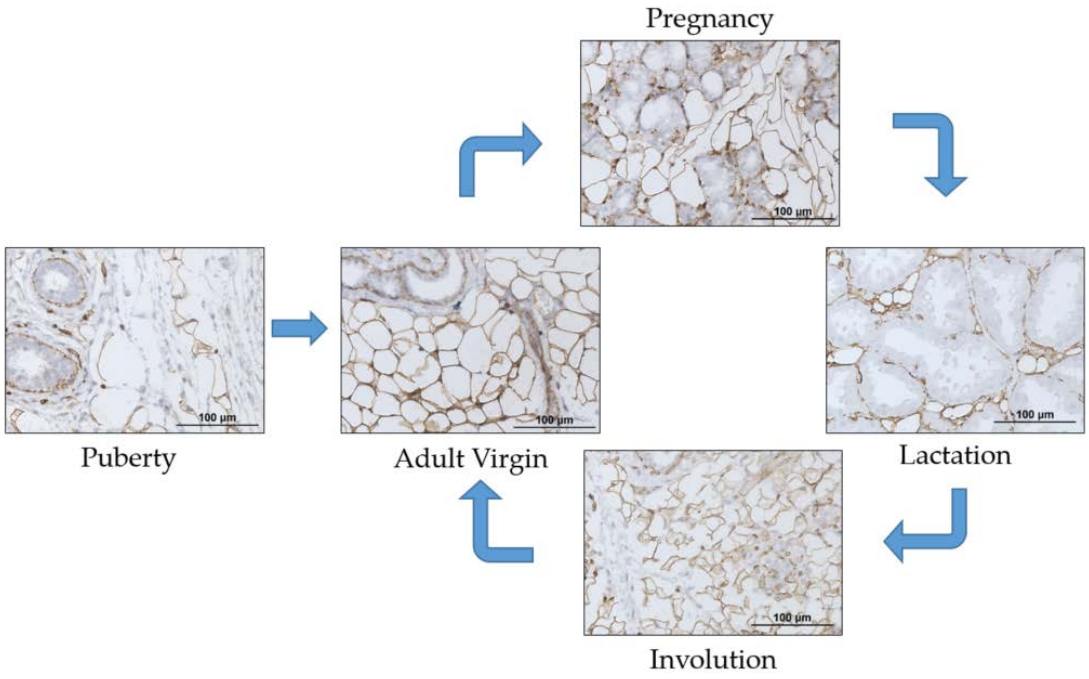
Pregnancy
100 µm
Puberty
100 µm
Adult Virgin
100 µm
Lactation
100 µm
Involution
100 µm

Figure 3.4. EHD2 is consistently expressed and localized to the myoepithelial/basal layer of the mammary duct. a, Immunohistochemical staining of EHD2 in normal human breast tissue sections. Selected area demonstrates the localization of EHD2 within the human myoepithelial/basal layer. **b,** Immunohistochemical analysis of EHD2 in murine mammary gland sections throughout various timepoints of development. Images are arranged to show the dynamic cycle of mammary gland development. Scale bars, 100 μm.

Figure 3.5

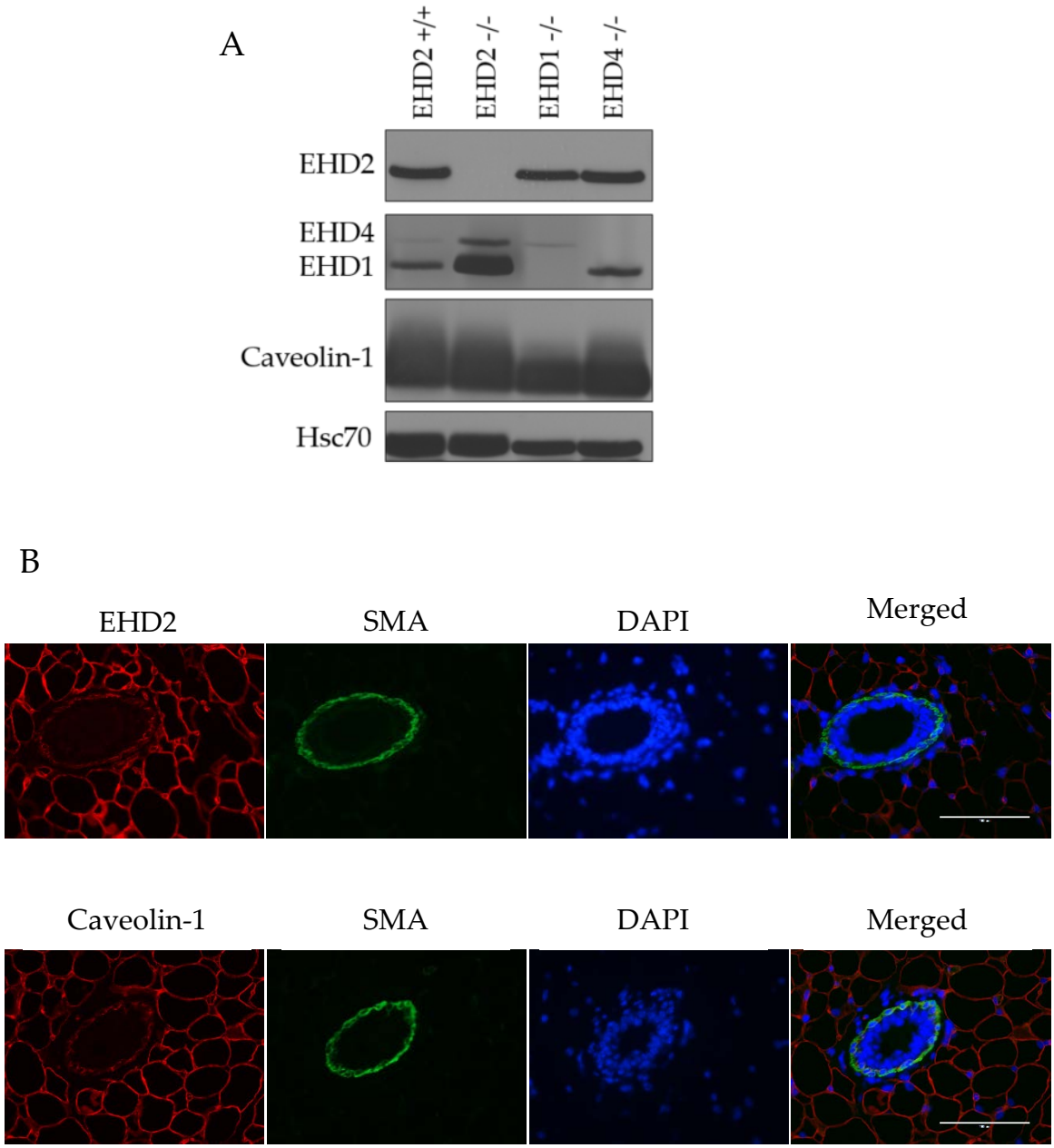
A
EHD2 +/+
EHD2 -/-
EHD1 -/-
EHD4 -/-
EHD2
EHD4
EHD1
Caveolin-1
Hsc70
B
EHD2
SMA
DAPI
Merged
Caveolin-1
SMA
DAPI
Merged

Figure 3.5. EHD2 and caveolin-1 occupy the same compartments of the mammary gland. a, Immunoblot analysis of EHD levels and caveolin-1 levels in normal murine mammary gland, EHD2, EHD1, and EHD4 null mammary gland; Hsc70 loading control is shown on the bottom panel. **b,** Immunofluorescence images of 12-week old female inguinal mammary glands of mice stained for EHD2 (red, top row) or caveolin-1 (red, bottom row), and smooth muscle actin (green), and DAPI (blue). Scale bars, 200 μm.

Figure 3.6

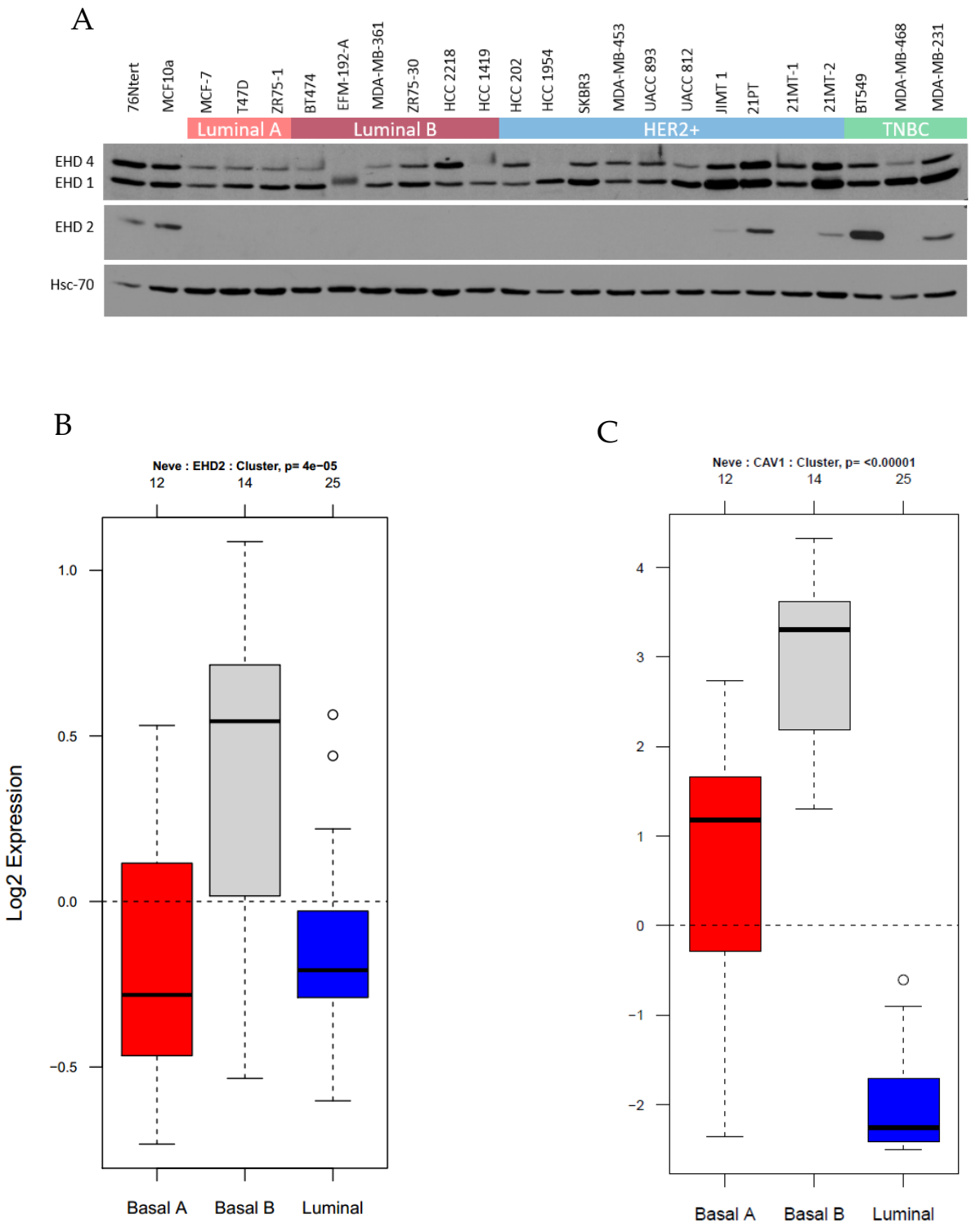
A
76Ntert
MCF10a
MCF-7
T47D
ZR75-1
BT474
EFM-192-A
MDA-MB-361
ZR75-30
HCC 2218
HCC 1419
HCC 202
HCC 1954
SKBR3
MDA-MB-453
UACC 893
UACC 812
JIMT 1
21PT
21MT-1
21MT-2
BT549
MDA-MB-468
MDA-MB-231
Luminal A
Luminal B
HER2+
TNBC
EHD 4
EHD 1
EHD 2
Hsc-70
B
Neve : EHD2 : Cluster, p= 4e−05
12
14
25
1.0
0.5
0.0
−0.5
Log2 Expression
Basal A
Basal B
Luminal
C
Neve : CAV1 : Cluster, p= <0.00001
12
14
25
4
3
2
1
0
−1
−2
Basal A
Basal B
Luminal

Figure 3.6. EHD2 and caveolin-1 are primarily expressed in triple-negative breast cancer cell lines. a, Immunoblot analysis of EHD levels in non-tumorigenic immortalized mammary epithelial cells (76Ntert, MCF10a), luminal A breast cancer cell lines (ER+/PR+), luminal B breast cancer cell lines (ER+/PR+, ErbB2+), HER2+ breast cancer cell lines (ErbB2+), and Triple-negative breast cancer cell lines (ER-/PR-, ErbB2-); Hsc70 loading control is shown on the bottom panel. **b,** Box-and-whisker plot of EHD2 mRNA expression levels in Basal A, Basal B, and Luminal cell lines. **c,** Box-and-whisker plot of caveolin-1 mRNA expression levels in Basal A, Basal B, and Luminal cell lines.

Figure 3.7

A

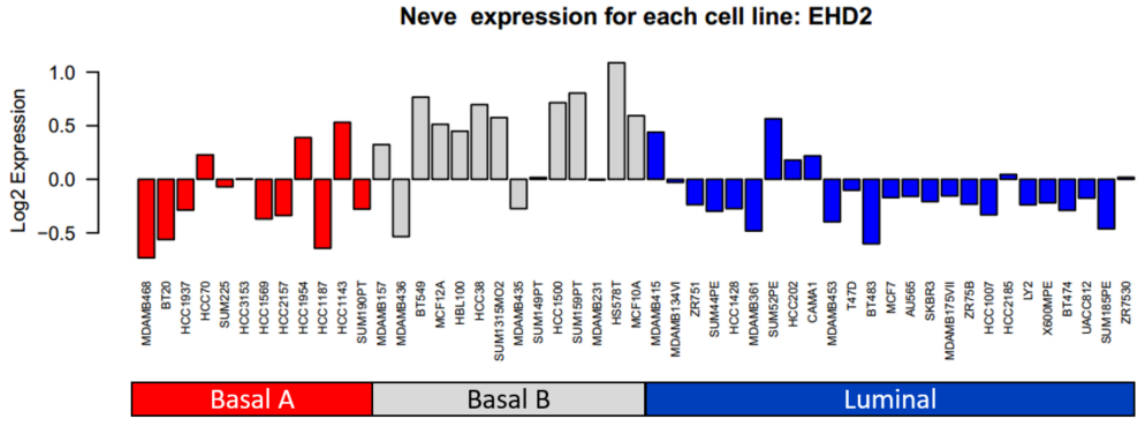
Neve expression for each cell line: EHD2
Log2 Expression
1.0
0.5
0.0
−0.5
MDAMB468 BT20 HCC1937 HCC70 SUM225 HCC3153 HCC1569 HCC2157 HCC1954 HCC1187 HCC1143 SUM190PT MDAMB157 MDAMB436 BT549 MCF12A HBL100 HCC38 SUM1315MO2 MDAMB435 SUM149PT HCC1500 SUM159PT MDAMB231 HS578T MCF10A MDAMB415 MDAMB134VI ZR751 SUM44PE HCC1428 MDAMB361 SUM52PE HCC202 CAMA1 MDAMB453 T47D BT483 MCF7 AU565 SKBR3 MDAMB175VII ZR75B HCC1007 HCC2185 LY2 X600MPE BT474 UACC812 SUM185PE ZR7530
Basal A
Basal B
Luminal

B

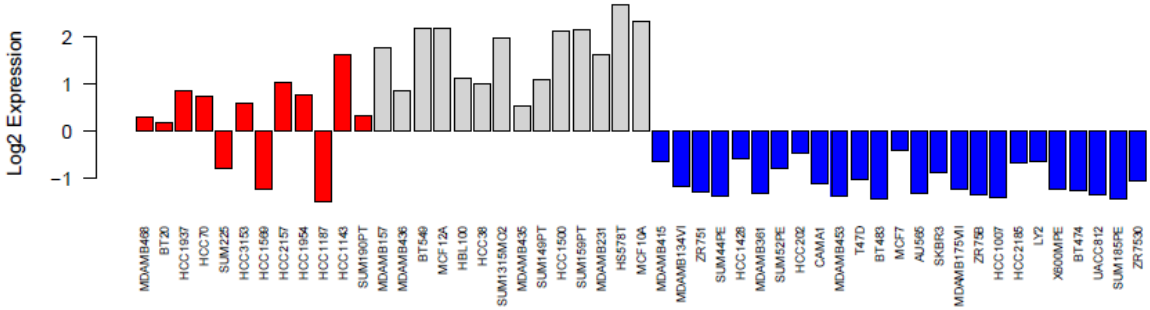
Neve expression for each cell line: MergedGeneSet
Log2 Expression
2
1
0
−1
MDAMB468 BT20 HCC1937 HCC70 SUM225 HCC3153 HCC1569 HCC2157 HCC1954 HCC1187 HCC1143 SUM190PT MDAMB157 MDAMB436 BT549 MCF12A HBL100 HCC38 SUM1315MO2 MDAMB435 SUM149PT HCC1500 SUM159PT MDAMB231 HS578T MCF10A MDAMB415 MDAMB134VI ZR751 SUM44PE HCC1428 MDAMB361 SUM52PE HCC202 CAMA1 MDAMB453 T47D BT483 MCF7 AU565 SKBR3 MDAMB175VII ZR75B HCC1007 HCC2185 LY2 X600MPE BT474 UACC812 SUM185PE ZR7530

Figure 3.7. Cell lines with high EHD2 mRNA expression and high EHD2 and caveolin-1 mRNA expression. a, Relative mRNA expression of EHD2 across individual basal A, basal B, and luminal cell lines. **b,** Relative mRNA expression of EHD2 and caveolin-1 across individual Basal A, Basal B, and Luminal cell lines.

Figure 3.8

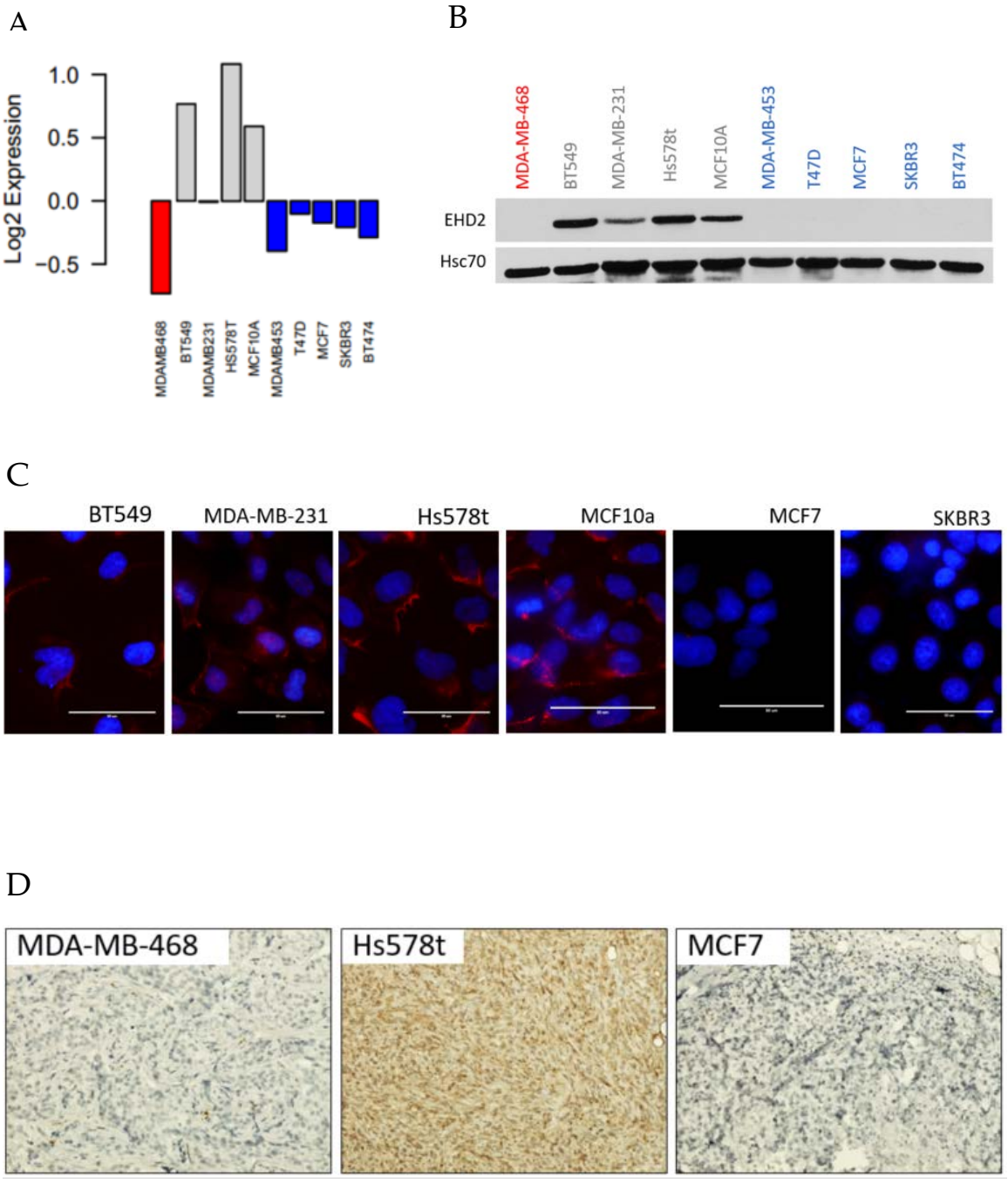
A
Log2 Expression
1.0
0.5
0.0
−0.5
MDAMB468
BT549
MDAMB231
HS578T
MCF10A
MDAMB453
T47D
MCF7
SKBR3
BT474
B
MDA-MB-468
BT549
MDA-MB-231
Hs578t
MCF10A
MDA-MB-453
T47D
MCF7
SKBR3
BT474
EHD2
Hsc70
C
BT549
MDA-MB-231
Hs578t
MCF10a
MCF7
SKBR3
D
MDA-MB-468
Hs578t
MCF7

Figure 3.8. EHD2 mRNA expression correlates with protein expression in breast cancer cell lines. a, EHD2 mRNA is highly expressed primarily within basal-like and triple-negative cell lines. **b,** EHD2 protein is highly expressed within basal-like and triple-negative cell lines. **c,** Immunofluorescence microscopy of EHD2 (red) localizes primarily to the plasma membrane of basal-like and triple-negative cell lines. DAPI (blue) was used to stain the nucleus. Scale bar indicates 50 μm. **d,** immunohistochemical staining of EHD2 in FFPE sections from xenograft tumors shown at 10x magnification.

Figure 3.9

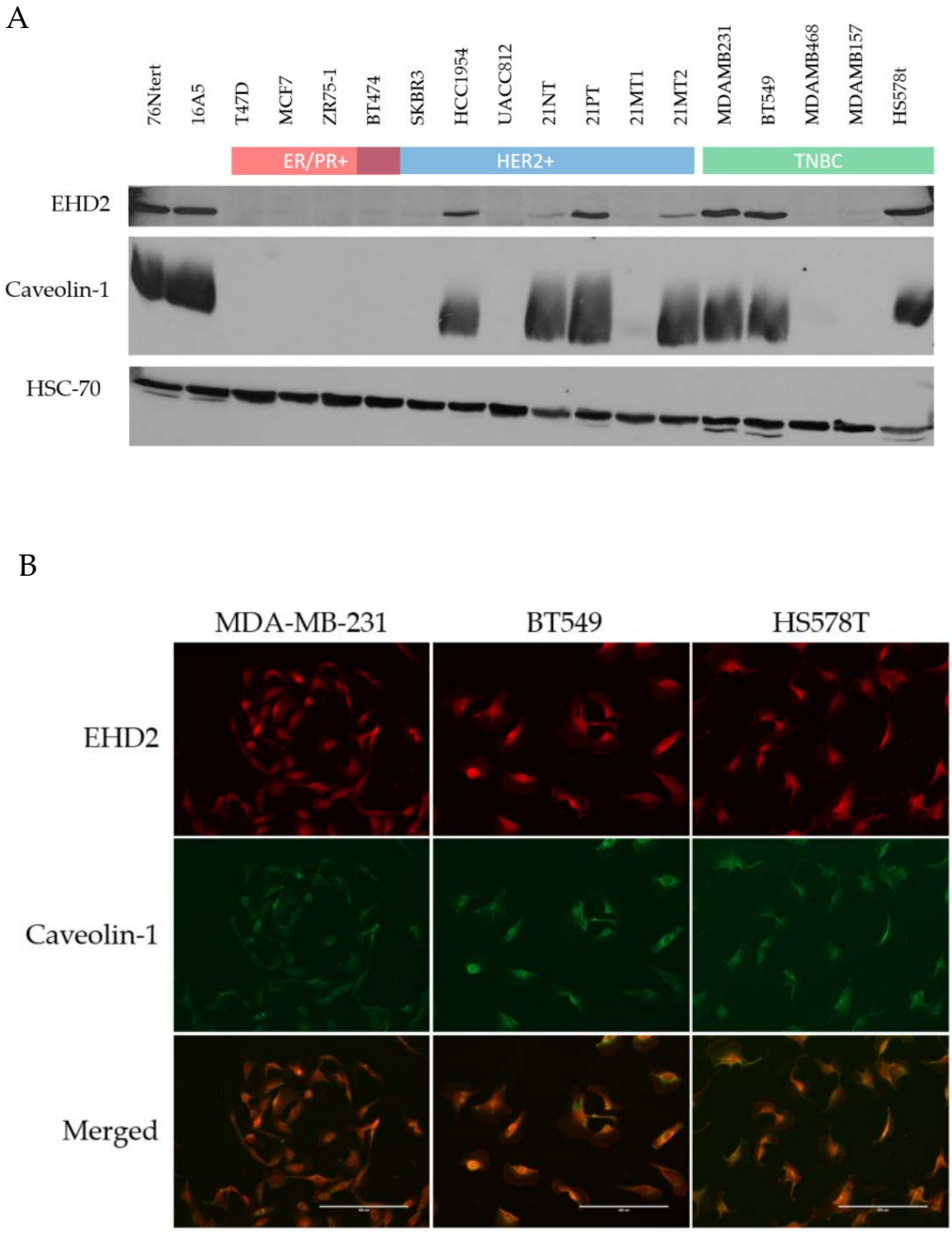
A
76Ntert
16A5
T47D
MCF7
ZR75-1
BT474
SKBR3
HCC1954
UACC812
21NT
21PT
21MT1
21MT2
MDAMB231
BT549
MDAMB468
MDAMB157
HS578t
ER/PR+
HER2+
TNBC
EHD2
Caveolin-1
HSC-70
B
MDA-MB-231
BT549
HS578T
EHD2
Caveolin-1
Merged

Figure 3.9. EHD2 is co-expressed and co-localizes with caveolin-1 in breast cancer cells. a, Western blot analysis of multiple breast cancer cell lines shows that EHD2 is expressed in triple-negative breast cancer (TNBC) and HER2 positive (HER2+) cells expressing caveolin-1. Non-tumorigenic cell lines (76Ntert and 16A5) also express EHD2 and caveolin-1. **b,** Immunofluorescence of anti-EHD2 (red) and anti-caveolin-1 (green) in TNBC cell lines shows co-localization of both proteins. Scale bar indicates 100 μm.

Figure 3.10

A

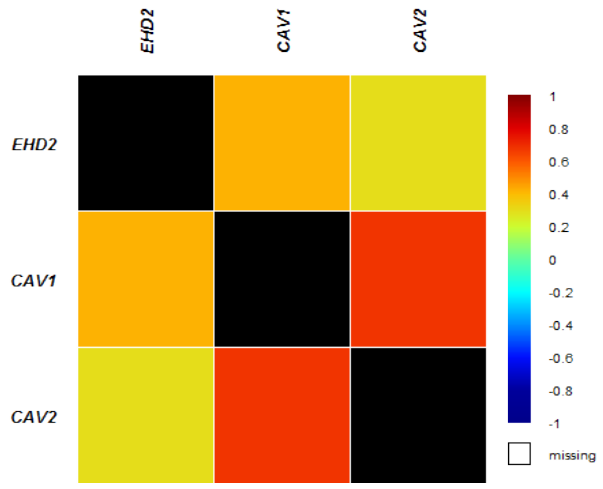

B

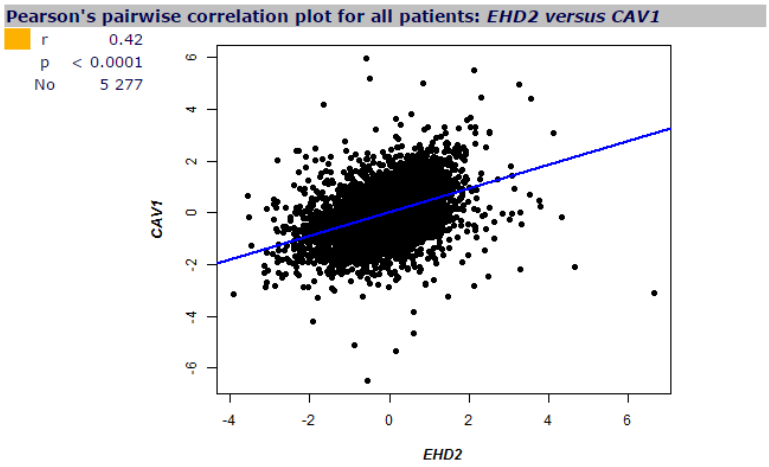

C

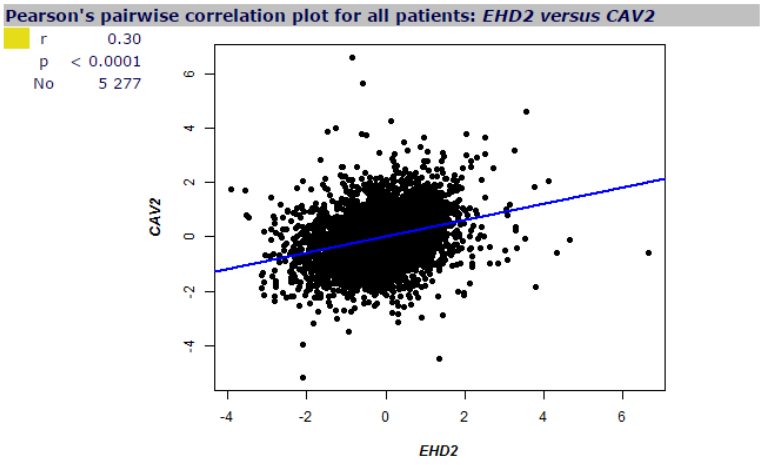

Figure 3.10. EHD2 mRNA expression positively correlates with caveolin-1 and caveolin-2 mRNA expression in human breast cancer. a, Pearson's pairwise correlation heatmap of EHD2, caveolin-1 (CAV1), and caveolin-2 (CAV2) mRNA expression across 5,277 human breast cancer samples. Red hue indicates strong positive correlation. **b,** Pearson's pairwise correlation plot of EHD2 and CAV1 mRNA expression for 5,277 human breast cancer samples. **c,** Pearson's pairwise correlation plot of EHD2 and CAV2 mRNA expression for 5,277 human breast cancer samples. Data obtained from bc-genExMiner.

Figure 3.11

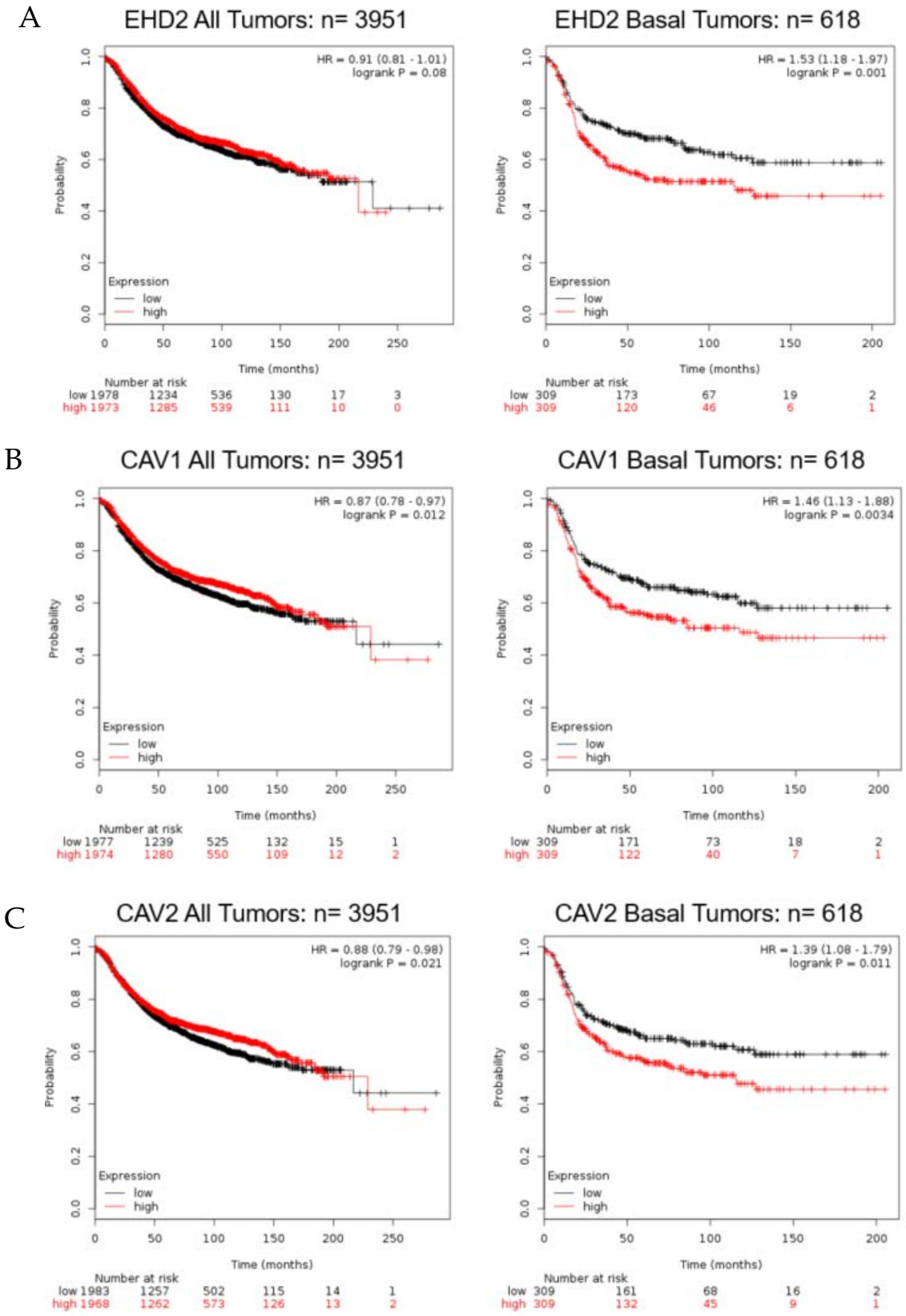
A
EHD2 All Tumors: n= 3951
HR = 0.91 (0.81 - 1.01)
logrank P = 0.08
Probability
Expression
low
high
Time (months)
Number at risk
low 1978 1234 536 130 17 3
high 1973 1285 539 111 10 0
EHD2 Basal Tumors: n= 618
HR = 1.53 (1.18 - 1.97)
logrank P = 0.001
Probability
Expression
low
high
Time (months)
Number at risk
low 309 173 67 19 2
high 309 120 46 6 1
B
CAV1 All Tumors: n= 3951
HR = 0.87 (0.78 - 0.97)
logrank P = 0.012
Probability
Expression
low
high
Time (months)
Number at risk
low 1977 1239 525 132 15 1
high 1974 1280 550 109 12 2
CAV1 Basal Tumors: n= 618
HR = 1.46 (1.13 - 1.88)
logrank P = 0.0034
Probability
Expression
low
high
Time (months)
Number at risk
low 309 171 73 18 2
high 309 122 40 7 1
C
CAV2 All Tumors: n= 3951
HR = 0.88 (0.79 - 0.98)
logrank P = 0.021
Probability
Expression
low
high
Time (months)
Number at risk
low 1983 1257 502 115 14 1
high 1968 1262 573 126 13 2
CAV2 Basal Tumors: n= 618
HR = 1.39 (1.08 - 1.79)
logrank P = 0.011
Probability
Expression
low
high
Time (months)
Number at risk
low 309 161 68 16 2
high 309 132 45 9 1

Figure 3.11. EHD2 and caveolin mRNA expression is associated with lower probability of survival in basal breast cancer. a, Kaplan-Meier survival curve for all tumors (left panel) and basal tumors (right panel) for low EHD2 mRNA (black) and high EHD2 mRNA (red) **b,** Kaplan-Meier survival curve for all tumors (left panel) and basal tumors (right panel) for low CAV1 mRNA (black) and high CAV1 mRNA (red). **c,** Kaplan-Meier survival curve for all tumors (left panel) and basal tumors (right panel) for low CAV2 mRNA (black) and high CAV2 mRNA (red). All data obtained from kmplot.com.

Figure 3.12

A

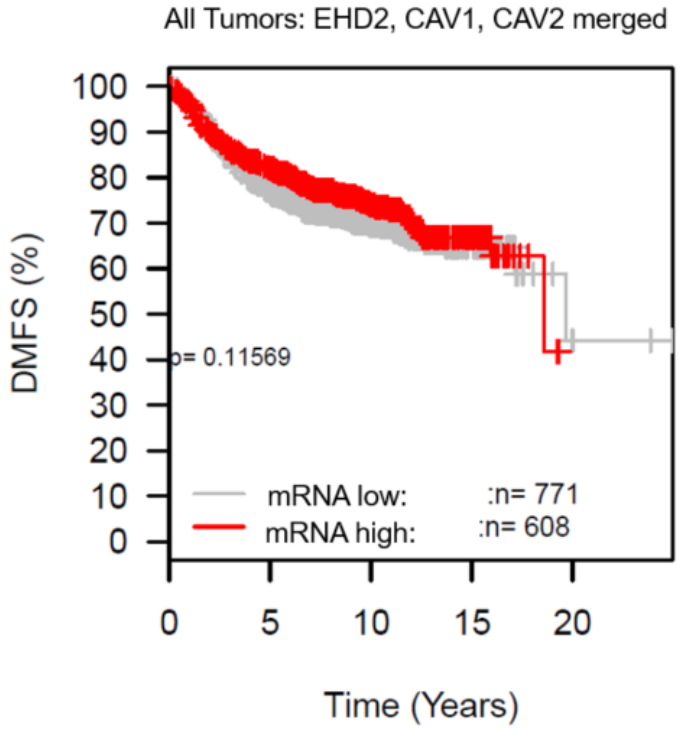

B

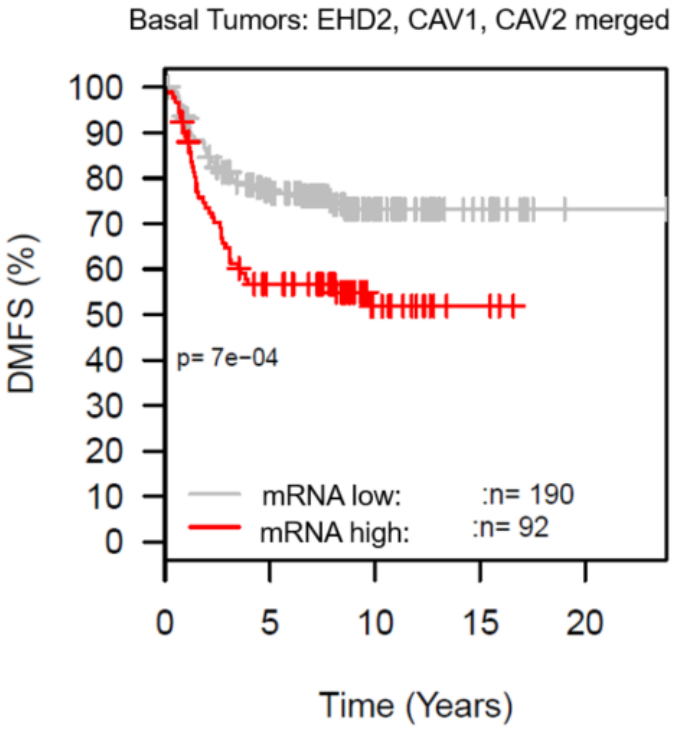

Figure 3.12. Combined EHD2, caveolin-1, and caveolin-2 mRNA expression is associated with lower probability of survival in basal breast cancer. a, Kaplan-Meier survival curve for distant metastasis-free survival (DMFS) percentage in all tumors for low EHD2 mRNA (gray) and high EHD2 mRNA (red) **b,** Kaplan-Meier survival curve for DMFS percentage in basal tumors for low EHD2 mRNA (gray) and high EHD2 mRNA (red)

Figure 3.13

A

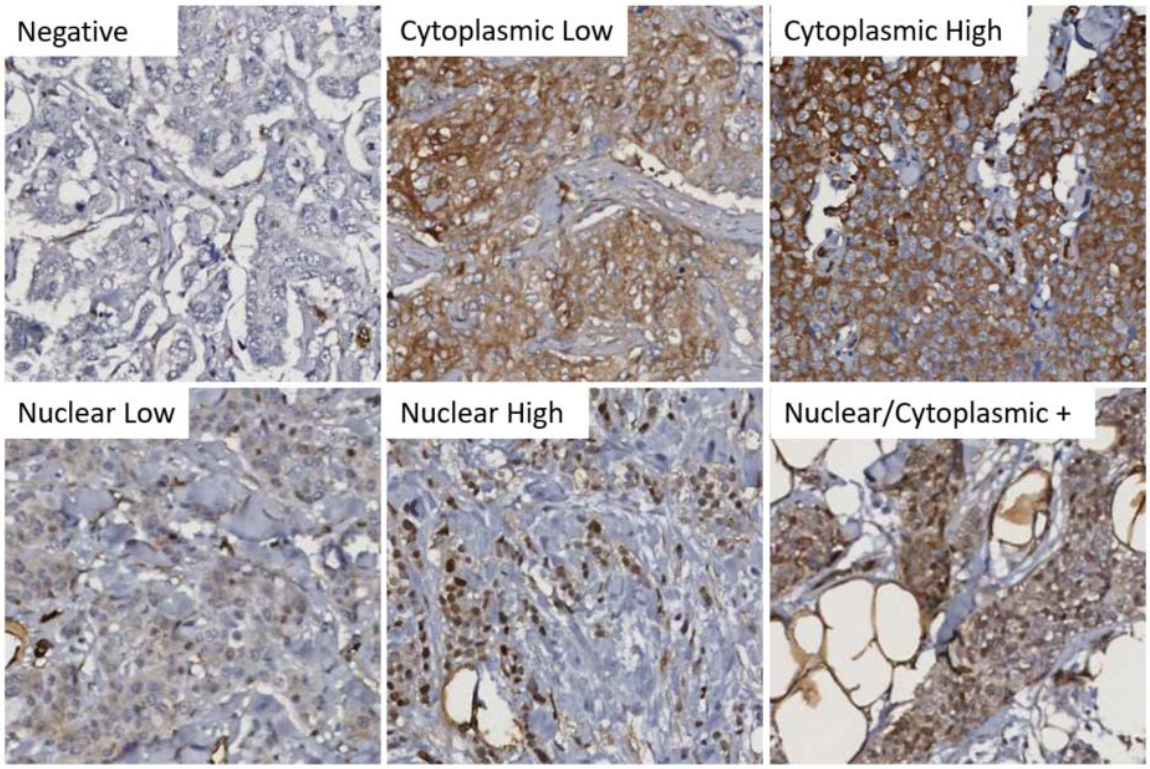

B

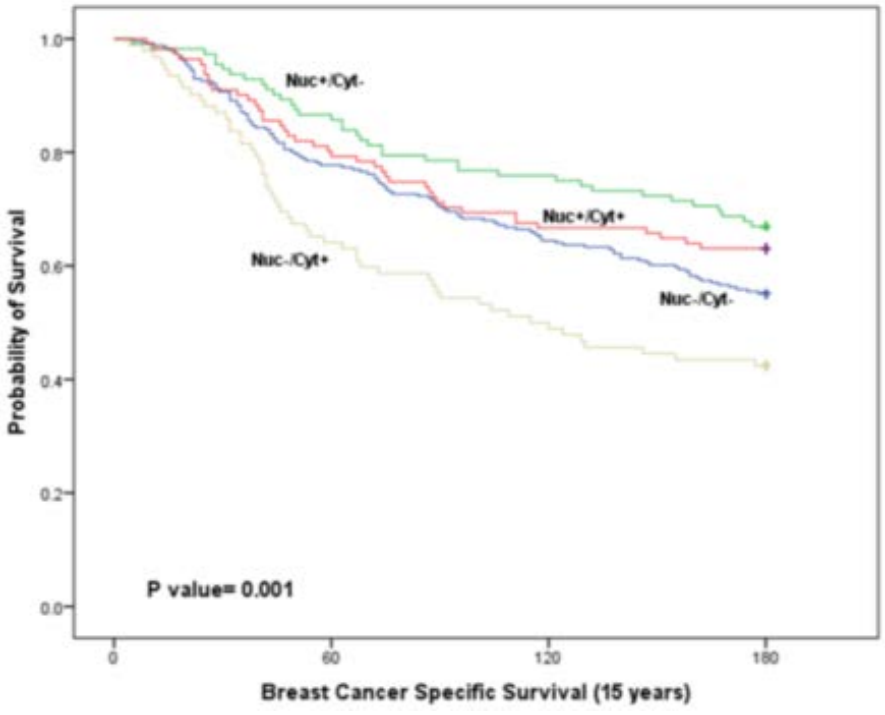

Figure 3.13. EHD2 protein expression and localization determines survival probability across a cohort of 840 human breast cancer tissue samples. a, Representative images (20x magnification) of EHD2 expression levels and nuclear/cytoplasmic localization throughout a tumor microarray of 840 human breast cancer samples. Immunohistochemistry staining for anti-EHD2 was performed and sent for pathologist scoring to Nottingham, U.K. **b,** Kaplan-Meier survival curve for breast cancer specific survival (BCSS) probability in all tumors scored for nuclear positive and cytoplasmic negative (green), nuclear positive and cytoplasmic positive (red), nuclear negative and cytoplasmic negative (blue), and nuclear negative and cytoplasmic positive (gray) expression of EHD2 throughout 840 human breast cancer samples.

Figure 3.14

A

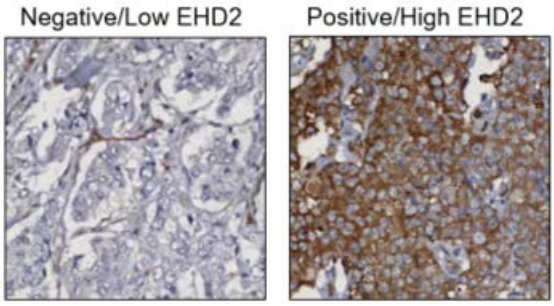

B

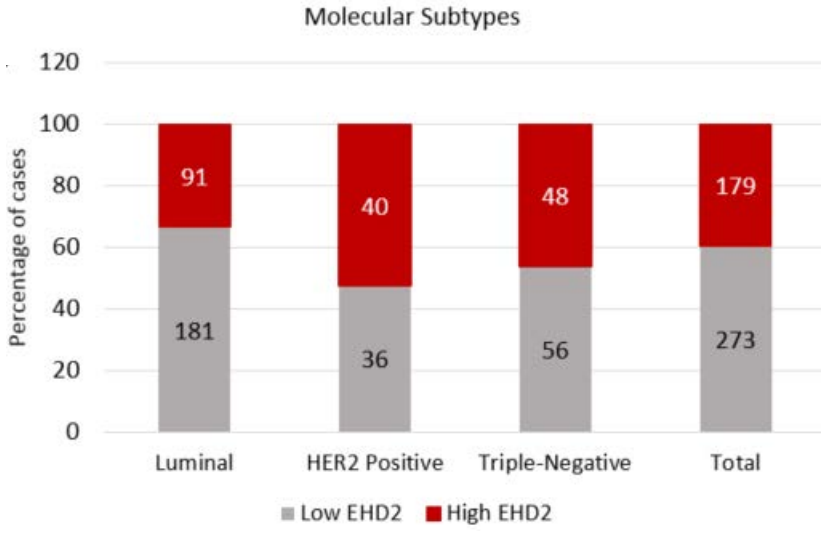

C

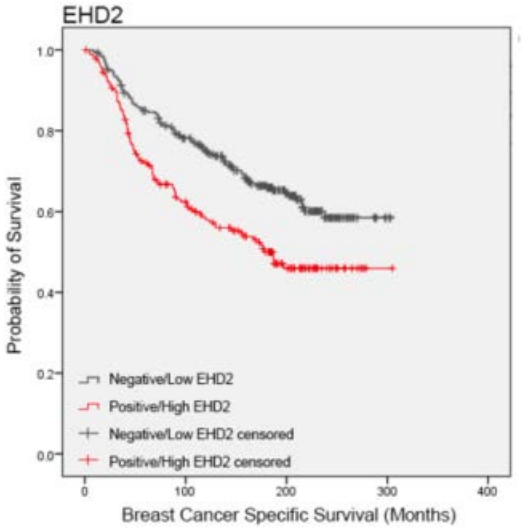

Figure 3.14. Cytoplasmic EHD2 expression is associated with TNBC and lower probability of survival across a cohort of 840 human breast cancer samples. a, Representative images (20x magnification) of negative/low cytoplasmic (left) and positive/high cytoplasmic EHD2 expression levels throughout a tumor microarray of 840 human breast cancer samples. Immunohistochemistry staining for anti-EHD2 was performed and sent for pathologist scoring to Nottingham, U.K. **b,** percentage of negative/low (gray) and positive/high cytoplasmic EHD2 samples in luminal, HER2+, TN, and all tumors throughout a tumor microarray of 840 human breast cancer samples. **c,** Kaplan-Meier survival curve for Breast Cancer Specific Survival (BCSS) probability in all tumors scored for nuclear/low (black) and positive/high cytoplasmic expression of EHD2 throughout 840 human breast cancer samples.

Figure 3.15

A

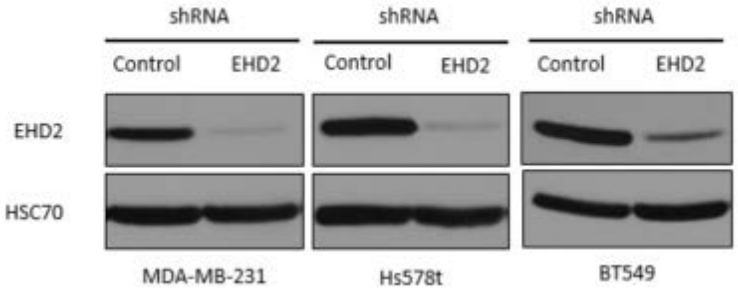

B

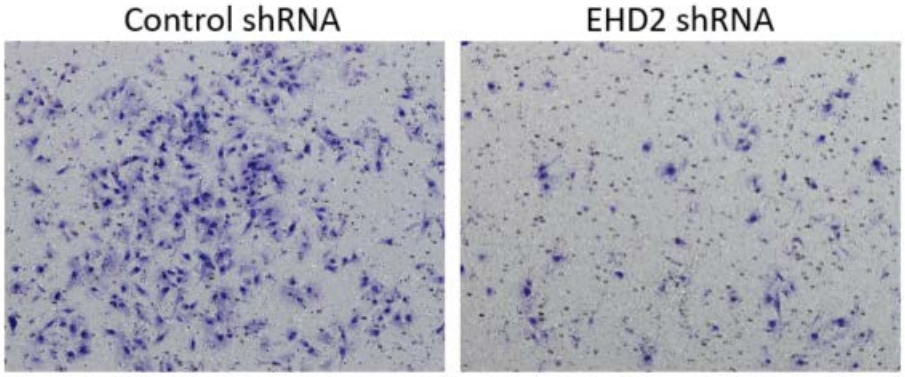

C

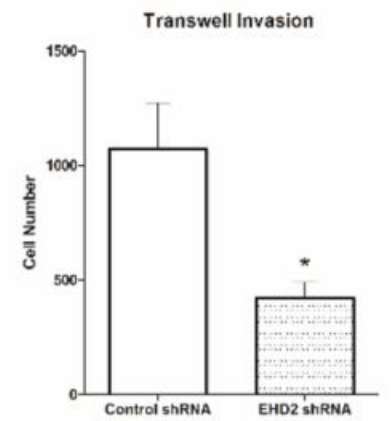

Figure 3.15. EHD2 shRNA knockdown reduces invasiveness of TNBC cell lines *in vitro*. a, Western blot analysis of EHD2 expression by MDA-MB-231, BT549, and Hs578t cells after retroviral transduction with control or EHD2 shRNA. HSC70 was used as a loading control. **b,** Representative image of transwell invasion extent for TNBC cells with control or EHD2 shRNA. Cells were seeded in the top chamber and allowed to invade through a Matrigel-coated membrane for 22 hours. **c,** Quantification of invasiveness for TNBC cells with control or EHD2 shRNA after 22 hours. Cells were fixed in methanol, stained with HEMA solution, and counted per high power field. * = $p < 0.05$

Figure 3.16

A

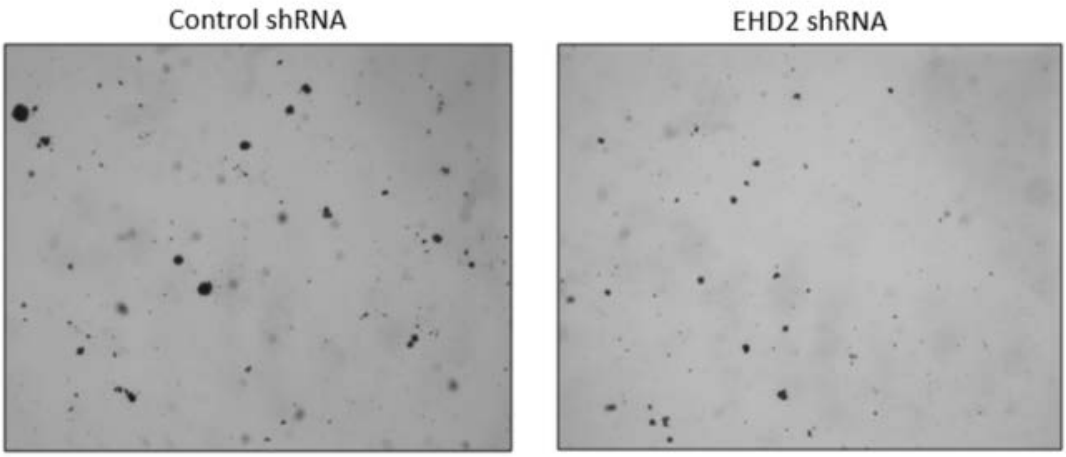

B

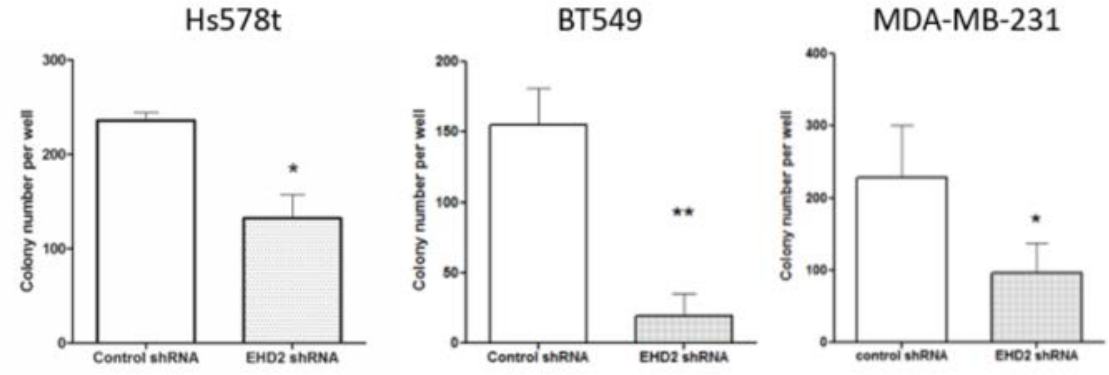

Figure 3.16. EHD2 shRNA knockdown reduces growth of soft-agar colonies for TNBC cell lines. a, Representative image of soft-agar colonies for TNBC cells with control or EHD2 shRNA. **b,** Quantification of the number of soft-agar colonies for TNBC cells with control or EHD2 shRNA after two weeks. Cells were fixed in methanol, stained with crystal violet, and counted per well. (error bar indicates s.e.m., n=3 experiments, * indicates $P<0.05$, ** indicates $P<0.01$).

Figure 3.17

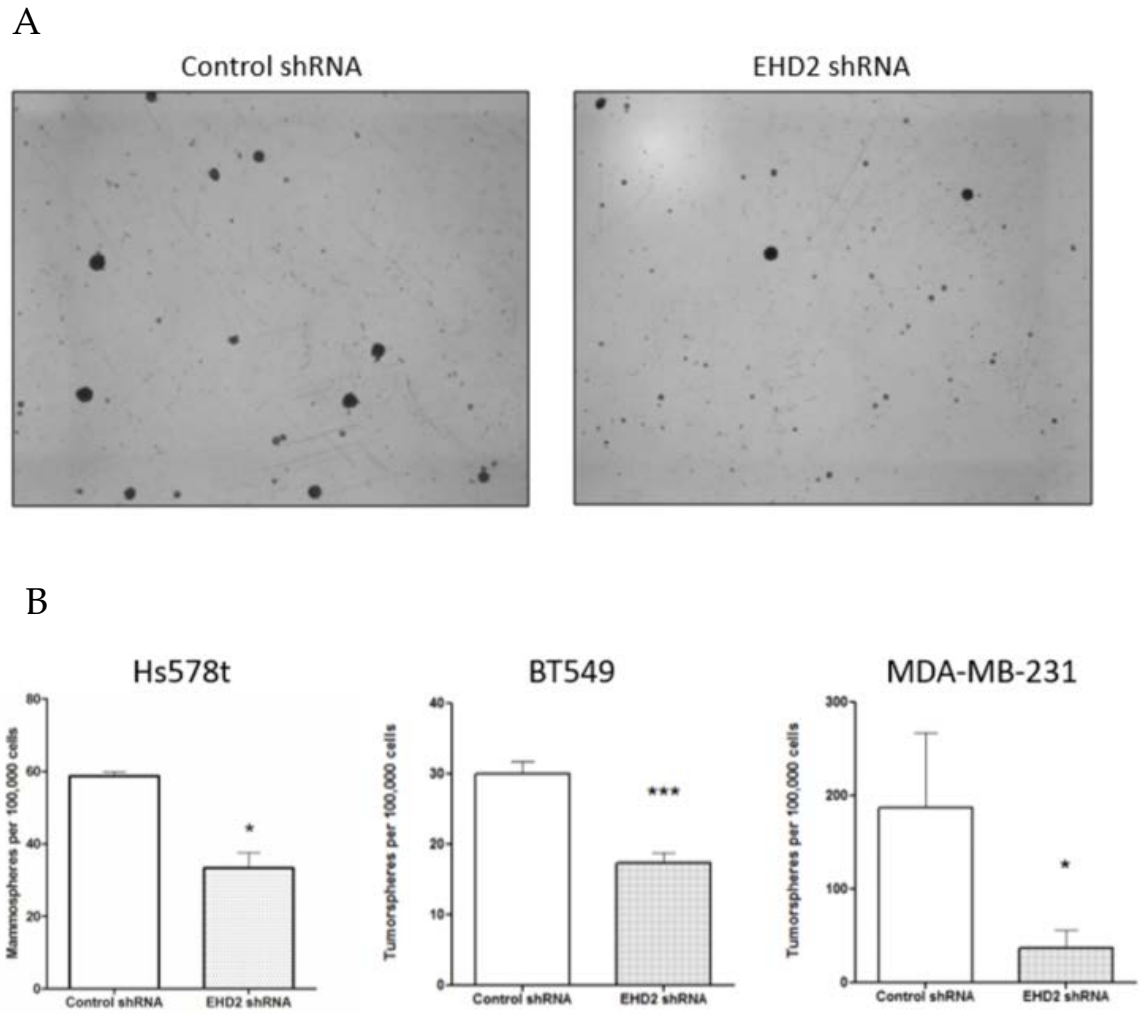
A
Control shRNA
EHD2 shRNA
B
Hs578t
Mammospheres per 100,000 cells
Control shRNA
EHD2 shRNA
BT549
Tumorspheres per 100,000 cells
***
Control shRNA
EHD2 shRNA
MDA-MB-231
Tumorspheres per 100,000 cells
*
Control shRNA
EHD2 shRNA

Figure 3.17. EHD2 shRNA knockdown reduces tumorsphere formation in TNBC cell lines. a, Representative image of tumorspheres for TNBC cells with control or EHD2 shRNA. **b,** Quantification of the number of tumorsphers for TNBC cells with control or EHD2 shRNA after one week. Tumorspheres over 40 μm in diameter were counted per well. (error bar indicates s.e.m., n=3 experiments, * indicates $P<0.05$, *** indicates $P<0.005$).

Figure 3.18

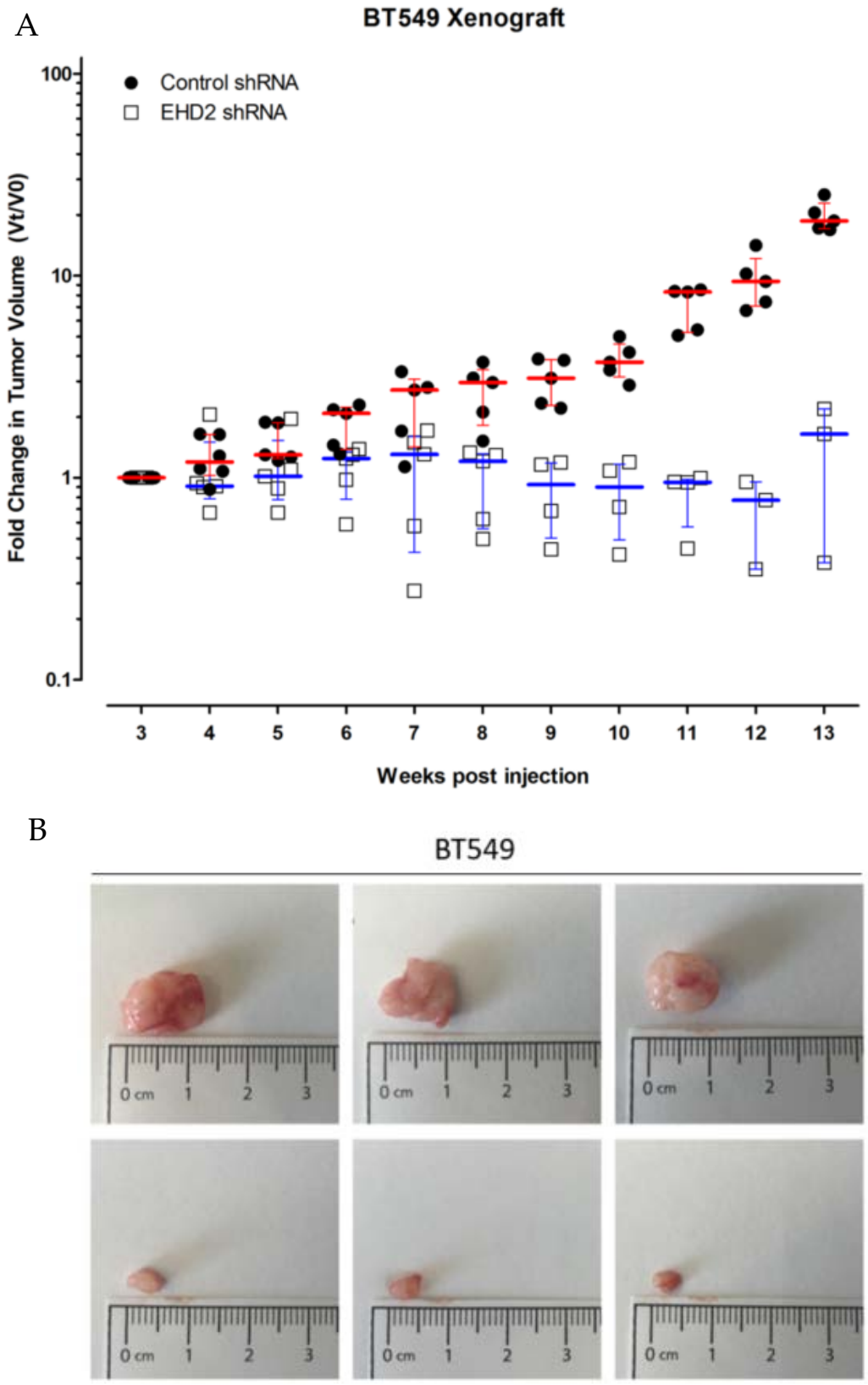
A
BT549 Xenograft
Control shRNA
EHD2 shRNA
Fold Change in Tumor Volume (Vt/V0)
100
10
1
0.1
3
4
5
6
7
8
9
10
11
12
13
Weeks post injection
B
BT549
0 cm
1
2
3

Figure 3.18. EHD2 shRNA-mediated knockdown reduces tumorigenicity of BT549 cells *in vivo*. Reduced fold change in tumor volumes in fat pads of athymic mice injected with EHD2 shRNA cells compared to control shRNA cells. **a,** $5x10^6$ BT549 cells with control shRNA (filled dots) or EHD2 shRNA (open squares) were injected into 4-week old aythmic mice, and followed for 13 weeks to estimate fold change in tumor volume after injection (each dot or square represents an individual tumor). Each data point is the volume of a single tumor (lines indicate median, error bars indicate interquartile range). **b,** Representative images of BT549 xenograft tumors with control shRNA (top row) or EHD2 shRNA (bottom row) from athymic mice at the experiment endpoint. Tumors shown are representative of the median from each group.

Figure 3.19

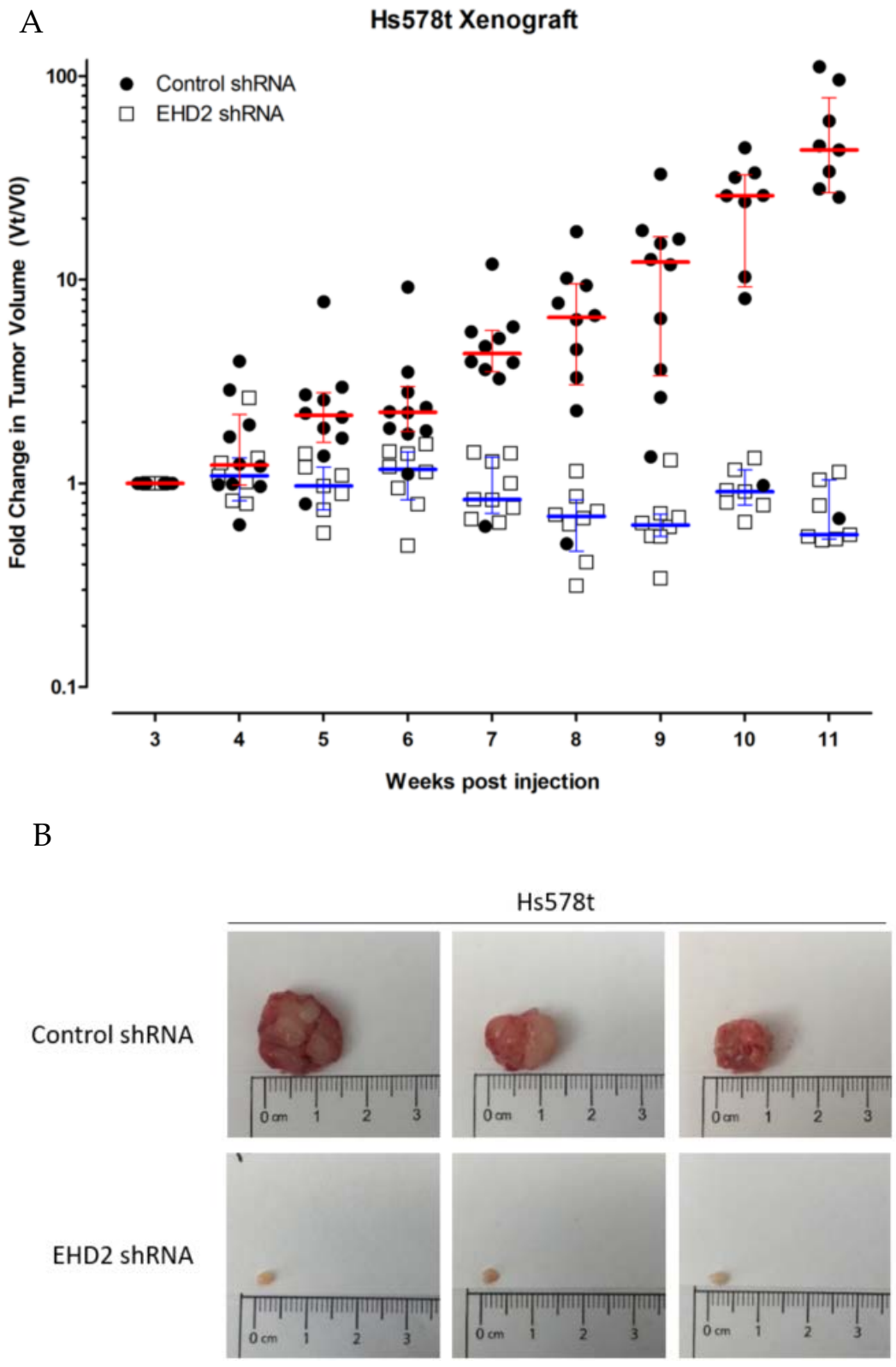
A
Hs578t Xenograft
Control shRNA
EHD2 shRNA
Fold Change in Tumor Volume (Vt/V0)
100
10
1
0.1
3
4
5
6
7
8
9
10
11
Weeks post injection
B
Hs578t
Control shRNA
EHD2 shRNA
0 cm
1
2
3

Figure 3.19. EHD2 shRNA-mediated knockdown reduces tumorigenicity of HS578t cells *in vivo*. Reduced fold change in tumor volumes in fat pads of athymic mice injected with EHD2 shRNA cells compared to control shRNA cells. **a,** $5x10^6$ Hs578t cells with control shRNA (filled dots) or EHD2 shRNA (open squares) were injected into 4-week old aythmic mice, and followed for 11 weeks to estimate fold change in tumor volume after injection (each dot or square represents an individual tumor). **b,** Representative images of Hs578t xenograft tumors with control shRNA (top row) or EHD2 shRNA (bottom row) from athymic mice at the experiment endpoint. Tumors shown are representative of the median from each group.

Figure 3.20

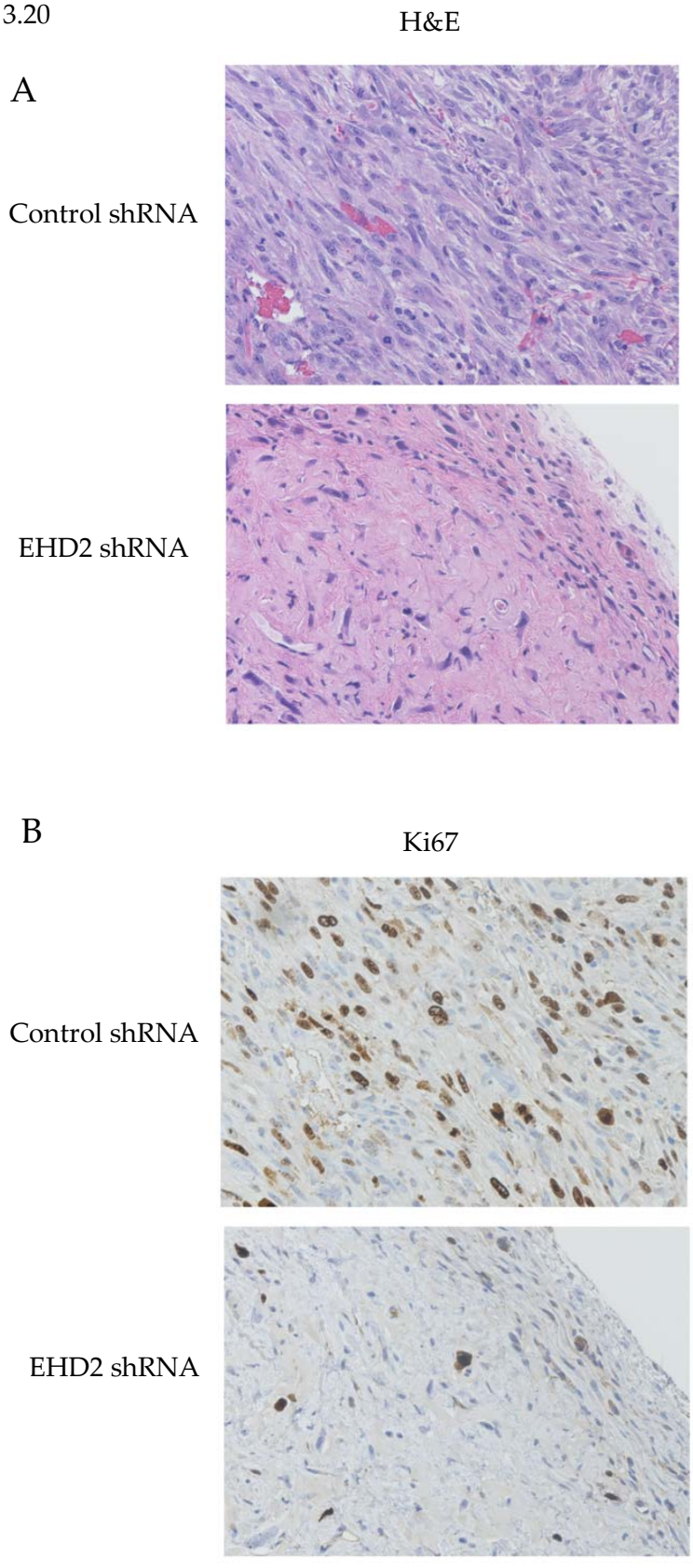
H&E
A
Control shRNA
EHD2 shRNA
B
Ki67
Control shRNA
EHD2 shRNA

Figure 3.20. EHD2 shRNA-mediated knockdown alters tumor cell morphology and reduces proliferation of TNBC cells *in vivo*. a, Representative images of H&E staining of xenograft tumor sections from HS578t cells with control or EHD2 shRNA to demonstrate tumor cell morphology. **b,** Representative images (20x magnification) of Ki67 staining of xenograft tumor sections from HS578t cells with control or EHD2 shRNA.

F 3.21
A

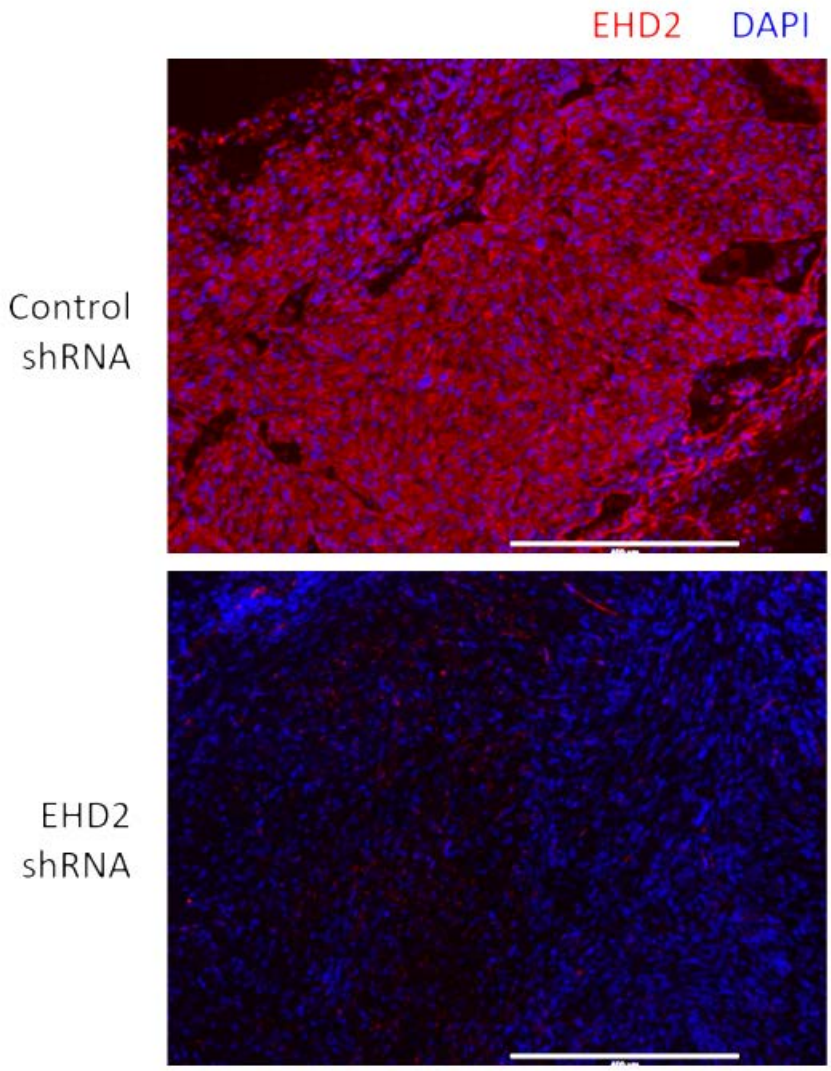

Figure 3.21. Validation of EHD2 shRNA-mediated knockdown in TNBC cells *in vivo*. **a,** Representative images of xenograft tumor sections from HS578t cells with control or EHD2 shRNA stained with anti-EHD2 (red) and DAPI (blue). Scale bars represent 200 μm.

Figure 3.22

A

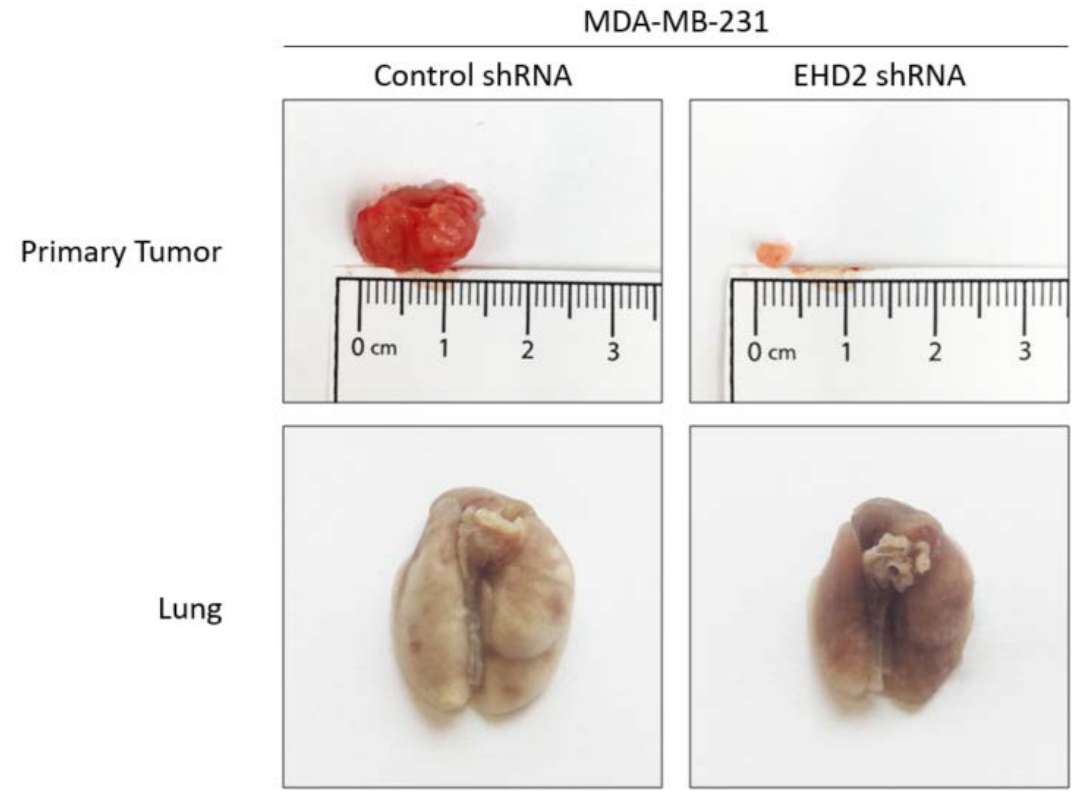

Tumors Formed	6/6	4/6
Lung Metastasis	5/6	1/4

Figure 3.22. EHD2-shRNA mediated knockdown reduces metastatic potential of TNBC cells *in vivo*. a, Representative images of primary xenograft tumors and lungs from mice injected with 5 x 10^6 MDA-MB-231 cells with control or EHD2 shRNA. Tumors and lungs were harvested 13 weeks after injection of MDA-MB-231 cells. Lung metastases were visually counted for each group.

Figure 3.23

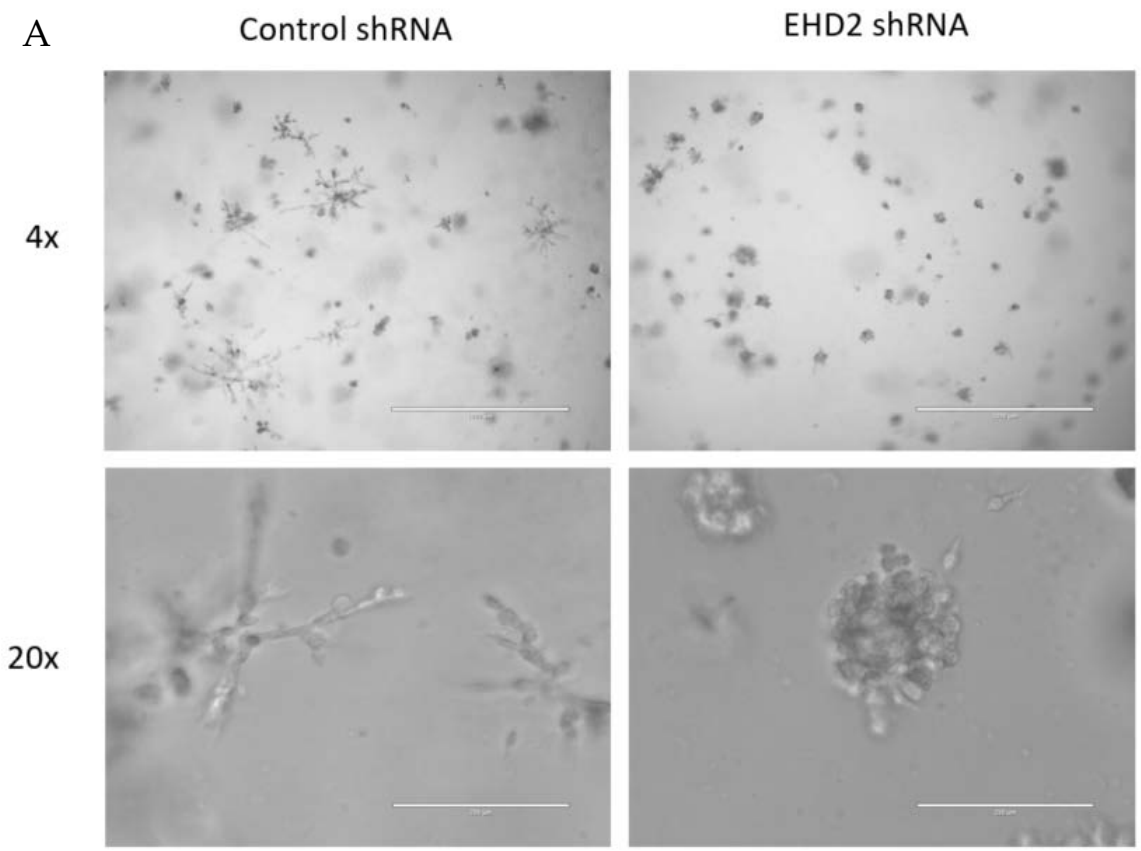
A
Control shRNA
EHD2 shRNA
4x
20x

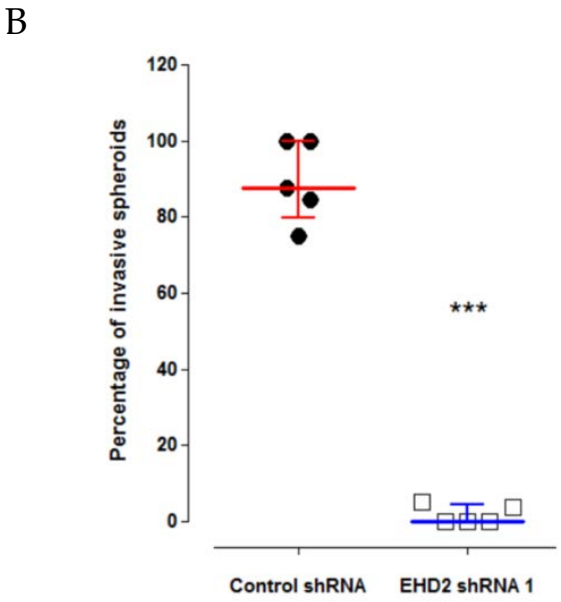
B
Percentage of invasive spheroids
120
100
80
60
40
20
0
***
Control shRNA
EHD2 shRNA 1

Figure 3.23. EHD2 knockdown reduces invasive growth of MDA-MB-231 cells in Matrigel culture. a, MDA-MB-231 cells were plated as single cells in 100% Matrigel and allowed to grow for 7 days in culture. Cell invasion through Matrigel was imaged at day 7. Scale bar represents 1000 μm. Magnified image scale bar represents 200 μm. **b,** The percentage of invasive spheroids per field was quantified for MDA-MB-231 cells with control or EHD2 shRNA (Each dot represents a field, *** indicates $p<0.001$).

Figure 3.24

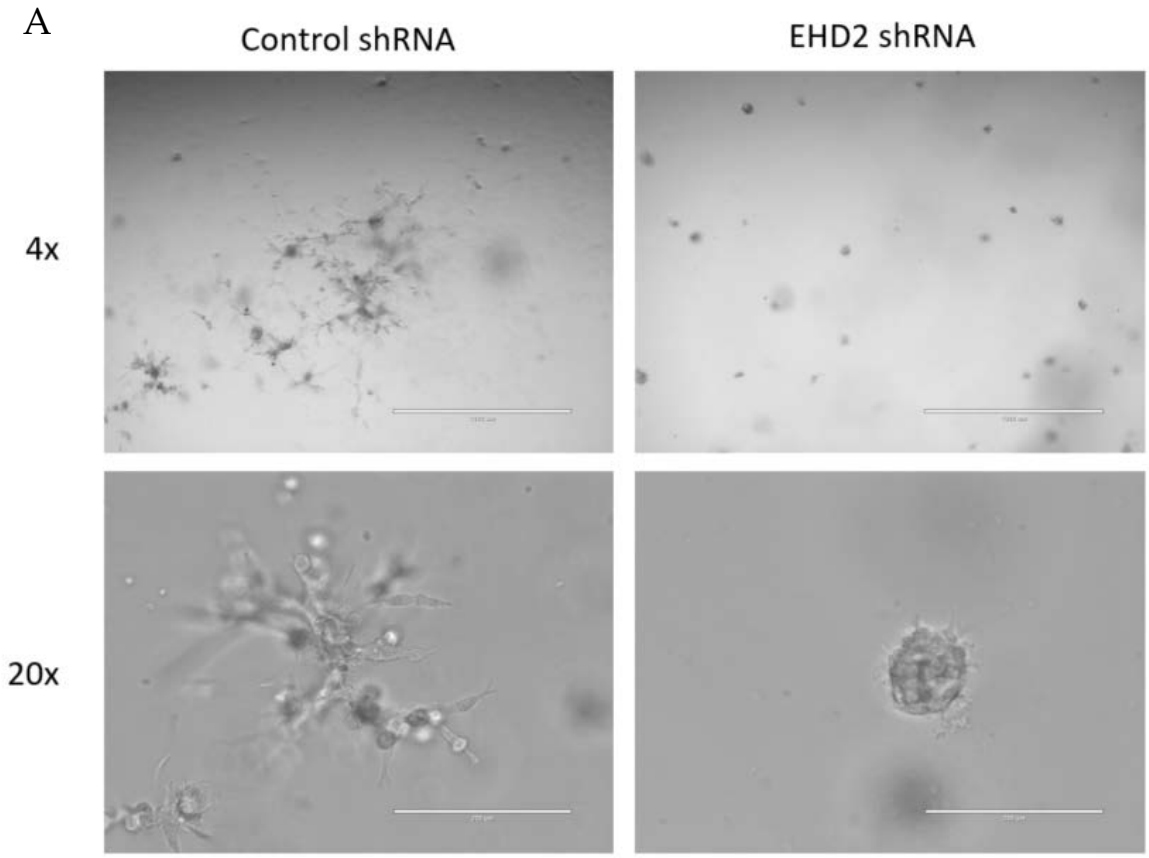
A
Control shRNA
EHD2 shRNA
4x
20x

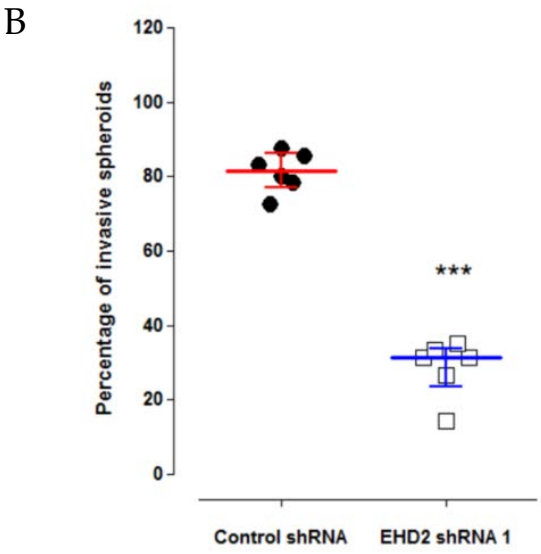
B
Percentage of invasive spheroids
120
100
80
60
40
20
0
***
Control shRNA
EHD2 shRNA 1

Figure 3.24. EHD2 knockdown reduces invasive growth of BT549 cells in Matrigel culture. a, BT549 cells were plated as single cells in 100% Matrigel and allowed to grow for 7 days in culture. Cell invasion through Matrigel was imaged at day 7. Scale bar represents 1000 μm. Magnified image scale bar represents 200 μm. **b,** The percentage of invasive spheroids per field was quantified for BT549 cells with control or EHD2 shRNA (Each dot represents a field, *** indicates $p<0.001$).

Figure 3.25

A

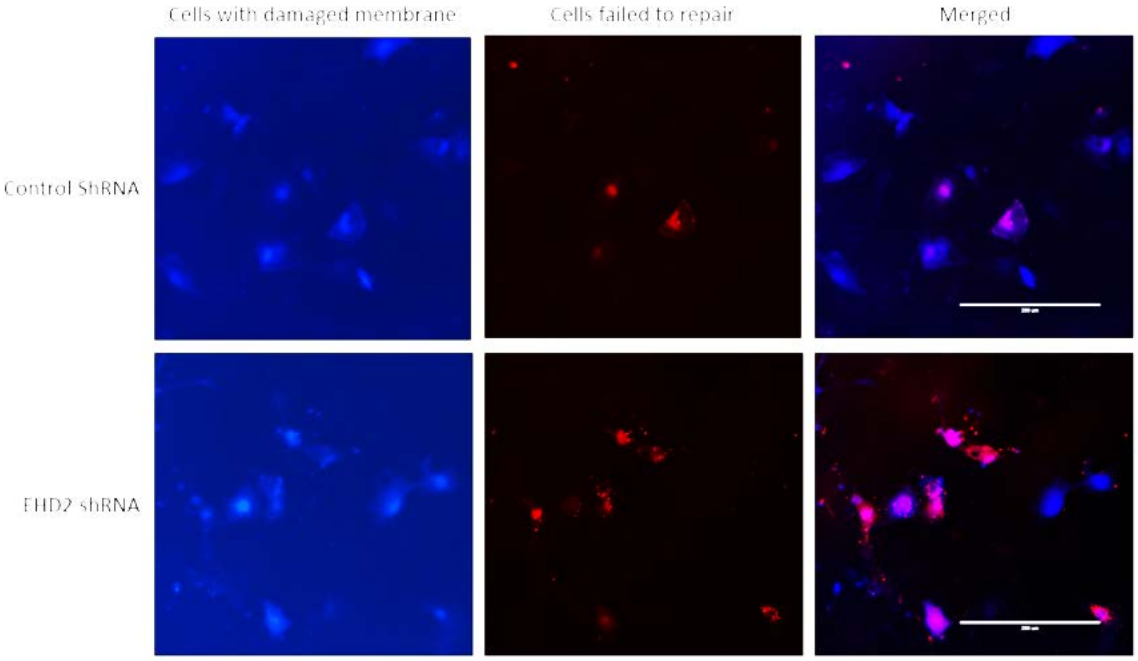

B

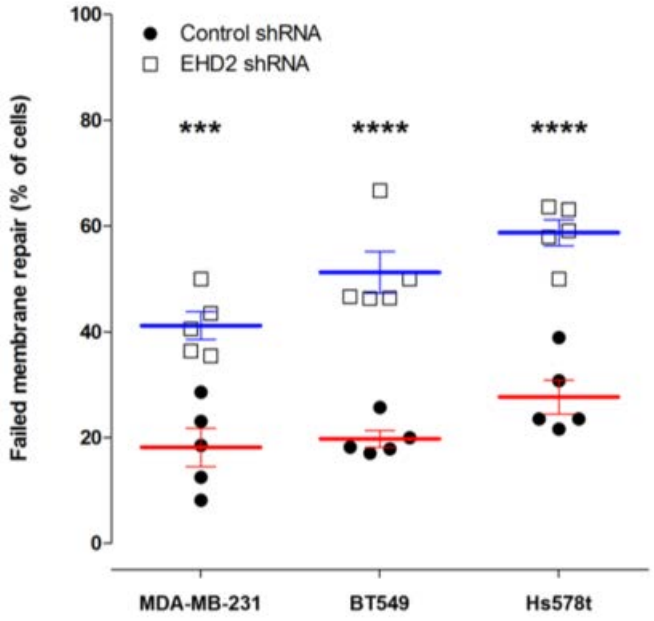

Figure 3.25. EHD2 knockdown reduces TNBC cell membrane repair ability *in vitro*. a, TNBC cells with control or EHD2 shRNA were incubated with CascadeBlue-conjugated dextran to label cells with damaged membranes via bulk membrane wounding from glass bead rolling. Five minutes after wounding, cells were rinsed and incubated with TRITC-conjugated dextran to label cells that failed to repair. Hs578t cells are shown as representative for the effects of EHD2 knockdown on membrane repair. Scale bar represents 200 μm. **b,** The number of wounded cells with repaired membranes were compared to the number cells with failed membrane repair and represented as a percentage for MDA-MB-231, BT549, and Hs578t cells. Quantification represents three independent experiments. P<0.001 (***), p<0.0001 (****)

III.4 Discussion

In this chapter, we have shown that EHD2 is a novel marker and important regulator of membrane repair and tumorigenicity in triple-negative breast cancer. We first demonstrated that EHD2 is exclusively expressed within the myoepithelial/basal layer of the murine and human mammary duct. We used a newly developed EHD2$^{-/-}$ mouse strain to validate our EHD2 antibody specificity and confirmed the exclusive expression of EHD2 throughout the major timepoints of mammary gland development. In accordance with its role as an essential regulator of caveolae dynamics, EHD2 localization in the mammary duct was consistent with the known expression pattern of the caveolae structural proteins, caveolin-1 and caveolin-2 (Pinilla et al. 2006; Savage et al. 2008). While EHD2 knockout in mice did not result in an obvious phenotype, we did observe a distinct increase of EHD1 expression within the myoepithelial/basal layer of the mammary duct. This suggests that EHD1 may serve a functionally redundant role to EHD2 within these compartments. Interestingly, other tissues of EHD2$^{-/-}$ mice did not exhibit similar increases in EHD1 expression (data not shown), and shRNA-mediated knockdown of EHD2 in mammary epithelial cells and breast cancer cells did not elicit increased EHD1 protein expression. This suggests that the observed increase of EHD1 in EHD2$^{-/-}$ mice may be regulated via genomic mechanisms instead of through protein expression levels. More research into this phenomenon would be interesting since the members of the EHD family of proteins have many overlapping cellular functions (George et al. 2007; Cai et al. 2013). Regardless, this compartment-specific redundancy

role of EHDs has been observed previously in other EHD knockout mice (Sengupta et al. 2009; George et al. 2011).

Our findings in normal mammary gland tissue were paralleled by the expression of EHD2 in breast cancer cell line subtypes. Most triple-negative breast cancers are often referred to as basal-like breast cancer because they have a gene expression profile similar to the myoepithelial/basal layer of the mammary duct (Savage et al. 2007; Charafe-Jauffret et al. 2006; Jacquemier et al. 2005; Neve et al. 2006; Chin et al. 2006). Our initialing screening of 24 breast cancer cell lines demonstrated that EHD2 protein expression levels were indeed present in basal-like cells and mostly absent in luminal and HER2-positive breast cancer lines. These results were further validated by using a publicly available breast cancer cell line expression database (Ringnér et al. 2011) based on gene expression data and molecular subtype classifications that were previously described (Neve et al. 2006). Moreover, EHD2 mRNA expression was positively correlated with both caveolin-1 and caveolin-2 mRNA, and was primarily expressed within the highly-metastatic basal B molecular subtype.

To expand our use of the publicly-available breast cancer gene expression databases, we showed that EHD2 mRNA expression correlated with EHD2 protein expression in a select set of breast cancer cell lines both *in vitro* and *in vivo*. Importantly, we also presented the novel finding that EHD2 and caveolin-1 protein expression was co-expressed and co-localized nearly perfect throughout our selected breast cancer cell lines. The co-localization of caveolin-1 and EHD2 in TNBC cell lines was predominantly

in the rear of motile cells *in vitro.* While the caveolin-1 localization was consistent with what has been shown for other cell systems (Masuelli et al. 2012; H. Yang et al. 2016), there was a fraction of EHD2 that was localized near the cell front and not co-localized with caveolin-1. This suggests that EHD2 is serving a role at the leading edge of motile TNBC cells that is independent of any regulatory roles involving caveolae. However, this could also be a misinterpretation since caveolae can also exist in a flattened state (Nassoy and Lamaze 2012; Senju and Suetsugu 2016) and the rear of the cell may simply represent a more concentrated pool of caveolae. This question could be answered in the future with additional imaging experiments using electron microscopy (Sinha et al. 2011).

Our findings also demonstrated that EHD2 mRNA was positively correlated with caveolin-1 and caveolin-2 mRNA expression in human breast cancer samples. While EHD2 mRNA expression was not associated with any significant difference in survival probability across all breast tumor subtypes, we did find that high EHD2 mRNA expression was significantly associated with lower survival probability in patients with basal tumors. Caveolin-1 and caveolin-2 mRNA expression analysis yielded similar results, once again confirming the close association between EHD2 and the structural proteins of caveolae in TNBC. It is important to note that we also observe high EHD2 expression within the stromal compartment of the mammary gland, mainly adipocytes and endothelial cells. This could skew EHD2 mRNA expression levels if the samples weren't dissected carefully or analyzed via a process such as laser capture microdissection (Braakman et al. 2017). However, given the similar survival probability

profiles of caveolin-1 and caveolin-2 and the fact that they are expressed in the same stromal compartments as EHD2, we can assume that the results from the mRNA expression database are an accurate representation of tumor expression. This is supported by research indicating that low stromal caveolin-1 expression is associated with a lower probability of survival in breast cancer (Qian et al. 2011; Goetz et al. 2011). Therefore, we can presume that any lower probability of survival from high caveolin-1 mRNA expression stems from tumor expression rather than stromal expression.

We followed up our findings from the mRNA expression database by validating EHD2 protein expression in TNBC in a well-annotated TMA of 840 breast cancer samples. Interestingly, we found that EHD2 protein localization within tumor samples influence survival probability and varied by subtype. Although cytoplasmic EHD2 expression was consistent with our mRNA data and associated with TNBC and lower probability of survival, EHD2 expression in the nucleus was associated with luminal subtypes of breast cancer and a higher probability of survival. This nuclear expression of EHD2 could explain the discrepancies we observed regarding EHD2 mRNA expression and survival probability. Specifically, nuclear expression of EHD2 could be the reason why high EHD2 mRNA expression does not show a significant difference in survival across all breast tumor subtypes. It is also possible that our observations of nuclear EHD2 are simply an artifact of sample preparation through immunohistochemistry. Future experiments to isolate cytoplasmic and nuclear fractions of breast cancer cells could help validate our IHC findings. Still, EHD2 does have a nuclear localization sequence and has been shown to traffic to the nucleus (Pekar et al. 2012; Bahl,

Naslavsky, and Caplan 2015). While the function of EHD2 shuttling to the nucleus is mostly unclear, our observations are the first time that differential nuclear and cytoplasmic expression of EHD2 has been documented in cancer.

Disregarding nuclear expression, however, our TMA results did indicate a significant association between cytoplasmic EHD2 and caveolin-2 expression. Although caveolin-1 did not exhibit the same significant association, caveolin-1 and caveolin-2 were shown to be associated with TNBC in the same cohort of patient samples (Elsheikh et al. 2008). The expression of EHD2, caveolin-1/2, and other basal-like markers in TNBC could be a due to the cancer originating from the myoepithelial/basal layer or simply part of a transcriptomic program that leads to a basal-like phenotype (Savage et al. 2008). Regardless, these findings demonstrate that EHD2 is a novel marker of TNBC and an indicator of poor outcome, and may be serving an important regulatory role for caveolae in TNBC.

Metastasis is the ultimate cause of death among the overwhelming majority of breast cancer patients (Kast et al. 2015; Gerratana et al. 2015; Wu et al. 2016). Triple-negative breast cancer comprises only 10%- 15% of all breast cancer cases, yet it is clinically challenging due to its highly metastatic nature (Marmé and Schneeweiss 2015; Molnár et al. 2017). To expand upon our observational findings, we selected three cell lines (MDA-MB-231, BT549, and HS578T) to test the functional effects of EHD2 shRNA-mediated knockdown in TNBC. Our initial findings demonstrated that EHD2 knockdown resulted in decreased invasiveness and tumorigenicity of TNBC both *in vitro*

and *in vivo*. EHD2 knockdown did not significantly affect proliferation, migration, or morphology of TNBC cells in normal 2D culture conditions. However, we found that EHD2 knockdown significantly reduced invasiveness and anchorage-independent growth *in vitro*. These results conform with our observational findings but also suggest that EHD2 could be regulating the tumorigenicity or viability of the cancer stem cell population in TNBC. Interestingly, previous studies of EHD2 in breast cancer described the opposite effect (X. Yang et al. 2015; Yuhua Shi et al. 2015). Briefly, EHD2 was suggested to serve as a tumor suppressor since siRNA-mediated knockdown led to enhanced migration and invasion in MDA-MB-231 and MCF7 cells. Our findings suggest the contrary. Not only did our study utilize a well-annotated and 10-fold larger cohort of breast cancer patient samples, but we also confirmed that the MCF7 cell line lacks EHD2 expression through western blotting, immunofluorescence, and multiple publicly available mRNA expression databases. Furthermore, we demonstrated that EHD2 knockdown dramatically reduces tumor growth and metastasis *in vivo* using MDA-MB-231, BT549, and HS578T orthotopic tumors. We also validated the specificity of our EHD2-antibody through western blot and immunofluorescence analysis of cells with EHD2 shRNA and tissue from $EHD2^{-/-}$ mice. These findings suggest that EHD2 plays a novel role as an indispensable regulator of tumorigenicity and metastatic potential in TNBC.

In breast cancer, breast density and matrix-stiffness are associated with poorer outcome (Wei et al. 2015; Provenzano et al. 2009). Breast cancer cells rely on mechano-protective and membrane repair processes to maintain their high growth rate and to

survive in hostile tumor microenvironments. Furthermore, caveolin-1, a required structural component of caveolae, has recently been shown to be upregulated in TNBC cells subjected to fluid shear stress, indicating that caveolae serve a mechanoprotective role during breast cancer metastasis (H. Yang et al. 2016). Previous studies have confirmed that EHD2-interacting proteins such as myoferlin localize to caveolae and regulate membrane repair in TNBC and lung carcinomas (Turtoi et al. 2013; Leung et al. 2013). While caveolae and EHD2 have established roles in membrane repair (Doherty et al. 2008; Marg et al. 2012; Schilling and Patel 2015; Yin Shi et al. 2015; Echarri and Del Pozo 2015), little is known about the role of EHD2 in regulating caveolae-mediated membrane repair. Although our orthotopic tumor model results showed that EHD2 knockdown decreased tumor growth, the tumors with EHD2 shRNA were still able to grow to an extent. We found that the tumors with EHD2 shRNA grew at rate similar to control shRNA tumors up to four weeks after implantation. After week four, the EHD2 shRNA tumors halted growth and maintained their volume until the end of the experiment (11 – 13 weeks), indicating that the tumors were unable to maintain a larger burden. Although we observed decreased proliferation in EHD2 shRNA tumors, we also saw a dramatic loss of the stellate tumor cell morphology characteristic of MDA-MB-231, BT549, and HS578T cell lines (Hughes et al. 2008; Nguyen-Ngoc et al. 2015). This observation was repeated *in vitro* by 3D-culturing of TNBCs in Matrigel, indicating a defect in the membrane protective processes required for TNBC invadopodia. Further analysis confirmed that EHD2 regulates membrane repair in TNBC, consistent with its established role in controlling caveolar dynamics and membrane repair in other models.

Altogether, these findings suggest that EHD2 is serving a novel role as an essential regulator of caveolar-mediated membrane-protective functions in TNBC.

Chapter IV: Conclusions and Future Directions

IV.1 Conclusions

In summary, we used publicly available gene expression databases, clinical breast cancer samples, and shRNA-mediated knockdown within *in vitro* and *in vivo* breast cancer models to provide evidence that EHD2, a member of the EHD protein family of endocytic recycling regulators, serves a novel and critical role in regulating caveolar-mediated mechanisms of plasma membrane maintenance essential for tumor growth and development in Triple-negative breast cancer.

Based on our studies, EHD2 is fundamentally important for triple-negative breast cancer invasiveness and tumor growth. Moreover, EHD2 is a key regulator of caveolae dynamics and interacts with proteins that regulate the caveolae-mediated membrane repair and protection processes. These mechanoprotective functions of caveolae allow TNBC cells to maintain their high growth rate, survive in the hostile tumor microevironment, and metastasize. Given our observations that EHD2 is highly expressed and critical for tumorigenesis in TNBC, as well as previous studies that have solved the structure of EHD2 and found it to be an important regulator of caveolae dynamics and stability through ATP binding, our findings here have uncovered a novel function of EHD2 as regulator of caveolae-mediated mechanoprotection in cancer that may be a potential therapy target for TNBC via specific inhibition of EHD2 ATPase activity. Further exploration of other human cancers may show a broader role of EHD2 across human cancer pathogenesis.

IV.2 Future Directions

In this thesis, we demonstrated the co-expression of and co-localization of EHD2 and caveolin-1 in triple-negative breast cancer. We also showed that EHD2 was indispensable for plasma membrane repair and invasive spheroid formation in TNBC cell lines. While this is consistent with the role of caveolae in membrane repair and role of EHD2 in regulating caveolae, we still need to confirm that EHD2 is directly influencing caveolar-mediated membrane repair processes. To accomplish task, future studies will need to perform structure function analysis to determine which domains of EHD2 are required for efficient plasma membrane repair. Transfection of EHD2 mutant constructs into TNBC cells to recapitulate the membrane repair phenotype will help establish which domains are essential for this process. While many EHD2 mutants have been generated and discussed in the literature, the EHD2 mutant unable to bind ATP (EHD2 T72A) has been shown to be unable to interact and regulate caveolae (Moren et al. 2012; Stoeber et al. 2012). However, it would also be prudent to instigate the many EHD2 interacting partners (myoferlin, pacsin 2, cavin 1, and cavin 2) that are also known to be associated and/or important for caveolae formation and regulation. Additional shRNA-mediated knockdown of caveolin-1 and caveolin-1 in TNBC cells would aslo help confirm our hypothesis if knockdown is able to recapitulate our observed phenotypes of defective membrane repair and reduced tumorigenicity.

Despite the clear association of EHD2 with triple-negative breast cancer, most breast cancer samples and cell lines do not express EHD2. This is an interesting finding

that needs to be examined further. Moreover, previous studies have shown that membrane repair is essential to the invasiveness of these breast cancer cells lacking EHD2, specifically the luminal subtype cell lines MCF7 (Jaiswal et al. 2014). The MCF7 cells were found to rely mostly on annexin and s100 protein mediated repair pathways, indicating that caveolae-independent repair mechanisms are present in these cells, but it would be crucial to investigate other luminal A, luminal B, and HER2+ cell lines. While we show that caveolin-1 is primarily expressed in TNBC, some TNBC cell lines like MDA-MB-468 do not express the protein or EHD2. These cells would also be important to investigate. Moreover, although EHD2 is absent, we have shown that EHD1 and EHD4 are highly expressed in luminal and most HER2+ cell lines. It would be prudent to investigate the role of these EHDs in regard to plasma membrane repair. Additionally, our lab has demonstrated that EHD1 is a critical component in the trafficking and signaling of the receptor tyrosine kinase CSF1-R in macrophages (Cypher et al. 2016). Given that HER2 is a receptor tyrosine kinase, it would interesting to examine the effects of EHD1 shRNA-mediate knockdown within these cells. The same experiments would be worthy of investigating within the EHD2-absent, TNBC cell lines that are high in EGFR expression.

Finally, if the ATP-binding deficient mutant, EHD2 T72A, is able to recapitulate the plasma membrane repair defects observed in TNBC cells with EHD2 knockdown, development of an ATP-binding pocket specific inhibitor could provide enormous therapeutic potential to TNBC patients in the future.

Bibliography

Aoki, M N, M K Amarante, J M M Oda, and M A E Watanabe. 2011. "Caveolin Involvement and Modulation in Breast Cancer." *Mini Reviews in Medicinal Chemistry* 11 (13): 1143–52. http://www.ncbi.nlm.nih.gov/pubmed/22353223.

Bahl, Kriti, Naava Naslavsky, and Steve Caplan. 2015. "Role of the EHD2 Unstructured Loop in Dimerization, Protein Binding and Subcellular Localization." Edited by Ruben Claudio Aguilar. *PLOS ONE* 10 (4): e0123710. doi:10.1371/journal.pone.0123710.

Bailey, Tameka A, Haitao Luan, Eric Tom, Timothy Alan Bielecki, Bhopal Mohapatra, Gulzar Ahmad, Manju George, et al. 2014. "A Kinase Inhibitor Screen Reveals Protein Kinase C-Dependent Endocytic Recycling of ErbB2 in Breast Cancer Cells." *The Journal of Biological Chemistry* 289 (44): 30443–58. doi:10.1074/jbc.M114.608992.

Bernatchez, Pascal N, Arpeeta Sharma, Pinar Kodaman, and William C Sessa. 2009. "Myoferlin Is Critical for Endocytosis in Endothelial Cells." *American Journal of Physiology. Cell Physiology* 297 (3): C484-92. doi:10.1152/ajpcell.00498.2008.

Blouin, Cédric M, Cécilia Prado, Karen K Takane, Françoise Lasnier, Adolfo Garcia-Ocana, Pascal Ferré, Isabelle Dugail, and Eric Hajduch. 2010. "Plasma Membrane Subdomain Compartmentalization Contributes to Distinct Mechanisms of Ceramide Action on Insulin Signaling." *Diabetes* 59 (3): 600–610. doi:10.2337/db09-0897.

Braakman, René B. H., Christoph Stingl, Madeleine M. A. Tilanus-Linthorst, Carolien H. M. van Deurzen, Mieke A. M. Timmermans, Marcel Smid, John A. Foekens, Theo M. Luider, John W. M. Martens, and Arzu Umar. 2017. "Proteomic Characterization of Microdissected Breast Tissue Environment Provides a Protein-Level Overview of Malignant Transformation." *PROTEOMICS* 17 (5): 1600213. doi:10.1002/pmic.201600213.

Briand, Nolwenn, Cécilia Prado, Guillaume Mabilleau, Françoise Lasnier, Xavier Le Lièpvre, Jeffrey D Covington, Eric Ravussin, Soazig Le Lay, and Isabelle Dugail. 2014. "Caveolin-1 Expression and Cavin Stability Regulate Caveolae Dynamics in Adipocyte Lipid Store Fluctuation." *Diabetes* 63 (12): 4032–44. doi:10.2337/db13-1961.

Cai, Bishuang, Sai Srinivas Panapakkam Giridharan, Jing Zhang, Sugandha Saxena, Kriti Bahl, John a Schmidt, Paul L Sorgen, Wei Guo, Naava Naslavsky, and Steve Caplan. 2013. "Differential Roles of C-Terminal Eps15 Homology Domain Proteins as Vesiculators and Tubulators of Recycling Endosomes." *The Journal of Biological Chemistry* 288 (42): 30172–80. doi:10.1074/jbc.M113.488627.

Charafe-Jauffret, E, C Ginestier, F Monville, and P Finetti. 2006. "Gene Expression Profiling of Breast Cell Lines Identifies Potential New Basal Markers." *Oncogene*. http://www.nature.com/onc/journal/v25/n15/abs/1209254a.html.

Cheng, Jade P X, Carolina Mendoza-Topaz, Gillian Howard, Jessica Chadwick, Elena Shvets, Andrew S Cowburn, Benjamin J Dunmore, Alexi Crosby, Nicholas W Morrell, and Benjamin J Nichols. 2015. "Caveolae Protect Endothelial Cells from Membrane Rupture during Increased Cardiac Output." *The Journal of Cell Biology* 211 (1): 53–61. doi:10.1083/jcb.201504042.

Chin, Koei, Sandy DeVries, Jane Fridlyand, Paul T. Spellman, Ritu Roydasgupta, Wen-Lin Kuo, Anna Lapuk, et al. 2006. "Genomic and Transcriptional Aberrations Linked to Breast Cancer Pathophysiologies." *Cancer Cell* 10 (6): 529–41. doi:10.1016/j.ccr.2006.10.009.

Cipta, Stephanie, and Hemal H Patel. 2009. "Molecular Bandages: Inside-Out, Outside-in Repair of Cellular Membranes. Focus on 'Myoferlin Is Critical for Endocytosis in Endothelial Cells'." *American Journal of Physiology. Cell Physiology* 297 (3): C481-3. doi:10.1152/ajpcell.00288.2009.

Corrotte, Matthias, Patricia E Almeida, Christina Tam, Thiago Castro-Gomes, Maria Cecilia Fernandes, Bryan A Millis, Mauro Cortez, et al. 2013. "Caveolae Internalization Repairs Wounded Cells and Muscle Fibers." *eLife* 2 (January): e00926. doi:10.7554/eLife.00926.

Cypher, Luke R, Timothy Alan Bielecki, Lu Huang, Wei An, Fany Iseka, Eric Tom, Matthew D Storck, Adam D Hoppe, Vimla Band, and Hamid Band. 2016. "CSF-1 Receptor Signalling Is Governed by Pre-Requisite EHD1 Mediated Receptor Display on the Macrophage Cell Surface." *Cellular Signalling* 28 (9): 1325–35. doi:10.1016/j.cellsig.2016.05.013.

Daumke, Oliver, Richard Lundmark, Yvonne Vallis, Sascha Martens, P Jonathan G Butler, and Harvey T McMahon. 2007. "Architectural and Mechanistic Insights into an EHD ATPase Involved in Membrane Remodelling." *Nature* 449 (7164): 923–27. doi:10.1038/nature06173.

Defour, Aurelia, S C Sreetama, and Jyoti K Jaiswal. 2014. "Imaging Cell Membrane Injury and Subcellular Processes Involved in Repair." *Journal of Visualized Experiments : JoVE*, no. 85(January). doi:10.3791/51106.

Demonbreun, Alexis R., Mattia Quattrocelli, David Y. Barefield, Madison V. Allen, Kaitlin E. Swanson, and Elizabeth M. McNally. 2016. "An Actin-Dependent Annexin Complex Mediates Plasma Membrane Repair in Muscle." *The Journal of Cell Biology* 213 (6): 705–18. doi:10.1083/jcb.201512022.

Dimri, Manjari, Mayumi Naramura, Lei Duan, Jing Chen, Cesar Ortega-Cava, Gengsheng Chen, Rasna Goswami, et al. 2007. "Modeling Breast Cancer-Associated c-Src and EGFR Overexpression in Human MECs: C-Src and EGFR Cooperatively Promote Aberrant Three-Dimensional Acinar Structure and Invasive Behavior." *Cancer Research* 67 (9): 4164–72. doi:10.1158/0008-5472.CAN-06-2580.

Doherty, Katherine R, Alexis R Demonbreun, Gregory Q Wallace, Andrew Cave, Avery D Posey, Konstantina Heretis, Peter Pytel, and Elizabeth M McNally. 2008. "The Endocytic Recycling Protein EHD2 Interacts with Myoferlin to Regulate Myoblast Fusion." *The Journal of Biological Chemistry* 283 (29): 20252–60. doi:10.1074/jbc.M802306200.

Echarri, Asier, and Miguel A Del Pozo. 2015. "Caveolae - Mechanosensitive Membrane Invaginations Linked to Actin Filaments." *Journal of Cell Science* 128 (15): 2747–58. doi:10.1242/jcs.153940.

Elsheikh, S E, A R Green, E A Rakha, R M Samaka, A A Ammar, D Powe, J S Reis-Filho, and I O Ellis. 2008. "Caveolin 1 and Caveolin 2 Are Associated with Breast Cancer Basal-like and Triple-Negative Immunophenotype." *British Journal of Cancer* 99 (2): 327–34. doi:10.1038/sj.bjc.6604463.

Engelman, J A, R J Lee, A Karnezis, D J Bearss, M Webster, P Siegel, W J Muller, J J Windle, R G Pestell, and M P Lisanti. 1998. "Reciprocal Regulation of Neu Tyrosine Kinase Activity and Caveolin-1 Protein Expression in Vitro and in Vivo. Implications for Human Breast Cancer." *The Journal of Biological Chemistry* 273 (32): 20448–55. http://www.ncbi.nlm.nih.gov/pubmed/9685399.

Feldman, Rebecca, Zoran Gatalica, Sandeep K. Reddy, Michael Castro, and Jasgit C. Sachdev. 2015. "Caveolin-1: Oncogenic Role in Breast Cancer? Clues from Molecular Profiling." *ASCO Meeting Abstracts* 33 (28_suppl): 134. http://hwmaint.meeting.ascopubs.org/cgi/content/abstract/33/28_suppl/134.

Fellmann, Christof, Thomas Hoffmann, Vaishali Sridhar, Barbara Hopfgartner, Matthias Muhar, Mareike Roth, Dan Yu Lai, et al. 2013. "An Optimized microRNA Backbone for Effective Single-Copy RNAi." *Cell Reports* 5 (6): 1704–13. doi:10.1016/j.celrep.2013.11.020.

George, Manju, Mark A Rainey, Mayumi Naramura, Kirk W Foster, Melissa S Holzapfel, Laura L Willoughby, GuoGuang Ying, et al. 2011. "Renal Thrombotic Microangiopathy in Mice with Combined Deletion of Endocytic Recycling Regulators EHD3 and EHD4." *PloS One* 6 (3). Public Library of Science: e17838. doi:10.1371/journal.pone.0017838.

George, Manju, GuoGuang Ying, Mark A Rainey, Aharon Solomon, Pankit T Parikh, Qingshen Gao, Vimla Band, and Hamid Band. 2007. "Shared as Well as Distinct Roles of EHD Proteins Revealed by Biochemical and Functional Comparisons in Mammalian Cells and C. Elegans." *BMC Cell Biology* 8 (January): 3. doi:10.1186/1471-2121-8-3.

Gerratana, L., V. Fanotto, M. Bonotto, S. Bolzonello, A. M. Minisini, G. Fasola, and F. Puglisi. 2015. "Pattern of Metastasis and Outcome in Patients with Breast Cancer." *Clinical & Experimental Metastasis* 32 (2): 125–33. doi:10.1007/s10585-015-9697-2.

Goetz, Jacky G, Susana Minguet, Inmaculada Navarro-Lérida, Juan José Lazcano, Rafael Samaniego, Enrique Calvo, Marta Tello, et al. 2011. "Biomechanical Remodeling of the Microenvironment by Stromal Caveolin-1 Favors Tumor Invasion and Metastasis." *Cell* 146 (1). Elsevier: 148–63. doi:10.1016/j.cell.2011.05.040.

Gudmundsson, Hjalti, Thomas J Hund, Patrick J Wright, Crystal F Kline, Jedidiah S Snyder, Lan Qian, Olha M Koval, et al. 2010. "EH Domain Proteins Regulate Cardiac Membrane Protein Targeting." *Circulation Research* 107 (1): 84–95. doi:10.1161/CIRCRESAHA.110.216713.

Győrffy, Balazs, Andras Lanczky, Aron C Eklund, Carsten Denkert, Jan Budczies, Qiyuan Li, and Zoltan Szallasi. 2010. "An Online Survival Analysis Tool to Rapidly Assess the Effect of 22,277 Genes on Breast Cancer Prognosis Using Microarray Data of 1,809 Patients." *Breast Cancer Research and Treatment* 123 (3): 725–31. doi:10.1007/s10549-009-0674-9.

Hansen, Carsten Gram, Gillian Howard, and Benjamin J Nichols. 2011. "Pacsin 2 Is Recruited to Caveolae and Functions in Caveolar Biogenesis." *Journal of Cell Science* 124 (Pt 16): 2777–85. doi:10.1242/jcs.084319.

Hashimoto, Shigeru, Yasuhito Onodera, Ari Hashimoto, Miwa Tanaka, Michinari Hamaguchi, Atsuko Yamada, and Hisataka Sabe. 2004. "Requirement for Arf6 in Breast Cancer Invasive Activities." *Proceedings of the National Academy of Sciences of the United States of America* 101 (17): 6647–52. doi:10.1073/pnas.0401753101.

Hughes, Linda, Catherine Malone, Saranya Chumsri, Angelika M Burger, and Susan McDonnell. 2008. "Characterisation of Breast Cancer Cell Lines and Establishment of a Novel Isogenic Subclone to Study Migration, Invasion and Tumourigenicity." *Clinical & Experimental Metastasis* 25 (5): 549–57. doi:10.1007/s10585-008-9169-z.

Inman, J. L., C. Robertson, J. D. Mott, and M. J. Bissell. 2015. "Mammary Gland Development: Cell Fate Specification, Stem Cells and the Microenvironment." *Development* 142 (6): 1028–42. doi:10.1242/dev.087643.

Jacquemier, Jocelyne, Laetitia Padovani, Laetitia Rabayrol, Sunil R Lakhani, Frédérique Penault-Llorca, Yves Denoux, Maryse Fiche, et al. 2005. "Typical Medullary Breast Carcinomas Have a Basal/myoepithelial Phenotype." *The Journal of Pathology* 207 (3): 260–68. doi:10.1002/path.1845.

Jézéquel, Pascal, Mario Campone, Wilfried Gouraud, Catherine Guérin-Charbonnel, Christophe Leux, Gabriel Ricolleau, and Loïc Campion. 2012. "Bc-GenExMiner: An Easy-to-Use Online Platform for Gene Prognostic Analyses in Breast Cancer." *Breast Cancer Research and Treatment* 131 (3): 765–75. doi:10.1007/s10549-011-1457-7.

Jézéquel, Pascal, Jean-Sébastien Frénel, Loïc Campion, Catherine Guérin-Charbonnel, Wilfried Gouraud, Gabriel Ricolleau, and Mario Campone. 2013. "Bc-GenExMiner 3.0: New Mining Module Computes Breast Cancer Gene Expression Correlation

Analyses." *Database : The Journal of Biological Databases and Curation* 2013 (0): bas060. doi:10.1093/database/bas060.

Kast, Karin, Theresa Link, Katrin Friedrich, Andrea Petzold, Antje Niedostatek, Olaf Schoffer, Carmen Werner, et al. 2015. "Impact of Breast Cancer Subtypes and Patterns of Metastasis on Outcome." *Breast Cancer Research and Treatment* 150 (3): 621–29. doi:10.1007/s10549-015-3341-3.

Lehmann, Brian D, Joshua A Bauer, Xi Chen, Melinda E Sanders, A Bapsi Chakravarthy, Yu Shyr, and Jennifer A Pietenpol. 2011. "Identification of Human Triple-Negative Breast Cancer Subtypes and Preclinical Models for Selection of Targeted Therapies." *The Journal of Clinical Investigation* 121 (7): 2750–67. doi:10.1172/JCI45014.

Leung, Cleo, Carol Yu, Michelle I. Lin, Cristina Tognon, and Pascal Bernatchez. 2013. "Expression of Myoferlin in Human and Murine Carcinoma Tumors: Role in Membrane Repair, Cell Proliferation, and Tumorigenesis." *American Journal of Pathology* 182 (5): 1900–1909. doi:10.1016/j.ajpath.2013.01.041.

Lo, Harriet P, Susan J Nixon, Thomas E Hall, Belinda S Cowling, Charles Ferguson, Garry P Morgan, Nicole L Schieber, et al. 2015. "The Caveolin-Cavin System Plays a Conserved and Critical Role in Mechanoprotection of Skeletal Muscle." *The Journal of Cell Biology* 210 (5): 833–49. doi:10.1083/jcb.201501046.

Ludwig, Alexander, Gillian Howard, Carolina Mendoza-Topaz, Thomas Deerinck, Mason Mackey, Sara Sandin, Mark H Ellisman, and Benjamin J Nichols. 2013. "Molecular Composition and Ultrastructure of the Caveolar Coat Complex." *PLoS Biology* 11 (8): e1001640. doi:10.1371/journal.pbio.1001640.

Malhotra, Gautam K, Xiangshan Zhao, Hamid Band, and Vimla Band. 2010. "Histological, Molecular and Functional Subtypes of Breast Cancers." *Cancer Biology & Therapy* 10 (10): 955–60. http://www.pubmedcentral.nih.gov/articlerender.fcgi?artid=3047091&tool=pmcentrez&rendertype=abstract.

Marg, Andreas, Verena Schoewel, Tobias Timmel, Anne Schulze, Claudio Shah, Oliver Daumke, and Simone Spuler. 2012. "Sarcolemmal Repair Is a Slow Process and Includes EHD2." *Traffic (Copenhagen, Denmark)* 13 (9): 1286–94. doi:10.1111/j.1600-0854.2012.01386.x.

Marmé, Frederik, and Andreas Schneeweiss. 2015. "Targeted Therapies in Triple-Negative Breast Cancer." *Breast Care (Basel, Switzerland)* 10 (3): 159–66. doi:10.1159/000433622.

Martinez-Outschoorn, Ubaldo E, Federica Sotgia, and Michael P Lisanti. 2015. "Caveolae and Signalling in Cancer." *Nature Reviews. Cancer* 15 (4). Nature Publishing Group, a division of Macmillan Publishers Limited. All Rights Reserved.: 225–37.

doi:10.1038/nrc3915.

Masuelli, Laura, Alfredo Budillon, Laura Marzocchella, Marie-Agnes Mrozek, Domenico Vitolo, Elena Di Gennaro, Simona Losito, et al. 2012. "Caveolin-1 Overexpression Is Associated with Simultaneous Abnormal Expression of the E-Cadherin/α-β Catenins Complex and Multiple ErbB Receptors and with Lymph Nodes Metastasis in Head and Neck Squamous Cell Carcinomas." *Journal of Cellular Physiology* 227 (9): 3344–53. doi:10.1002/jcp.24034.

Mercier, Isabelle, Mathew C Casimiro, Jie Zhou, Chenguang Wang, Christopher Plymire, Kelly G Bryant, Kristin M Daumer, et al. 2009. "Genetic Ablation of Caveolin-1 Drives Estrogen-Hypersensitivity and the Development of DCIS-like Mammary Lesions." *The American Journal of Pathology* 174 (4): 1172–90. doi:10.2353/ajpath.2009.080882.

Mercier, Isabelle, and Michael P Lisanti. 2012. "Caveolin-1 and Breast Cancer: A New Clinical Perspective." *Advances in Experimental Medicine and Biology* 729 (January): 83–94. doi:10.1007/978-1-4614-1222-9_6.

Mohan, Jagan, Björn Morén, Elin Larsson, Mikkel R Holst, and Richard Lundmark. 2015. "Cavin3 Interacts with cavin1 and caveolin1 to Increase Surface Dynamics of Caveolae." *Journal of Cell Science* 128 (5): 979–91. doi:10.1242/jcs.161463.

Molnár, István Artúr, Béla Ákos Molnár, Laura Vízkeleti, Krisztina Fekete, Judit Tamás, Péter Deák, Csilla Szundi, et al. 2017. "Breast Carcinoma Subtypes Show Different Patterns of Metastatic Behavior." *Virchows Archiv* 470 (3): 275–83. doi:10.1007/s00428-017-2065-7.

Moren, B., C. Shah, M. T. Howes, N. L. Schieber, H. T. McMahon, R. G. Parton, O. Daumke, and R. Lundmark. 2012. "EHD2 Regulates Caveolar Dynamics via ATP-Driven Targeting and Oligomerization." *Molecular Biology of the Cell*. doi:10.1091/mbc.E11-09-0787.

Morén, Björn, Claudio Shah, Mark T Howes, Nicole L Schieber, Harvey T McMahon, Robert G Parton, Oliver Daumke, and Richard Lundmark. 2012. "EHD2 Regulates Caveolar Dynamics via ATP-Driven Targeting and Oligomerization." *Molecular Biology of the Cell* 23 (7): 1316–29. doi:10.1091/mbc.E11-09-0787.

Nassoy, Pierre, and Christophe Lamaze. 2012. "Stressing Caveolae New Role in Cell Mechanics." *Trends in Cell Biology* 22 (7). Elsevier Ltd: 381–89. doi:10.1016/j.tcb.2012.04.007.

Nawaz, Z, D M Lonard, A P Dennis, C L Smith, and B W O'Malley. 1999. "Proteasome-Dependent Degradation of the Human Estrogen Receptor." *Proceedings of the National Academy of Sciences of the United States of America* 96 (5): 1858–62. http://www.pubmedcentral.nih.gov/articlerender.fcgi?artid=26701&tool=pmcentrez&rendertype=abstract.

Neve, Richard M., Koei Chin, Jane Fridlyand, Jennifer Yeh, Frederick L. Baehner, Tea Fevr, Laura Clark, et al. 2006. "A Collection of Breast Cancer Cell Lines for the Study of Functionally Distinct Cancer Subtypes." *Cancer Cell* 10 (6): 515–27. doi:10.1016/j.ccr.2006.10.008.

Nguyen-Ngoc, Kim-Vy, Eliah R. Shamir, Robert J. Huebner, Jennifer N. Beck, Kevin J. Cheung, and Andrew J. Ewald. 2015. "3D Culture Assays of Murine Mammary Branching Morphogenesis and Epithelial Invasion." In , 135–62. doi:10.1007/978-1-4939-1164-6_10.

Okamoto, T, A Schlegel, P E Scherer, and M P Lisanti. 1998. "Caveolins, a Family of Scaffolding Proteins for Organizing 'preassembled Signaling Complexes' at the Plasma Membrane." *The Journal of Biological Chemistry* 273 (10): 5419–22. http://www.ncbi.nlm.nih.gov/pubmed/9488658.

Ortega-Cava, Cesar F, Srikumar M Raja, Zenab Laiq, Tameka a Bailey, Haitao Luan, Bhopal Mohapatra, Stetson H Williams, et al. 2011. "Continuous Requirement of ErbB2 Kinase Activity for Loss of Cell Polarity and Lumen Formation in a Novel ErbB2/Neu-Driven Murine Cell Line Model of Metastatic Breast Cancer." *Journal of Carcinogenesis* 10 (January): 29. doi:10.4103/1477-3163.90443.

Parton, Robert G, and Miguel A del Pozo. 2013. "Caveolae as Plasma Membrane Sensors, Protectors and Organizers." *Nature Reviews. Molecular Cell Biology* 14 (2): 98–112. doi:10.1038/nrm3512.

Patani, Neill, Lesley-Ann Martin, Jorge S Reis-Filho, and Mitch Dowsett. 2012. "The Role of Caveolin-1 in Human Breast Cancer." *Breast Cancer Research and Treatment* 131 (1): 1–15. doi:10.1007/s10549-011-1751-4.

Pekar, Olga, Sigi Benjamin, Hilla Weidberg, Silvia Smaldone, Francesco Ramirez, and Mia Horowitz. 2012. "EHD2 Shuttles to the Nucleus and Represses Transcription." *Biochemical Journal*. doi:10.1042/BJ20111268.

Pelkmans, L, J Kartenbeck, and A Helenius. 2001. "Caveolar Endocytosis of Simian Virus 40 Reveals a New Two-Step Vesicular-Transport Pathway to the ER." *Nature Cell Biology* 3 (5): 473–83. doi:10.1038/35074539.

Pelkmans, Lucas, Thomas Bürli, Marino Zerial, and Ari Helenius. 2004. "Caveolin-Stabilized Membrane Domains as Multifunctional Transport and Sorting Devices in Endocytic Membrane Traffic." *Cell* 118 (6): 767–80. doi:10.1016/j.cell.2004.09.003.

Pinilla, Socorro María Rodríguez, Emiliano Honrado, David Hardisson, Javier Benítez, and José Palacios. 2006. "Caveolin-1 Expression Is Associated with a Basal-like Phenotype in Sporadic and Hereditary Breast Cancer." *Breast Cancer Research and Treatment* 99 (1): 85–90. doi:10.1007/s10549-006-9184-1.

Posey, Avery D, Peter Pytel, Konstantina Gardikiotes, Alexis R Demonbreun, Mark Rainey, Manju George, Hamid Band, and Elizabeth M McNally. 2011. "Endocytic

Recycling Proteins EHD1 and EHD2 Interact with Fer-1-like-5 (Fer1L5) and Mediate Myoblast Fusion." *The Journal of Biological Chemistry* 286 (9): 7379–88. doi:10.1074/jbc.M110.157222.

Provenzano, P P, D R Inman, K W Eliceiri, and P J Keely. 2009. "Matrix Density-Induced Mechanoregulation of Breast Cell Phenotype, Signaling and Gene Expression through a FAK-ERK Linkage." *Oncogene* 28 (49): 4326–43. doi:10.1038/onc.2009.299.

Qian, Niansong, Takayuki Ueno, Nobuko Kawaguchi-Sakita, Masahiro Kawashima, Noriyuki Yoshida, Yoshiki Mikami, Tomoko Wakasa, et al. 2011. "Prognostic Significance of Tumor/stromal Caveolin-1 Expression in Breast Cancer Patients." *Cancer Science* 102 (8): 1590–96. doi:10.1111/j.1349-7006.2011.01985.x.

Rainey, Mark a, Manju George, GuoGuang Ying, Reiko Akakura, Daniel J Burgess, Ed Siefker, Tom Bargar, et al. 2010. "The Endocytic Recycling Regulator EHD1 Is Essential for Spermatogenesis and Male Fertility in Mice." *BMC Developmental Biology* 10 (January): 37. doi:10.1186/1471-213X-10-37.

Ringnér, Markus, Erik Fredlund, Jari Häkkinen, Åke Borg, and Johan Staaf. 2011. "GOBO: Gene Expression-Based Outcome for Breast Cancer Online." *PloS One* 6 (3). Public Library of Science: e17911. doi:10.1371/journal.pone.0017911.

Savage, Kay, Maryou B K Lambros, David Robertson, Robin L Jones, Chris Jones, Alan Mackay, Michelle James, et al. 2007. "Caveolin 1 Is Overexpressed and Amplified in a Subset of Basal-like and Metaplastic Breast Carcinomas: A Morphologic, Ultrastructural, Immunohistochemical, and in Situ Hybridization Analysis." *Clinical Cancer Research : An Official Journal of the American Association for Cancer Research* 13 (1): 90–101. doi:10.1158/1078-0432.CCR-06-1371.

Savage, Kay, Samuel Leung, S Katrina Todd, Lindsay A Brown, Robin L Jones, David Robertson, Michelle James, et al. 2008. "Distribution and Significance of Caveolin 2 Expression in Normal Breast and Invasive Breast Cancer: An Immunofluorescence and Immunohistochemical Analysis." *Breast Cancer Research and Treatment* 110 (2): 245–56. doi:10.1007/s10549-007-9718-1.

Schilling, Jan M, and Hemal H Patel. 2015. "Non-Canonical Roles for Caveolin in Regulation of Membrane Repair and Mitochondria: Implications for Stress Adaptation with Age." *The Journal of Physiology*, September. doi:10.1113/JP270591.

Sengupta, Soma, Manju George, Katharine K Miller, Khurram Naik, Jonathan Chou, Mary Ann Cheatham, Peter Dallos, Mayumi Naramura, Hamid Band, and Jing Zheng. 2009. "EHD4 and CDH23 Are Interacting Partners in Cochlear Hair Cells." *The Journal of Biological Chemistry* 284 (30): 20121–29. doi:10.1074/jbc.M109.025668.

Senju, Yosuke, and Shiro Suetsugu. 2016. "Possible Regulation of Caveolar Endocytosis and Flattening by Phosphorylation of F-BAR Domain Protein PACSIN2/Syndapin II." *BioArchitecture*, January, 00–00. doi:10.1080/19490992.2015.1128604.

Shah, Claudio, Balachandra G Hegde, Björn Morén, Elmar Behrmann, Thorsten Mielke, Gregor Moenke, Christian M T Spahn, Richard Lundmark, Oliver Daumke, and Ralf Langen. 2014. "Structural Insights into Membrane Interaction and Caveolar Targeting of Dynamin-like EHD2." *Structure (London, England : 1993)* 22 (3): 409–20. doi:10.1016/j.str.2013.12.015.

Shaw, Frances L., Hannah Harrison, Katherine Spence, Matthew P. Ablett, Bruno M. Simões, Gillian Farnie, and Robert B. Clarke. 2012. "A Detailed Mammosphere Assay Protocol for the Quantification of Breast Stem Cell Activity." *Journal of Mammary Gland Biology and Neoplasia* 17 (2). Springer US: 111–17. doi:10.1007/s10911-012-9255-3.

Shi, Yin, Shi-Hao Tan, Shukie Ng, Jing Zhou, Na-Di Yang, Gi-Bang Koo, Kerrie-Ann McMahon, et al. 2015. "Critical Role of CAV1/caveolin-1 in Cell Stress Responses in Human Breast Cancer Cells via Modulation of Lysosomal Function and Autophagy." *Autophagy* 11 (5): 769–84. doi:10.1080/15548627.2015.1034411.

Shi, Yuhua, Xiaobing Liu, Yongfang Sun, Dichen Wu, Aifeng Qiu, Haiyan Cheng, Cuigan Wu, and Xuebin Wang. 2015. "Decreased Expression and Prognostic Role of EHD2 in Human Breast Carcinoma: Correlation with E-Cadherin." *Journal of Molecular Histology* 46 (2): 221–31. doi:10.1007/s10735-015-9614-7.

Shiota, Takuya, Yuko Miyasato, Koji Ohnishi, Mutsuko Yamamoto-Ibusuki, Yutaka Yamamoto, Hirotaka Iwase, Motohiro Takeya, and Yoshihiro Komohara. 2016. "The Clinical Significance of CD169-Positive Lymph Node Macrophage in Patients with Breast Cancer." Edited by Fabrizio Mattei. *PLOS ONE* 11 (11): e0166680. doi:10.1371/journal.pone.0166680.

Siegel, Rebecca L., Kimberly D. Miller, and Ahmedin Jemal. 2017. "Cancer Statistics, 2017." *CA: A Cancer Journal for Clinicians* 67 (1): 7–30. doi:10.3322/caac.21387.

Simone, Laura C, Naava Naslavsky, and Steve Caplan. 2014. "Scratching the Surface: Actin' and Other Roles for the C-Terminal Eps15 Homology Domain Protein, EHD2." *Histology and Histopathology* 29 (3): 285–92. http://www.pubmedcentral.nih.gov/articlerender.fcgi?artid=4106284&tool=pmcentrez&rendertype=abstract.

Sinha, Bidisha, Darius Köster, Richard Ruez, Pauline Gonnord, Michele Bastiani, Daniel Abankwa, Radu V Stan, et al. 2011. "Cells Respond to Mechanical Stress by Rapid Disassembly of Caveolae." *Cell* 144 (3): 402–13. doi:10.1016/j.cell.2010.12.031.

Sohn, Jihee, Rachel M Brick, and Rocky S Tuan. 2016. "From Embryonic Development to Human Diseases: The Functional Role of Caveolae/caveolin." *Birth Defects Research. Part C, Embryo Today : Reviews* 108 (1): 45–64. doi:10.1002/bdrc.21121.

Stoeber, Miriam, Ina Karen Stoeck, Christine Hänni, Christopher Karl Ernst Bleck, Giuseppe Balistreri, and Ari Helenius. 2012. "Oligomers of the ATPase EHD2

Confine Caveolae to the Plasma Membrane through Association with Actin." *The EMBO Journal* 31 (10): 2350–64. doi:10.1038/emboj.2012.98.

Thomas, Nicholas B P, Iain R Hutcheson, Lee Campbell, Julia Gee, Kathryn M Taylor, Robert I Nicholson, and Mark Gumbleton. 2010. "Growth of Hormone-Dependent MCF-7 Breast Cancer Cells Is Promoted by Constitutive Caveolin-1 Whose Expression Is Lost in an EGF-R-Mediated Manner during Development of Tamoxifen Resistance." *Breast Cancer Research and Treatment* 119 (3): 575–91. doi:10.1007/s10549-009-0355-8.

Turtoi, Andrei, Arnaud Blomme, Akeila Bellahcène, Christine Gilles, Vincent Hennequière, Paul Peixoto, Elettra Bianchi, et al. 2013. "Myoferlin Is a Key Regulator of EGFR Activity in Breast Cancer." *Cancer Research* 73 (17): 5438–48. doi:10.1158/0008-5472.CAN-13-1142.

Wei, Spencer C, Laurent Fattet, Jeff H Tsai, Yurong Guo, Vincent H Pai, Hannah E Majeski, Albert C Chen, et al. 2015. "Matrix Stiffness Drives Epithelial-Mesenchymal Transition and Tumour Metastasis through a TWIST1-G3BP2 Mechanotransduction Pathway." *Nature Cell Biology* 17 (5): 678–88. doi:10.1038/ncb3157.

Wu, Xingrao, Ayesha Baig, Goulnar Kasymjanova, Kamran Kafi, Christina Holcroft, Hind Mekouar, Annie Carbonneau, Boris Bahoric, Khalil Sultanem, and Thierry Muanza. 2016. "Pattern of Local Recurrence and Distant Metastasis in Breast Cancer By Molecular Subtype." *Cureus*, December. doi:10.7759/cureus.924.

Yadav, Budhi S, Priyanka Chanana, and Swaty Jhamb. 2015. "Biomarkers in Triple Negative Breast Cancer: A Review." *World Journal of Clinical Oncology* 6 (6): 252–63. doi:10.5306/wjco.v6.i6.252.

Yamaguchi, Hideki, Yukiko Takeo, Shuhei Yoshida, Zen Kouchi, Yoshikazu Nakamura, and Kiyoko Fukami. 2009. "Lipid Rafts and Caveolin-1 Are Required for Invadopodia Formation and Extracellular Matrix Degradation by Human Breast Cancer Cells." *Cancer Research* 69 (22): 8594–8602. doi:10.1158/0008-5472.CAN-09-2305.

Yang, Hong, Liuyuan Guan, Shun Li, Ying Jiang, Niya Xiong, Li Li, Chunhui Wu, Hongjuan Zeng, and Yiyao Liu. 2016. "Mechanosensitive Caveolin-1 Activation-Induced PI3K/Akt/mTOR Signaling Pathway Promotes Breast Cancer Motility, Invadopodia Formation and Metastasis in Vivo." *Oncotarget*, February. doi:10.18632/oncotarget.7583.

Yang, Xiaojing, Hanru Ren, Li Yao, Xueyu Chen, and Aina He. 2015. "Role of EHD2 in Migration and Invasion of Human Breast Cancer Cells." *Tumour Biology : The Journal of the International Society for Oncodevelopmental Biology and Medicine* 36 (5): 3717–26. doi:10.1007/s13277-014-3011-9.

Appendix

CHIP/STUB1 ubiquitin ligase targets MZF1 and loss of CHIP in breast cancer unleashes the MZF1-cathepsin pro-oncogenic program

Haitao Luan[1,2,$], Bhopal C. Mohapatra[1,3,$], Timothy A. Bielecki[1,$], Sameer Mirza[2], Tameka A. Bailey[1,*], Robert J. Clubb[1,*], Wei An[1,2], Dena Ahmed[7], Matthew D. Storck[1], Yuri Sheinin[4,6], Jane L. Meza[5,6], Srikumar M. Raja[1,*], Emad A. Rakha[7], Vimla Band[1,2,3,6], Hamid Band[1,2,3,4,6,#]

[1]Eppley Institute for Research in Cancer and Allied Diseases; Departments of [2]Genetics, Cell Biology & Anatomy, [3]Biochemistry & Molecular Biology, and [4]Pathology & Microbiology, College of Medicine; [5]Department of Biostatistics, College of Public Health; and [6]Fred & Pamela Buffett Cancer Center, University of Nebraska Medical Center, NE 68198, USA; [7]Department of Pathology, University of Nottingham and Nottingham University Hospitals NHS Trust, City Hospital Campus, Nottingham, NG5 1PB, UK.

[*]**Current Addresses**: TAB, Department of Biology, University of Arkansas, Fayetteville, AR, USA; RC, Department of Oncology, Novartis Molecular Diagnostics, LLC, Cambridge, MA, USA; SMR, Robert H Lurie Comprehensive Cancer Center, Northwestern University, Chicago, IL, USA.

[$]Co-First Authors

Running title: Loss of CHIP E3 unleashes cathepsin expression

Keywords: CHIP/STUB1, ubiquitin ligase, breast cancer, ErbB2, matrix degradation

Financial support: Supported by the NIH grants CA116552 to HB, and CA96844 and CA144027 to VB; DOD grants W81WH-11-1-0167 to HB, and W81XWH-07-1-0351 and W81XWH-11-1-0171 to VB; NIGMS (NIH) Institutional Development Award P30 GM106397; and support to the Confocal, Flow Cytometry and other Cores from the NCI Cancer Center Support Grant (P30CA036727) to FPBCC and from Nebraska Research Initiative. TA Bielecki and TA Bailey were trainees under a NCI Cancer Biology Training Grant (T32CA009476). HL received a China Scholarship Council graduate fellowship. BCM and WA received UNMC graduate fellowships. TA Bailey was a Susan G. Komen Foundation postdoctoral fellow.

[#]**Corresponding Author:** Hamid Band, MD, PhD. Eppley Institute for Research in Cancer and Allied Disease, 985950 Nebraska Medical Center, Omaha, NE 68198-5950, USA; Email: hband@unmc.edu; Phone: 402-559-8572; FAX: 402-559-4651

Conflict of interest disclosure statement: None of the authors declare any conflicts.

Word count: Abstract - 249; Manuscript – 4,995

Abstract:

Biochemical pathways whose rewiring is required for tumor progression represent potential targets to devise new combinatorial therapies. CHIP/STUB1 ubiquitin ligase is a negative co-chaperone of HSP90/HSC70, and its expression is reduced or lost in several cancers, including breast cancer. Using an extensive and well-annotated breast cancer tissue collection, we identified the loss of nuclear but not cytoplasmic CHIP to predict more aggressive tumorigenesis and poorer patient survival, with loss of CHIP in two-thirds of ErbB2+ and triple-negative breast cancers and in one-third of ER+ breast cancers. Reduced CHIP expression was seen in breast cancer patient-derived xenograft tumors and in ErbB2+ and triple-negative breast cancer cell lines. Ectopic CHIP expression in ErbB2+ lines suppressed in vitro oncogenic traits and in vivo xenograft tumor growth. An unbiased screen for CHIP-regulated nuclear transcription factors identified a number of candidates whose DNA-binding activity is up- or down-regulated by CHIP. We validated Myeloid Zinc Finger 1 (MZF1) as a CHIP target as it has emerged as a key positive regulator of cathepsin B/L (CTSB/L)-mediated tumor cell invasion downstream of ErbB2. We show that CHIP negatively regulates CTSB/L expression in ErbB2+ and other breast cancer cell lines. CTSB inhibition abrogates invasion and matrix degradation in vitro and halts ErbB2+ breast cancer cell line xenograft growth. We conclude that loss of CHIP remodels cellular transcriptome to unleash critical pro-oncogenic pathways, such as the matrix-degrading enzymes of the cathepsin family, whose components can provide new therapeutic opportunities in breast and other cancers with loss of CHIP expression.

Introduction

The ubiquitin-proteasome system (UPS) plays diverse roles in normal cellular homeostasis. Ubiquitination cascade involves two ubiquitin-activating (E1) enzymes, a small group of ubiquitin-conjugating (E2) enzymes and a large repertoire of ubiquitin ligase (E3) enzymes. E3s dictate substrate specificity and comprise two broad groups: the human papilloma virus E6-interacting (HECT) domain and the really interesting new gene (RING) finger domain protein families (1).

Consistent with roles of the UPS as a contributor to oncogenesis, certain cancers, e.g., multiple myeloma, are clinically treated with proteasome inhibitors (1). Recent focus has shifted to substrate-specific elements of the UPS, such as E3s, with MDM2 inhibitors currently in clinical trials for several malignancies (clinicaltrials.gov). Notably, mutations of E3s, such as CBL (2) or FBW7 (3) convert them into oncogenes.

The C-terminus of HSC70-Interacting Protein (CHIP)/STIP1 homology and U-Box containing protein 1 (STUB1) is a U-box subfamily RING finger type E3 that regulates protein quality control as a negative co-chaperone of the HSP90/HSC70 chaperone by targeting unfolded or misfolded proteins for proteasomal degradation (4-9). CHIP-null mice exhibit strain-dependent embryonic lethality and hyper-sensitivity to stresses (10). CHIP also targets many mature proteins for ubiquitination and proteasomal degradation or degradation-independent regulation (11).

CHIP targeting of oncogenic driver/co-drivers, such as ErbB2, has prompted analyses of CHIP expression in human tumors. Analysis of matched normal and tumor

tissues from 27 breast cancer patients revealed progressive loss of CHIP mRNA expression with tumor progression; CHIP knockdown in CHIP-high MCF-7 (ER+) cells increased and CHIP overexpression in CHIP-low MDA-MB231 (triple-negative; TN) cells suppressed oncogenic traits in vitro and xenograft tumor growth and metastasis in vivo (12). Another study of 33 normal and 127 breast tumor samples also showed an inverse relation of CHIP mRNA levels with increasing grade and Nottingham Prognostic Index (13). A third study of 183 patient found an inverse correlation between ErbB2 and CHIP protein levels, with reduced CHIP expression associated with tumor progression (14). Thus, CHIP appears to function as a suppressor of breast cancer tumorigenesis. However, the extent of loss of CHIP expression in breast cancer subtypes is unknown.

Mechanistically, CHIP can target cell surface, cytoplasmic, nuclear or secreted proteins for ubiquitin-dependent degradation (11). Relevant to breast cancer, CHIP targets ERB2 (15-17), SRC-3 transcriptional coactivator (12), macrophage inhibitory factor (18), protein kinase 6/breast tumor kinase (19) and actin regulatory protein profilin-1 (20). However, how loss of CHIP promotes oncogenesis remains unclear.

Here, we assessed both nuclear and cytoplasmic CHIP expression in a well-annotated cohort of >900 breast cancer specimens. We show that a majority of ERBB2+ and TN, and a minority (but numerically large number) of ER+ breast cancers show loss of CHIP expression, and that loss of the nuclear and not the cytoplasmic CHIP expression predicts features of tumor progression and invasion, and poor patient

survival. Loss of CHIP expression in ERBB2+ breast tumor cell lines unleashes a program of increased tumor cell invasion and migration in vitro and tumorigenesis in vivo, as reported with a TN cell line model (12). Given the importance of the loss of nuclear CHIP, we performed an unbiased screen of the impact of low vs. high CHIP levels on DNA-binding activities of cellular transcription factors in ERBB2+ and TN breast cancer cell lines and identified a number of shared CHIP-regulated transcription factors. Here, we focus on CHIP regulation of MZF1 as it was recently identified as a key mediator of pro-invasive signaling downstream of ERBB2 through upregulation of the expression of matrix degrading cathepsin B and L enzymes (21). We show the CHIP dependence of this pathway in cell lines representing various breast cancer subtypes and demonstrate that chemical targeting of CTSB inhibits ERBB2-driven tumorigenesis. We conclude that loss of CHIP expression unleashes a MZF1-dependent and CTSB/L-mediated pro-oncogenic pathway in breast cancer.

Materials and Methods

Details methods are presented in Supplementary Methods.

Cell culture: ErbB2-overexpressing breast cancer cell lines SKBR3 and BT474 (ATCC) were cultured in complete α-MEM medium with 5% fetal bovine serum, 10 mM HEPES, 1 mM each of sodium pyruvate, nonessential amino acids and L-glutamine, 50 μM 2-ME, and 1% penicillin/ streptomycin (Life technologies, Carlsbad, CA). ErbB2-overexpressing breast cancer cell line 21MT1 (22) was cultured α-MEM medium supplemented as above and with 1 μg/mL hydrocortisone and 12.5 ng/mL epidermal growth factor (Sigma-Aldrich, St. Louis, MO). The lentiviral packaging cell line TSA-54 (23), the ER+ breast cancer cell line MCF7 and the ErbB2-negative and estrogen receptor/progesterone receptor-negative (TN) breast cancer cell line MDA-MB-231 (ATCC) were cultured in DMEM medium (Life technologies) and supplements as for BT474. For retroviral overexpression of Myc-tagged human CHIP (16), HEK-293T cells were transfected with pMSCV-CHIP and packaging vectors, and supernatants used to infect ErbB2+ breast cancer cell lines followed by selection in puromycin. Cell lines were regularly tested for mycoplasma. Cell lines were not continuously cultured for >3 months.

Antibodies and Reagents: Rabbit anti-CHIP antibody used for blotting has been described (16). Other primary antibodies or secondary conjugates for fluorescence or immunoblotting analyses are described under Supplementary Methods.

Cell lysis, immunoprecipitation and immunoblotting: Cells lysates were prepared in RIPA or Triton X-100 lysis buffers (as indicated in figure legends) and used for immunoprecipitation and immunoblotting analyses as described in Supplementary Methods.

Quantitative real-time PCR: Total RNA extracted using TRIzol reagent (Invitrogen) and reverse transcribed using Quantitative real-time PCR kit (cat. 204141, Qiagen, Germantown, MD) was used for real-time QPCR with primers described in Supplementary Methods.

Cell growth assays: Cell growth was analyzed as cumulative proliferation over 5 serial weekly passages and by soft agar anchorage-independent growth assay as described under Supplementary Methods.

Transwell migration and invasion assays: The migration or invasion of cells was analyzed using uncoated or Matrigel-coated Transwell chambers as described under Supplementary Methods.

Extracellular matrix (ECM) degradation assay: This assay was carried out using QCM™ Gelatin Invadopodia kit (Cat. ECM670, EMD Millipore, Billerica, MA) according to the manufacturer's protocol. Details are presented in Supplementary Methods. ECM degradation, seen as focal loss of fluorescent signal ("holes") in the labeled gelatin layer was quantified using Image J (NIH).

Xenograft tumorigenesis: 10^6 cells in Matrigel (BD Biosciences) were implanted in the mammary fat pad of female NSG mice (The Jackson Laboratory) primed with s/c estrogen pellet (0.72 mg/ 60 day pellets; Innovative Research of America, Sarasota, FL) and tumor growth monitored weekly for 10 weeks. After euthanasia, tumors were imaged, and formalin-fixed and paraffin-embedded for further analyses. Details are presented in Supplementary Methods.

Protein/DNA array: A protein/DNA combo-array kit (Cat. MA1215, Affymetrix, Santa Clara, CA) was used to simultaneously screen 345 transcription factors for DNA-binding activity per vendor protocol with signals detected using chemiluminescence (See Extended Methods).

Electrophoretic mobility shift assay (EMSA): EMSA was carried out using an EMSA kit (cat. 20148, Life Technologies, Waltham, MA) as described in Extended Methods.

Cathepsin B (CTSB)/Cathepsin L (CTSL) activity assay: CTSB/L activity was assayed using the Magic Red CTSB/L Activity Kit (Cat. 937 & 941, Immunochemistry Technologies, Bloomington, MN) according to the manufacturer's protocol (See Extended Methods). Experiments were run in triplicates and repeated thrice. Ten random fields per well were imaged and the fluorescence intensity was quantified using Image J (NIH).

Human and animal subjects: The use of human tissues was approved by the Ethics Committee of the University of Nottingham. Mouse studies were pre-approved by the

UNMC Institutional Review Board (IRB) Committee, in compliance with Federal and State guidelines.

IHC analysis of breast cancer tissue microarrays: Tissue microarrays (TMAs) corresponding to a well-annotated 971 breast cancer patient cohort at the University of Nottingham Hospital Breast Unit and a commercial TMA (BR20837, from US Biomax, INC.) were analyzed by IHC staining (see Extended Methods for details) with a previously described (27) anti-rabbit CHIP antibody that was further validated (Supplementary Figure 1).

Semi-quantitative assessment of staining intensity utilized a modified histochemical score (H-score) ranging from 0 to 300 based on multiplying staining intensity of 0 to 3 (negative, 0); weak, 1; moderate, 2; strong, 3) by the percentage of positive cells (See Extended Methods. Nuclear expression of >1 or cytoplasmic expression of >110 was considered positive (See Extended Methods). The IHC staining results were statistically analyzed using the SPSS 16.0 statistical software (SPSS Inc., Chicago, IL, USA) (See Extended Methods).

Results

Reduced nuclear CHIP expression in breast cancer correlates with tumor progression, invasion and poorer patient survival

As small previous studies (12-14) have not clarified which breast cancer subtypes lose CHIP expression, we performed immunohistochemistry (IHC) analysis of formalin-fixed and paraffin-embedded tissue microarrays (TMAs) from a well-annotated cohort of 971 breast cancer patients (Supplementary Table 1) (24-28) using an established rabbit anti-CHIP antibody (16) further validated in western blotting with lysates of CHIP-depleted or ectopic CHIP-expressing cell lines (Supplementary Figure S1). Initial IHC of a commercial breast cancer TMA (208 samples) detected both cytoplasmic and nuclear CHIP within tumor cells and in surrounding normal epithelium (Figure 1A). In the 971-sample TMA, 423 and 314 samples, respectively, were evaluable for cytoplasmic and nuclear staining, with multiple staining patterns: low cytoplasmic/low nuclear, low cytoplasmic/high nuclear, high cytoplasmic/low nuclear; or high cytoplasmic/high nuclear (Figure 1B; Supplementary Table1). Loss of nuclear CHIP staining showed a significant positive correlation with biochemical markers of tumor progression and metastasis, reduced ER and PR staining, altered cytokeratins (CK 18, CK19), increased expression of early epithelial-mesenchymal transition markers (N-cadherin, P-cadherin) and expression of EGFR family proteins (EGFR, ErbB2, ErbB4) (Supplementary Table 2). Only CK 18 ($p=0.001$) and ErbB2 ($p=0.016$) expression correlated with reduced cytoplasmic CHIP staining (Supplementary Table 2). Lower nuclear but not cytoplasmic

CHIP staining showed a significant positive correlation with clinical-pathological features of tumor progression (higher tumor size, tumor grade, pleomorphism and mitotic status) (Supplementary Table 1). Using the previously-established ER, PR and ErbB2/Her2 expression status of the TMA samples (25-29), low CHIP expression was seen in two-thirds of ErbB2+ and TN cases and about one-third of ER+ cases. Kaplan-Meier analysis revealed that low nuclear but not the cytoplasmic staining pattern correlated significantly with poorer breast cancer-specific survival (Nuclear CHIP, $p=0.003$ Vs. cytoplasmic CHIP, $p=0.469$; Figure 1C).

CHIP suppresses tumorigenic traits in ErbB2+ breast cancer cell lines

Validating IHC results, a majority of cell lines representing the ErbB2+ and TN breast cancer subtypes showed lower CHIP mRNA and protein levels compared to ER+ lines (Supplementary Figure 2A and 2B); the ER+ and TN cell line results confirm a previous report (12). Western blotting of 12 breast cancer patient-derived xenograft (29) lysates confirmed the lower or absent CHIP expression in TN, ErbB2+ and some ER+ breast cancers (Supplementary Figure 2C). The CHIP expression status in the commercial TMA was consistent with these results (Supplementary Figure 2D).

To gain mechanistic insights into how the loss of nuclear CHIP promotes oncogenic progression, we utilized ErbB2+ breast cancer cell lines (BT474, SK-BR3 and 21-MT1) as primary models, confirming key findings in TN (MDA-MB231) and ER+ (MCF-7) lines. We engineered 3 ErbB2+ lines and MDA-MB231 cells to stably

overexpress Myc-CHIP (CHIP-hi lines) (or vector control; CHIP-lo lines) and MCF-7 cells with CHIP shRNA (CHIP-lo) to deplete the endogenous CHIP expression (or a control shRNA; CHIP-hi) (Supplementary Figure 1). As CHIP expression in MDA-MB-231 cells is known to suppress oncogenic attributes (12), these served as controls.

While no significant differences in cell proliferation were observed over a single passage, confirming previous MDA-MB231 results (12), cumulative cell proliferation over multiple passages was modestly but significantly lower in CHIP-hi vs. control cells (Figure 2A). CHIP-high cells exhibited a significantly lower number of colonies in soft agar compared to control cells (Figure 2B). CHIP-hi cells exhibited significantly reduced Transwell migration (Figure 2C). Finally, CHIP-hi 21MT1 cells exhibited significantly reduced invasion through Matrigel compared to CHIP-lo control cells (Figure 2D).

Analysis of CHIP-lo vs. CHIP-hi MDA-MB231 cells, as controls, confirmed the expected reduction in primary tumor growth and lung metastasis upon CHIP overexpression (12) (Supplementary Figure 3). Notably, the CHIP-hi BT474 cells formed significantly smaller xenograft tumors compared to those with CHIP-lo cells (Figure 3A and 3B). Exogenous CHIP overexpression in tumors was confirmed by western blotting (Figure 3C). Histologically, the CHIP-hi BT474 tumors showed lower nuclear atypia and mitotic index (Figure 3D), and reduced Ki67+ proliferating cells (Figure 3E and 3F) compared to CHIP-lo BT474 tumors. No significant difference in immunostaining for the apoptotic marker cleaved-caspase 3 was noted (Figure 3E and 3G), suggesting a primarily cytostatic impact of CHIP overexpression. These studies support the tumor

suppressor role of CHIP in ErbB2+ breast cancer as suggested by our clinical-pathological analyses.

Identification of nuclear targets of CHIP in breast cancer

As loss of nuclear but not cytoplasmic CHIP expression predicted tumor progression and poor patient outcomes, we assessed the cognate DNA-binding activities of 345 cellular transcription factors in nuclear extracts of control vs. CHIP-hi ErbB2+ BT474 cells, using a commercially-available array platform, expressing the DNA-binding activity in CHIP-hi over CHIP-lo extracts as a fold ratio. Subsets of transcription factors showed changes in DNA-binding activities outside of the arbitrary 3-fold cut-off, representing potential direct or indirect targets of negative or positive regulation by CHIP (Figure 4A, left). These (Supplementary Table 3) included known CHIP targets, such as p53 and NFkB (30, 31) validating the approach. Analysis of CHIP-hi vs. CHIP-lo (control) MDA-MB231 cells (Fig 4A, right) showed that most CHIP targets were shared with the BT474 cell model (see Supplementary Table 4) (Fig 4A), although the extent of changes differed. Thus, our unbiased screen identified novel CHIP-targeted transcription factors whose deregulated function upon loss of CHIP expression may contribute to tumor progression.

MZF1 is a direct target of CHIP-mediated ubiquitination and degradation

We focused further on myeloid zinc finger 1 (MZF1), whose DNA-binding activity was down-regulated in CHIP-hi BT474 and MDA-MB231 cells (Figure 4A and 6A; MZF1 highlighted in red), as it was recently identified as a nexus of ErbB2 signaling that culminates in tumor cell invasiveness through increased transcription of matrix-degrading enzymes cathepsin B (CTSB) and L (CTSL) (21). Electrophoresis mobility shift assay (EMSA) using sequences corresponding to MZF1 binding sites on the CD34 gene promoter (32) confirmed reduced binding activity (shifted bands) in CHIP-hi vs. CHIP-lo BT474 cells (Figure 4B). The MZF1 mRNA level was reduced in CHIP-hi vs. CHIP-lo cells BT474 cells (Figure 4C), suggesting the regulation of upstream modulators of MZF1 transcription as part of CHIP-dependent reduction in DNA-binding activity. MZF1 protein level was reduced in CHIP-hi vs. CHIP-lo cells, and anti-ubiquitin blotting of MZF1 immunoprecipitations showed increased MZF1 ubiquitination in CHIP-hi vs CHIP-lo BT474 cells (Figure 4D). Co-transfection of CHIP and MZF1 in HEK-293T cells revealed CHIP dose-dependent MZF1 ubiquitination (Figure 4E, upper) and reduction in protein level (Figure 4E, bottom). These results support the conclusion that MZF1 is a bona-fide target of CHIP, involving indirect transcriptional downregulation and CHIP-dependent ubiquitination and degradation of MZF1.

CHIP is a negative regulator of MZF1-dependent and Cathepsin B/L-mediated ECM degradation

CTSB/L are key regulators of tumor invasion, angiogenesis and metastasis (33), and their MZF1-dependent transcriptional upregulation was shown to mediate in vitro tumor cell invasion upon ErbB2 overexpression in breast cancer cells (21). We therefore asked if CHIP regulation of MZF1 translates into control of CTSB/L expression. EMSA with a DNA probe from a known MZF1-binding site in the CTSB promoter (32) confirmed reduced DNA-binding activity in the nuclear extracts of CHIP-hi vs. control ErbB2+ cells (Figure 5A), with reduced CTSB and CTSL mRNA and protein levels (Figure 5B and 5C), reduced CTSB/L enzymatic activities (Figure 5D-F) measured with a fluorescent substrate (34), and reduced FITC-labeled gelatin degradation (35, 36) (Figure 5G and 5H). Thus, the MZF1/CTSB/L pro-invasion signaling axis is negatively regulated by CHIP in ErbB2+ breast cancer cells.

Consistent with CHIP-dependent reduction in the DNA-binding activity of MZF1 in CHIP-hi vs. CHIP-lo MDA-MB231 cells (Figure 4A), reduced mRNA and protein levels of CTSB/L (Figure 6A and 6B), reduced CTSB/L activity (Figure 6C, 6D and 6E) and reduced florescent gelatin degradation (Figure 6F and 6G) were observed in CHIP-hi vs. CHIP-lo MDA-MB231 cells. Increased CTSB expression was also seen in CHIP KD vs. control MCF7 cells (Supplementary Figure 4). Treatment of CHIP-lo 21MT1 cells (high CTSB/L activity; Figure 6D and 6E) with CA074, a specific inhibitor of CTSB (37), abrogated fluorescent gelatin degradation, and markedly inhibited the

transwell invasion of 21MT1 (Figure 7A-C) and MDA-MB-231 (7D-F) breast cancer cell lines. Thus, we conclude that loss of CHIP expression across breast cancer subtypes upregulates the pro-invasive MZF1-CTSB/L signaling axis.

To assess if the upregulation of CTSB expression and activity as a result of CHIP downregulation contributes to oncogenesis in vivo, we grew BT474 xenograft tumors to an average of 0.5 mm^3 and treated the mice with CA074 (25 mg/Kg body weight, i.p.), Trastuzumab (4 mg/Kg, tail vein injection) as a standard ErbB2-targeted therapeutic or the vehicle control, based on previously used dosages (37-39). CA074 treatment led to a marked and statistically-significant inhibition of tumor growth at multiple time points, comparable to that seen with Trastuzumab (Figure 7G), supporting the conclusion that one mechanism by which loss of CHIP promotes breast tumor progression is by eliminating the negative regulation of MZF1 and unleashing the cathepsin expression.

Discussion

Loss of expression of the HSP90/HSC70 co-chaperone CHIP E3 has emerged as a mechanism to promote tumor progression. Here, we demonstrate that loss of nuclear, and not cytoplasmic, CHIP expression is associated with tumor progression and shorter survival in breast cancer patients, and is a feature of about two-thirds of ErbB2+ and TN as well as a third of ER+ breast cancers. Importantly, we identify loss of CHIP as a key mechanism to alter the DNA-binding activities of a substantial subset of cellular transcription factors, and establish that loss of CHIP expression unleashes a pro-invasion signaling cascade in which the CHIP target MZF1 promotes cathepsin B and L expression. Using a chemical inhibitor strategy, we show that upregulation of MZF1-CTSB axis due to loss of CHIP expression contributes to tumorigenesis.

IHC analyses of an extensive collection of well-annotated breast cancer TMAs demonstrated that loss of nuclear CHIP signals correlates with markers of advanced tumor progression, including higher tumor grade, mitotic index and markers of early EMT (Supplementary Table 1), and significantly shorter breast cancer-specific and progression-free survival (Figure 1C). Loss of nuclear CHIP was a feature of nearly two-thirds of ErB2+ and TN subtypes, consistent with their poorer intrinsic patient outcomes and higher metastatic odds (40, 41), and about a third of ER+ breast cancers (Supplementary Table 2). In contrast, loss of cytoplasmic CHIP expression was only associated with ErbB2 positivity, and did not predict poor patient survival (Fig 1C). These results materially extend previous findings using smaller patient cohorts (12-14),

and highlight the subtype preference of CHIP loss and the importance of the loss of nuclear CHIP as a pro-oncogenic adaptation in breast cancer. Of note, the CHIP-low ER+ patients numerically exceed the CHIP-lo ErbB2+ and TN patients, and further studies are needed to assess if these patients belong to a particular molecular sub-class.

Analyses in breast cancer cell lines confirmed the predominant loss of CHIP expression in the ErbB2+ and TN subtypes. Using matched pairs of ErbB2+ breast cancer cell lines with low endogenous CHIP expression vs. their CHIP-hi derivatives in functional assays, we show that CHIP levels are a key determinant of ErbB2-driven cell growth and invasiveness in vitro and xenograft tumor growth in nude mice, extending previous findings using CHIP-reconstituted MDA-MB231 (TN) and CHIP-depleted MCF-7 (ER+) lines (12), which served as controls. While we confirmed the lack of impact of CHIP restoration on cell proliferation in a single passage (12), analyses over multiple passages revealed a subtle but significant proliferative disadvantage (Figure 2A), which is profound under anchorage-independent conditions (Figure 2B). Thus, CHIP serves as a tumor suppressor for ErbB2+, TN and a proportion of ER+ breast cancers.

Furthering our novel findings that loss of nuclear and not cytoplasmic CHIP correlates with tumor progression, an unbiased protein/DNA array screen identified a number of transcription factors whose DNA-binding activities are directly or indirectly up- or down-regulated by CHIP (Figure 4A), vastly expanding the list of potential targets of CHIP in the context of cancer (30, 31). Here, we have focused on MZF1, whose activity was downregulated by CHIP, since it was recently identified as a major

transcriptional activator of CTSB/L-mediated tumor cell invasion downstream of ErbB2 in breast cancer cells (42). CTSB/L are overexpressed in primary breast cancers and CTSB or MZF1 knockdown abrogated breast cancer cell invasiveness in vitro (42). Our EMSA analyses confirmed the reduced MZF1DNA-binding activity in CHIP-hi breast cancer cells (Figure 4B), and we show that MZF1 is both a direct target of CHIP for ubiquitination and destabilization (Figure 4D) and also indirectly regulated at the mRNA level, potentially due to CHIP regulation of upstream regulators of MZF1 expression such as MYC (43) (Figure 4A). Since intermediary kinases (CDC42BPβ, ERK2, PAK4, PKCα) were implicated in MZF1-mediated CTSB/L transcription downstream of ErbB2 (42), negative regulation of these kinases or ErbB2 (15, 16) may also contribute to CHIP regulation of MZF1.

Our analyses support a key role of loss of CHIP as a mechanism to unleash the MZF1-dependent transcriptional network that controls CTSB/L expression (Figure 5A) and extracellular matrix (ECM) degradation (Figure 5G), and to promote oncogenesis (Figure 2). CTSB is a well-established downstream mediator of invasive/metastatic signaling in various cancers (44, 45), including breast cancer (21, 37). Specific CTSB inhibition with CA074 reduced the matrix degradation and cell invasion in vitro and tumor growth in vivo (Figure 6), providing further support for loss of CHIP expression as a key breast cancer adaptation to unleash the pro-oncogenic MZF1-CTSB pathway. The strong effect of CTSB inhibition alone on matrix degradation and xenograft tumor growth, the latter comparable to Trastuzumab (Figure 7D), suggests that CTSB may be the dominant player in BT474 cells, consistent with strong reported impact of CTSB

depletion on in vitro invasiveness of ErbB2+ breast cancer cell lines (42). However, further studies to assess the contribution of CTSL and other potential targets of MZF1 are warranted. Our in vitro results in TN and ER+ cell lines (Figure 4) also support the unleashing of MZF1-CTSB/L pathway in the corresponding breast cancer subtypes, and further studies in these and other tumors with loss of CHIP expression (11) will be of interest.

In conclusion, our studies demonstrate that upregulation of MZF1/CTSB/L axis is an important pro-oncogenic mechanism unleashed by loss of CHIP expression in breast cancer. Given the established roles of cathepsins in matrix remodeling, invasion, angiogenesis and metastasis (44, 45), future studies to establish the role and targeting of MZF1-CTSB/L axis in metastatic tumor settings may provide new therapeutic opportunities for breast and other tumors with loss of CHIP expression (31, 46-49).

Acknowledgements

We thank the Band laboratory members for helpful discussions.

Authors' Contributions

HB and VB conceived and supervised the project, HL, BCM, WA, DA, SM, BCM, TA Bielecki, TA Bailey, RC, SMR, YS and EAR developed methodologies and/or acquired data, HL, HB, VB, JM, SMR, YS and EAR analyzed data, HL, DA, HB, VB and EAR wrote the manuscript, and MDS provided key technical support.

References

1. Ciechanover A, Schwartz AL. The ubiquitin system: Pathogenesis of human diseases and drug targeting. Biochim Biophys Acta 2004;1695(1-3):3-17.

2. Naramura M, Nadeau S, Mohapatra B, et al. Mutant cbl proteins as oncogenic drivers in myeloproliferative disorders. Oncotarget 2011;2(3):245-50.

3. Welcker M, Clurman BE. FBW7 ubiquitin ligase: A tumour suppressor at the crossroads of cell division, growth and differentiation. Nat Rev Cancer 2008;8(2):83-93.

4. Ballinger CA, Connell P, Wu Y, et al. Identification of CHIP, a novel tetratricopeptide repeat-containing protein that interacts with heat shock proteins and negatively regulates chaperone functions. Mol Cell Biol 1999;19(6):4535-45.

5. Connell P, Ballinger CA, Jiang J, et al. The co-chaperone CHIP regulates protein triage decisions mediated by heat-shock proteins. Nat Cell Biol 2001;3(1):93-6.

6. Murata S, Minami Y, Minami M, Chiba T, Tanaka K. CHIP is a chaperone-dependent E3 ligase that ubiquitylates unfolded protein. EMBO Rep 2001;2(12):1133-8.

7. Wiederkehr T, Bukau B, Buchberger A. Protein turnover: A CHIP programmed for proteolysis. Curr Biol 2002;12(1):R26-8.

8. McDonough H, Patterson C. CHIP: A link between the chaperone and proteasome systems. Cell Stress Chaperones 2003;8(4):303-8.

9. Kundrat L, Regan L. Balance between folding and degradation for Hsp90-dependent client proteins: A key role for CHIP. Biochemistry 2010;49(35):7428-38.

10. Min JN, Whaley RA, Sharpless NE, Lockyer P, Portbury AL, Patterson C. CHIP deficiency decreases longevity, with accelerated aging phenotypes accompanied by altered protein quality control. Mol Cell Biol 2008;28(12):4018-25.

11. Paul I, Ghosh MK. A CHIPotle in physiology and disease. Int J Biochem Cell Biol 2015;58:37-52.

12. Kajiro M, Hirota R, Nakajima Y, et al. The ubiquitin ligase CHIP acts as an upstream regulator of oncogenic pathways. Nat Cell Biol 2009;11(3):312-9.

13. Patani N, Jiang W, Newbold R, Mokbel K. Prognostic implications of carboxyl-terminus of Hsc70 interacting protein and lysyl-oxidase expression in human breast cancer. J Carcinog 2010;9:9,3163.72505.

14. Jan CI, Yu CC, Hung MC, et al. Tid1, CHIP and ErbB2 interactions and their prognostic implications for breast cancer patients. J Pathol 2011;225(3):424-37.

15. Xu W, Marcu M, Yuan X, Mimnaugh E, Patterson C, Neckers L. Chaperone-dependent E3 ubiquitin ligase CHIP mediates a degradative pathway for c-ErbB2/Neu. Proc Natl Acad Sci U S A 2002;99(20):12847-52.

16. Zhou P, Fernandes N, Dodge IL, et al. ErbB2 degradation mediated by the co-chaperone protein CHIP. J Biol Chem 2003;278(16):13829-37.

17. Jeong JH, An JY, Kwon YT, Li LY, Lee YJ. Quercetin-induced ubiquitination and down-regulation of her-2/neu. J Cell Biochem 2008;105(2):585-95.

18. Schulz R, Marchenko ND, Holembowski L, et al. Inhibiting the HSP90 chaperone destabilizes macrophage migration inhibitory factor and thereby inhibits breast tumor progression. J Exp Med 2012;209(2):275-89.

19. Kang SA, Cho HS, Yoon JB, Chung IK, Lee ST. Hsp90 rescues PTK6 from proteasomal degradation in breast cancer cells. Biochem J 2012;447(2):313-20.

20. Choi YN, Lee SK, Seo TW, Lee JS, Yoo SJ. C-terminus of Hsc70-interacting protein regulates profilin1 and breast cancer cell migration. Biochem Biophys Res Commun 2014;446(4):1060-6.

21. Rafn B, Nielsen CF, Andersen SH, et al. ErbB2-driven breast cancer cell invasion depends on a complex signaling network activating myeloid zinc finger-1-dependent cathepsin B expression. Mol Cell 2012;45(6):764-76.

22. Band V, Zajchowski D, Stenman G, et al. A newly established metastatic breast tumor cell line with integrated amplified copies of ERBB2 and double minute chromosomes. Genes Chromosomes Cancer 1989;1(1):48-58.

23. Dimri M, Naramura M, Duan L, et al. Modeling breast cancer-associated c-src and EGFR overexpression in human MECs: C-src and EGFR cooperatively promote aberrant three-dimensional acinar structure and invasive behavior. Cancer Res 2007;67(9):4164-72.

24. Mirza S, Rakha EA, Alshareeda A, et al. Cytoplasmic localization of alteration/deficiency in activation 3 (ADA3) predicts poor clinical outcome in breast cancer patients. Breast Cancer Res Treat 2013;137(3):721-31.

25. Mohibi S, Gurumurthy CB, Nag A, et al. Mammalian alteration/deficiency in activation 3 (Ada3) is essential for embryonic development and cell cycle progression. J Biol Chem 2012;287(35):29442-56.

26. Zhao X, Mirza S, Alshareeda A, et al. Overexpression of a novel cell cycle regulator ecdysoneless in breast cancer: A marker of poor prognosis in HER2/neu-overexpressing breast cancer patients. Breast Cancer Res Treat 2012;134(1):171-80.

27. Curtis C, Shah SP, Chin SF, et al. The genomic and transcriptomic architecture of 2,000 breast tumours reveals novel subgroups. Nature 2012;486(7403):346-52.

28. Aleskandarany MA, Soria D, Green AR, et al. Markers of progression in early-stage invasive breast cancer: A predictive immunohistochemical panel algorithm for distant recurrence risk stratification. Breast Cancer Res Treat 2015;151(2):325-33.

29. Bieniasz M, Radhakrishnan P, Faham N, De La OJP, Welm AL. Preclinical efficacy of ron kinase inhibitors alone and in combination with PI3K inhibitors for treatment of sfRon-expressing breast cancer patient-derived xenografts. Clin Cancer Res 2015;21(24):5588-600.

30. Cicalese A, Bonizzi G, Pasi CE, et al. The tumor suppressor p53 regulates polarity of self-renewing divisions in mammary stem cells. Cell 2009;138(6):1083-95.

31. Wang Y, Ren F, Wang Y, et al. CHIP/Stub1 functions as a tumor suppressor and represses NF-kappaB-mediated signaling in colorectal cancer. Carcinogenesis 2014;35(5):983-91.

32. Perrotti D, Melotti P, Skorski T, Casella I, Peschle C, Calabretta B. Overexpression of the zinc finger protein MZF1 inhibits hematopoietic development from embryonic stem cells: Correlation with negative regulation of CD34 and c-myb promoter activity. Mol Cell Biol 1995;15(11):6075-87.

33. Olson OC, Joyce JA. Cysteine cathepsin proteases: Regulators of cancer progression and therapeutic response. Nat Rev Cancer 2015;15(12):712-29.

34. Taniguchi M, Ogiso H, Takeuchi T, Kitatani K, Umehara H, Okazaki T. Lysosomal ceramide generated by acid sphingomyelinase triggers cytosolic cathepsin B-mediated degradation of X-linked inhibitor of apoptosis protein in natural killer/T lymphoma cell apoptosis. Cell Death Dis 2015;6:e1717.

35. Tu C, Ortega-Cava CF, Chen G, et al. Lysosomal cathepsin B participates in the podosome-mediated ECM degradation and invasion via secreted lysosomes in v-src fibroblasts. Cancer Res 2008;68(22):9147-56.

36. Bowden ET, Mueller S, Coopman PJ. In vitro invasion assays: Phagocytosis of the extracellular matrix. Curr Protoc Cytom 2001;Chapter 9:Unit 9.13.

37. Withana NP, Blum G, Sameni M, et al. Cathepsin B inhibition limits bone metastasis in breast cancer. Cancer Res 2012;72(5):1199-209.

38. Raja SM, Clubb RJ, Ortega-Cava C, et al. Anticancer activity of celastrol in combination with ErbB2-targeted therapeutics for treatment of ErbB2-overexpressing breast cancers. Cancer Biol Ther 2011;11(2):263-76.

39. Raja SM, Desale SS, Mohapatra B, et al. Marked enhancement of lysosomal targeting and efficacy of ErbB2-targeted drug delivery by HSP90 inhibition. Oncotarget 2016;7(9):10522-35.

40. Malhotra GK, Zhao X, Band H, Band V. Histological, molecular and functional subtypes of breast cancers. Cancer Biol Ther 2010;10(10):955-60.

41. Perou CM, Borresen-Dale AL. Systems biology and genomics of breast cancer. Cold Spring Harb Perspect Biol 2011;3(2):10.1101/cshperspect.a003293.

42. Rafn B, Kallunki T. A way to invade: A story of ErbB2 and lysosomes. Cell Cycle 2012;11(13):2415-6.

43. Eguchi T, Prince T, Wegiel B, Calderwood SK. Role and regulation of myeloid zinc finger protein 1 in cancer. J Cell Biochem 2015;116(10):2146-54.

44. Gondi CS, Rao JS. Cathepsin B as a cancer target. Expert Opin Ther Targets 2013;17(3):281-91.

45. Gora J, Latajka R. Involvement of cysteine proteases in cancer. Curr Med Chem 2015;22(8):944-57.

46. Liang ZL, Kim M, Huang SM, Lee HJ, Kim JM. Expression of carboxyl terminus of Hsp70-interacting protein (CHIP) indicates poor prognosis in human gallbladder carcinoma. Oncol Lett 2013;5(3):813-8.

47. Jang KW, Lee KH, Kim SH, et al. Ubiquitin ligase CHIP induces TRAF2 proteasomal degradation and NF-kappaB inactivation to regulate breast cancer cell invasion. J Cell Biochem 2011;112(12):3612-20.

48. Wang S, Wu X, Zhang J, et al. CHIP functions as a novel suppressor of tumour angiogenesis with prognostic significance in human gastric cancer. Gut 2013;62(4):496-508.

49. Wang T, Yang J, Xu J, et al. CHIP is a novel tumor suppressor in pancreatic cancer through targeting EGFR. Oncotarget 2014;5(7):1969-86.

Figure 1.

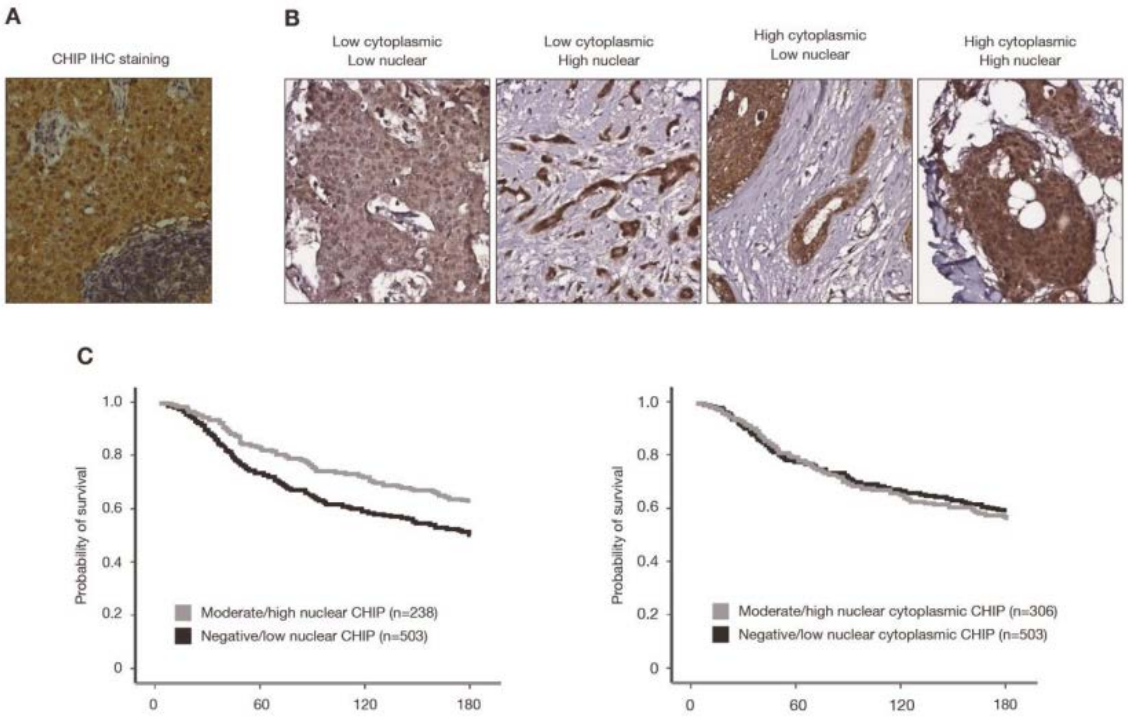
A
CHIP IHC staining
B
Low cytoplasmic
Low nuclear
Low cytoplasmic
High nuclear
High cytoplasmic
Low nuclear
High cytoplasmic
High nuclear
C
Probability of survival
1.0
0.8
0.6
0.4
0.2
0
0
60
120
180
Moderate/high nuclear CHIP (n=238)
Negative/low nuclear CHIP (n=503)
Probability of survival
1.0
0.8
0.6
0.4
0.2
0
0
60
120
180
Moderate/high nuclear cytoplasmic CHIP (n=306)
Negative/low nuclear cytoplasmic CHIP (n=503)

Figure 1. Reduced nuclear CHIP staining in primary breast cancer tissue microarrays (TMAs) specimens. (A) Anti-CHIP IHC staining of a representative breast cancer specimen vs. normal breast tissue to show cytoplasmic and nuclear staining. B. Representative IHC staining patterns of loss of nuclear vs. cytoplasmic CHIP expression in breast cancer TMAs. (C) Kaplan-Meier analysis of the correlation of breast cancer-specific survival (BCSS) with reduction in nuclear (left) or cytoplasmic (right) CHIP expression. Number of patients and p values are indicated.

Figure 2.

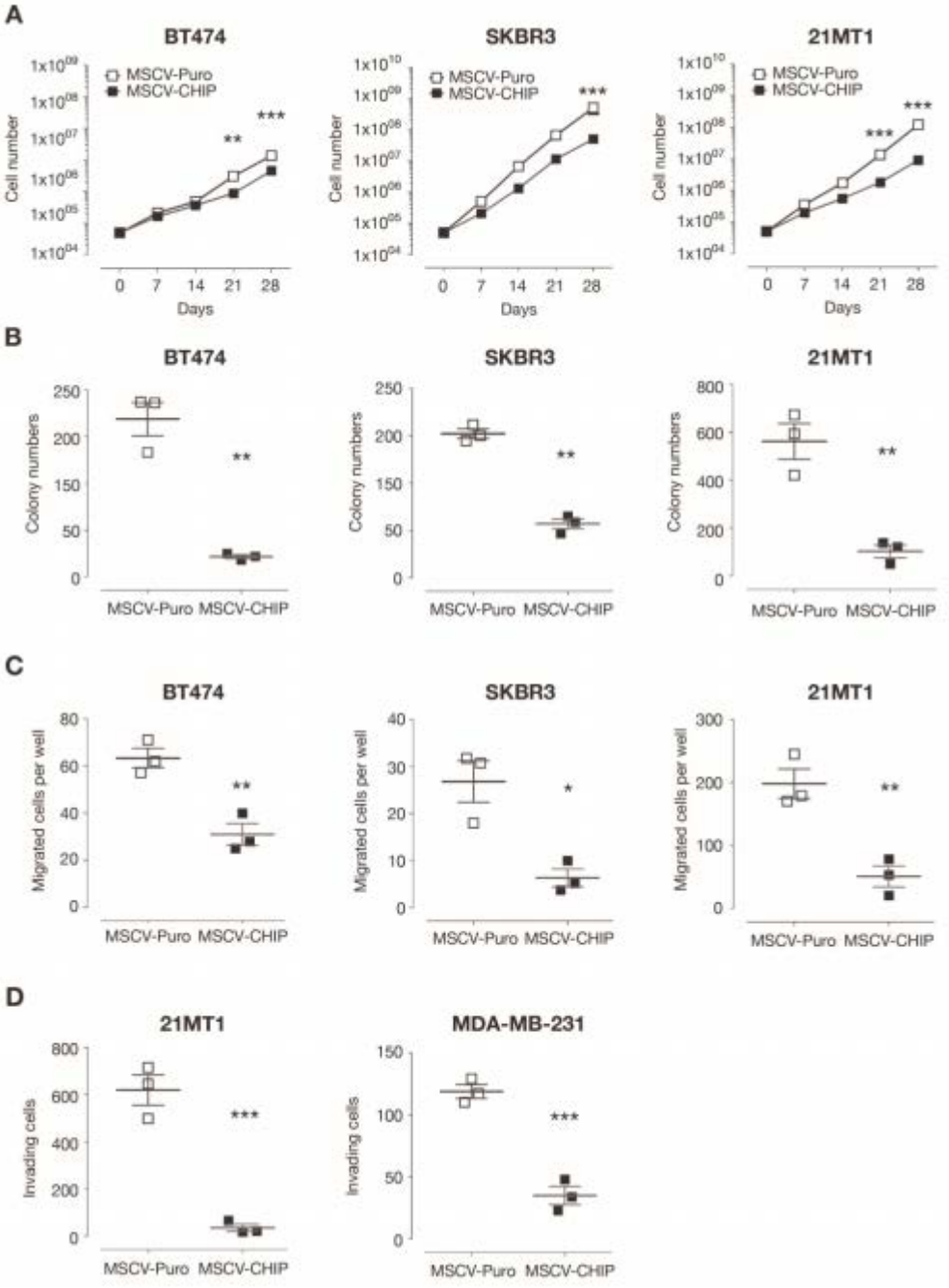
A
BT474
SKBR3
21MT1
MSCV-Puro
MSCV-CHIP
Cell number
Days
B
Colony numbers
C
Migrated cells per well
D
Invading cells
MDA-MB-231

Figure 2. Suppression of in vitro oncogenic attributes of CHIP-lo ErbB2+ breast cancer cell lines upon CHIP overexpression. (A) Cumulative proliferation of CHIP-lo control (MSCV-puro) vs. CHIP-hi (MSCV-CHIP) 21MT1, BT474 and SKBR3 cell lines. (B) Anchorage-independent cell growth in soft agar after 3 weeks of culture. Y-axis, number of colonies per 2500 cells. (C) Transwell migration assay. Y-axis, number of migrated cells per high power field (HPF). D. Transwell Matrigel-invasion assay. Y-axis, number of migrated cells per HPF. Data are mean +/- SEM of 3 experiments, each in triplicates.

Figure 3.

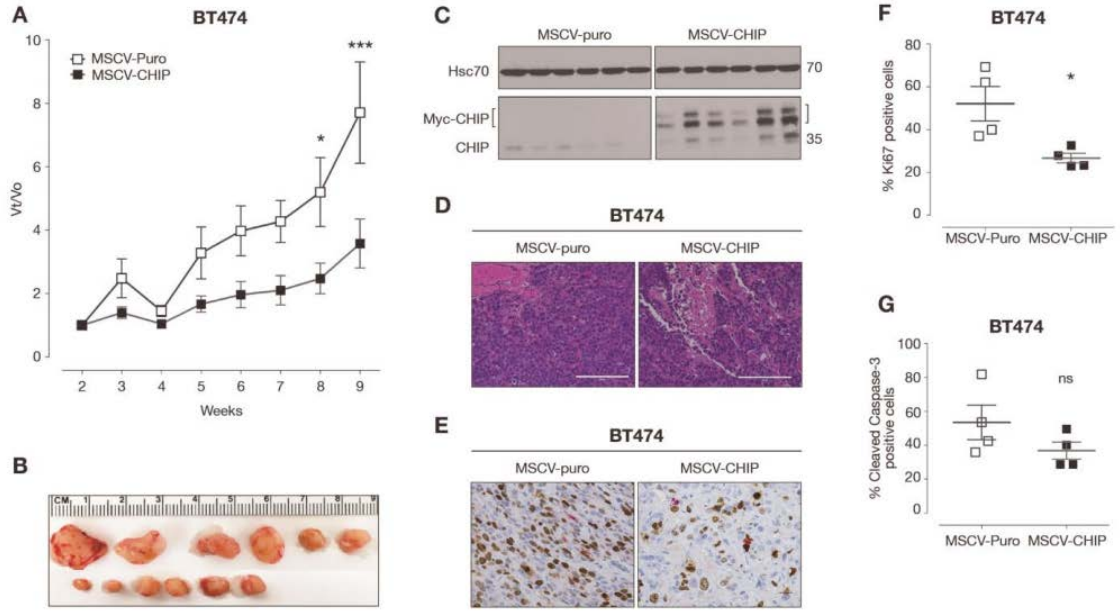
A
BT474
MSCV-Puro
MSCV-CHIP
Vt/Vo
Weeks
B
C
MSCV-puro
MSCV-CHIP
Hsc70
70
Myc-CHIP
CHIP
35
D
BT474
MSCV-puro
MSCV-CHIP
E
BT474
MSCV-puro
MSCV-CHIP
F
BT474
% Ki67 positive cells
MSCV-Puro
MSCV-CHIP
G
BT474
% Cleaved Caspase-3 positive cells
ns
MSCV-Puro
MSCV-CHIP

Figure 3. Reduced xenograft growth of CHIP-overexpressing BT474 cells in nude mice. (A) Tumor volume of CHIP-lo (MSCV-puro) control and CHIP-hi (MSCV-CHIP) BT474 xenografts over time N = 6 per group. *, $p < 0.05$. (B) Photograph of resected CHIP-lo (upper) and CHIP-hi (lower) BT474 cells. (C) Western blotting of endogenous and overexpressed (Myc-tagged) CHIP in resected BT474 xenografts; HSC70, loading control. (D & E) Representative H&E staining (D) or Ki67 (brown) plus cleaved caspase 3 (CC3; red) staining of CHIP-lo (left) and CHIP-hi (right) BT474 xenograft tumor sections. (F, G) Quantification of Ki67 (F) and CC3 (G) positive cells in Figure E. Mean +/- SD, n=6.

Figure 4.

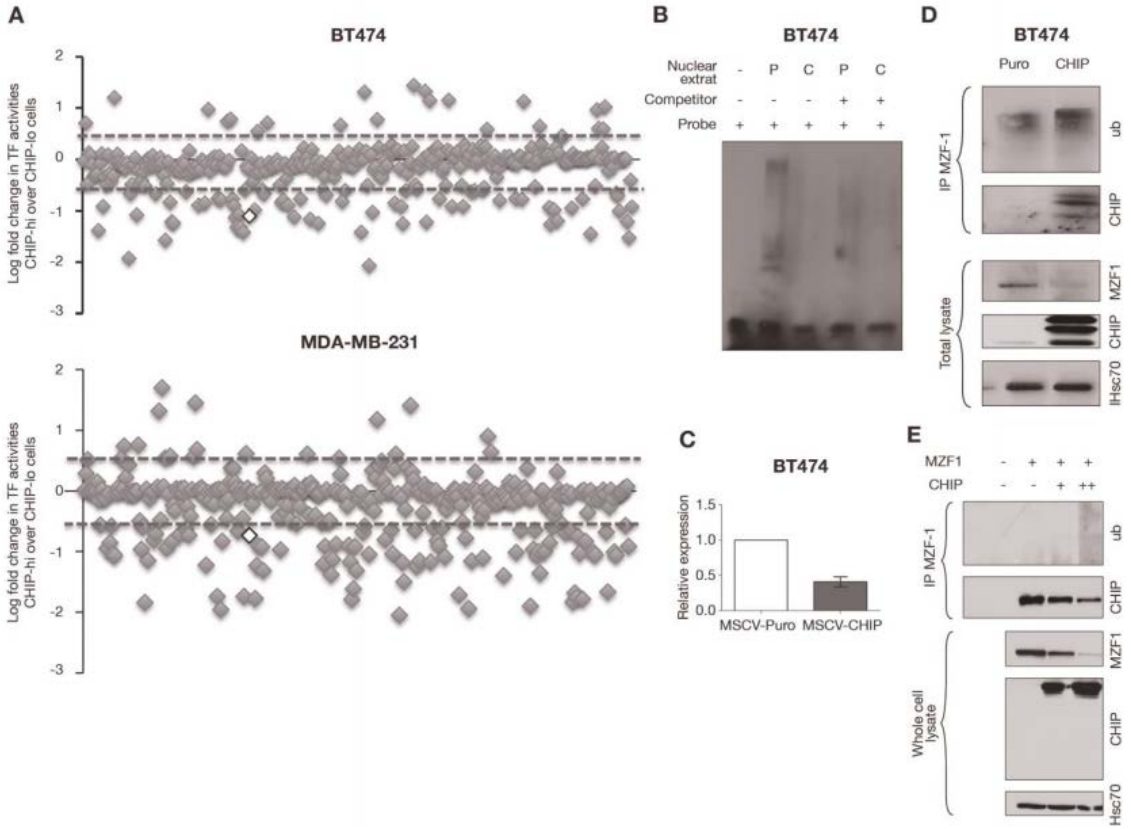
A
BT474
Log fold change in TF activities CHIP-hi over CHIP-lo cells
MDA-MB-231
B
BT474
Nuclear extrat
Competitor
Probe
C
BT474
Relative expression
MSCV-Puro
MSCV-CHIP
D
BT474
Puro
CHIP
IP MZF-1
ub
CHIP
Total lysate
MZF1
CHIP
lHsc70
E
MZF1
CHIP
IP MZF-1
ub
CHIP
Whole cell lysate
MZF1
CHIP
Hsc70

Figure 4. Identification of MZF1 as a CHIP-regulated transcription factor in ErbB2+ breast cancer cells. (A) DNA-binding activities of 345 transcription factors were analyzed in CHIP-lo (MSCV-puro control) vs. CHIP-hi (MSCV-CHIP) BT474 and MDA-MB-231cell lines. Y-axis, log-fold binding in CHIP-hi over CHIP-lo cells. The 3-fold increase (upper) or decrease (lower) in binding (dotted lines) was used as cut-off. MZF1 (Open symbol). (B) Biotin-labeled MZF1-specific DNA sequences was used as to probe nuclear extracts of CHIP-hi (MSCV-CHIP, C) vs. CHIP-lo (MSCV-puro, P) BT474 cells. 200-fold excess of non-labeled probe served as competitor. (C) Real-time qPCR analysis of MZF1 mRNA levels in CHIP-hi vs. CHIP-lo BT474 cells. (D) Immunoblotting of MZF1 protein levels in CHIP-hi vs. CHIP-lo BT474 cells. (E) CHIP-dependent ubiquitination and degradation of MZF1. Anti-MZF1 immunoprecipitations from lysates of HEK-293T cells transfected with GFP- MZF1 +/- Myc- CHIP (0.5 or 4 □g) were immunoblotted for ubiquitin or MZF1 (upper panel), and whole cell lysates (lower panel) for MZF1, CHIP or HSC70 (loading control).

Figure 5.

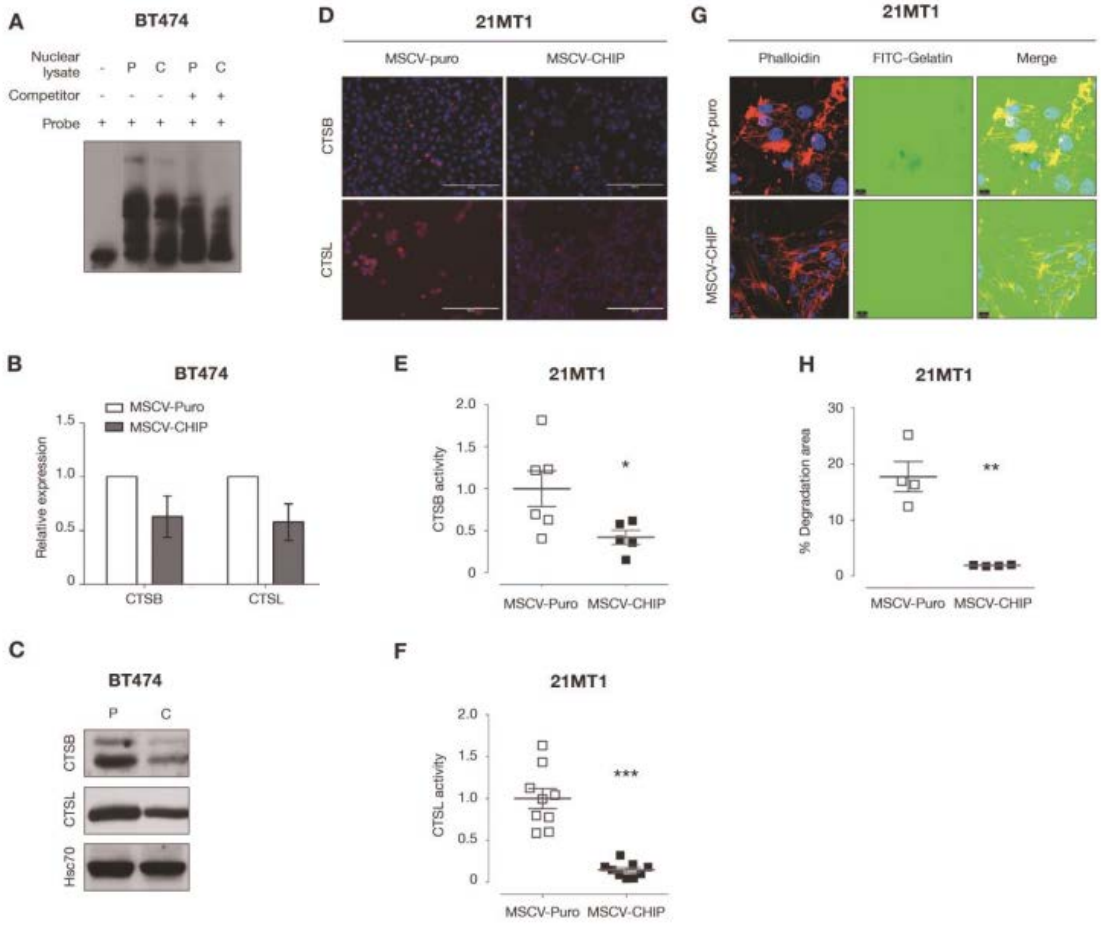
A
BT474
Nuclear lysate - P C P C
Competitor - - - + +
Probe + + + + +
D
21MT1
MSCV-puro
MSCV-CHIP
CTSB
CTSL
G
21MT1
Phalloidin
FITC-Gelatin
Merge
MSCV-puro
MSCV-CHIP
B
BT474
MSCV-Puro
MSCV-CHIP
Relative expression
CTSB
CTSL
E
21MT1
CTSB activity
MSCV-Puro MSCV-CHIP
H
21MT1
% Degradation area
MSCV-Puro MSCV-CHIP
C
BT474
P C
CTSB
CTSL
Hsc70
F
21MT1
CTSL activity
MSCV-Puro MSCV-CHIP

Figure 5. CHIP levels control the expression of MZF1 target genes cathepsins B and L. (A) EMSA analysis with CTSB promoter sequences in CHIP-hi vs. CHIP-lo BT474 cells was done as in Figure 4B. (B) CTSB/L mRNA expression in CHIP-hi vs. CHIP-lo BT474 cells was analyzed by real-time qPCR. (C) Immunoblotting for CTSB/L protein levels in CHIP-hi vs. CHIP-lo BT474 cells. (D) CTSB/L activities in CHIP-hi vs. CHIP-lo 21MT1 cells analyzed by the production of a red fluorescent cleavage product. (E, F) Quantification of CTSB (E) and CTSL (F) activities presented in D. Mean+/- S.D., n=10. (G) Degradation of FITC-labeled gelatin matrix (seen as black holes) by CHIP-lo vs. CHIP-hi 21MT1 cells seeded for 48 hours and stained for actin-containing invadopodia with phalloidin (red) and nuclei with DAPI (blue). (H) Quantification of gelatin degradation presented in G. Mean +/- SD., n=4.

Figure 6.

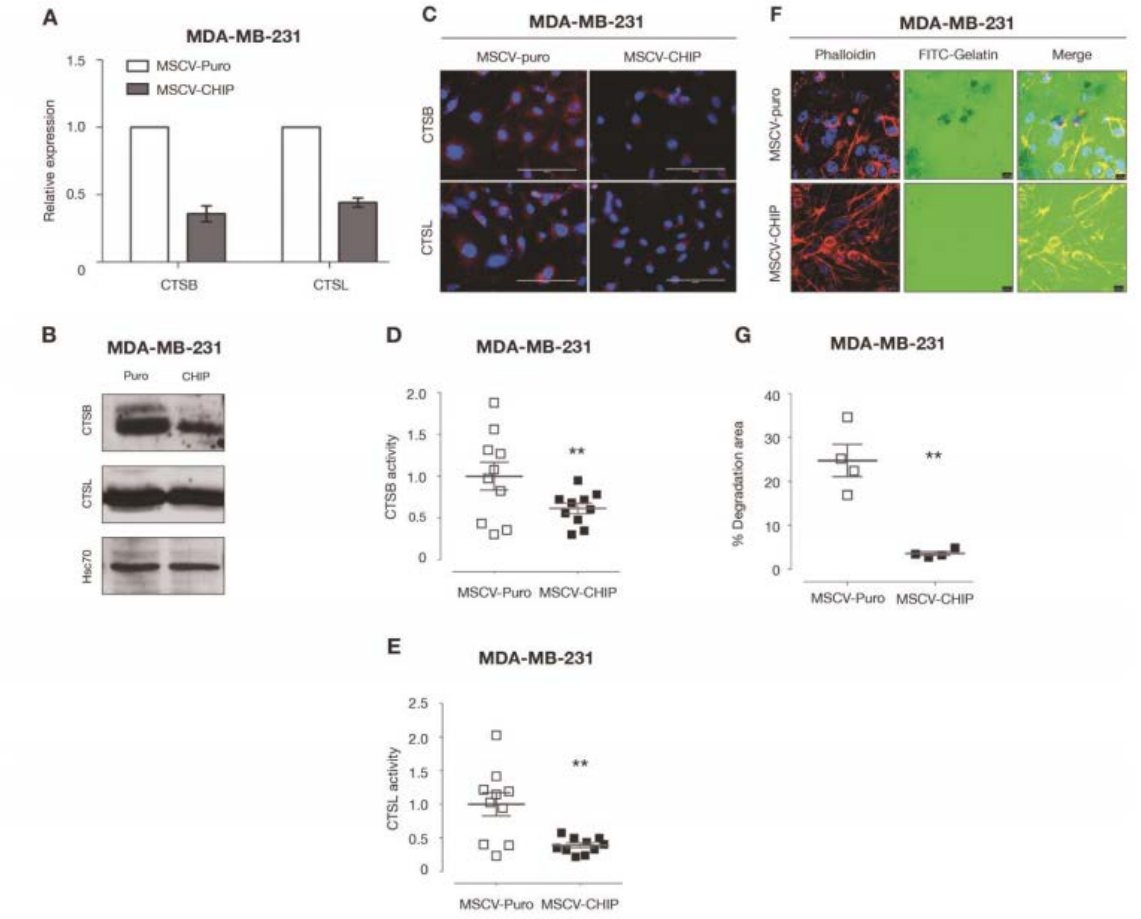
A
MDA-MB-231
MSCV-Puro
MSCV-CHIP
Relative expression
1.5
1.0
0.5
0
CTSB
CTSL
C
MDA-MB-231
MSCV-puro
MSCV-CHIP
CTSB
CTSL
F
MDA-MB-231
Phalloidin
FITC-Gelatin
Merge
MSCV-puro
MSCV-CHIP
B
MDA-MB-231
Puro
CHIP
CTSB
CTSL
Hsc70
D
MDA-MB-231
CTSB activity
2.0
1.5
1.0
0.5
0
**
MSCV-Puro
MSCV-CHIP
G
MDA-MB-231
% Degradation area
40
30
20
10
0
**
MSCV-Puro
MSCV-CHIP
E
MDA-MB-231
CTSL activity
2.5
2.0
1.5
1.0
0.5
0
**
MSCV-Puro
MSCV-CHIP

Figure 6. The CHIP-MZF1-CTSB axis also operates in triple-negative breast cancer cells. (A & B) CHIP-hi vs. CHIP-lo MDA-MB231 cells were analyzed by qPCR for CTSB/L mRNA (A) and immunoblotting for protein expression (B). (C) CTSB/L activity in CHIP-hi vs. CHIP-lo (MDA-MB231 cells analyzed as in Figure 4A. (D, E) Quantification of CTSB (D) and CTSL (E) activity shown in Figure D. Mean± S.D., n=10. (F) FITC-gelatin degradation (black holes) in CHIP-hi vs. CHIP-lo MDA-MB231 cells. (G) Quantification of FITC-gelatin degradation. Mean +/- SD., n=6.

Figure 7.

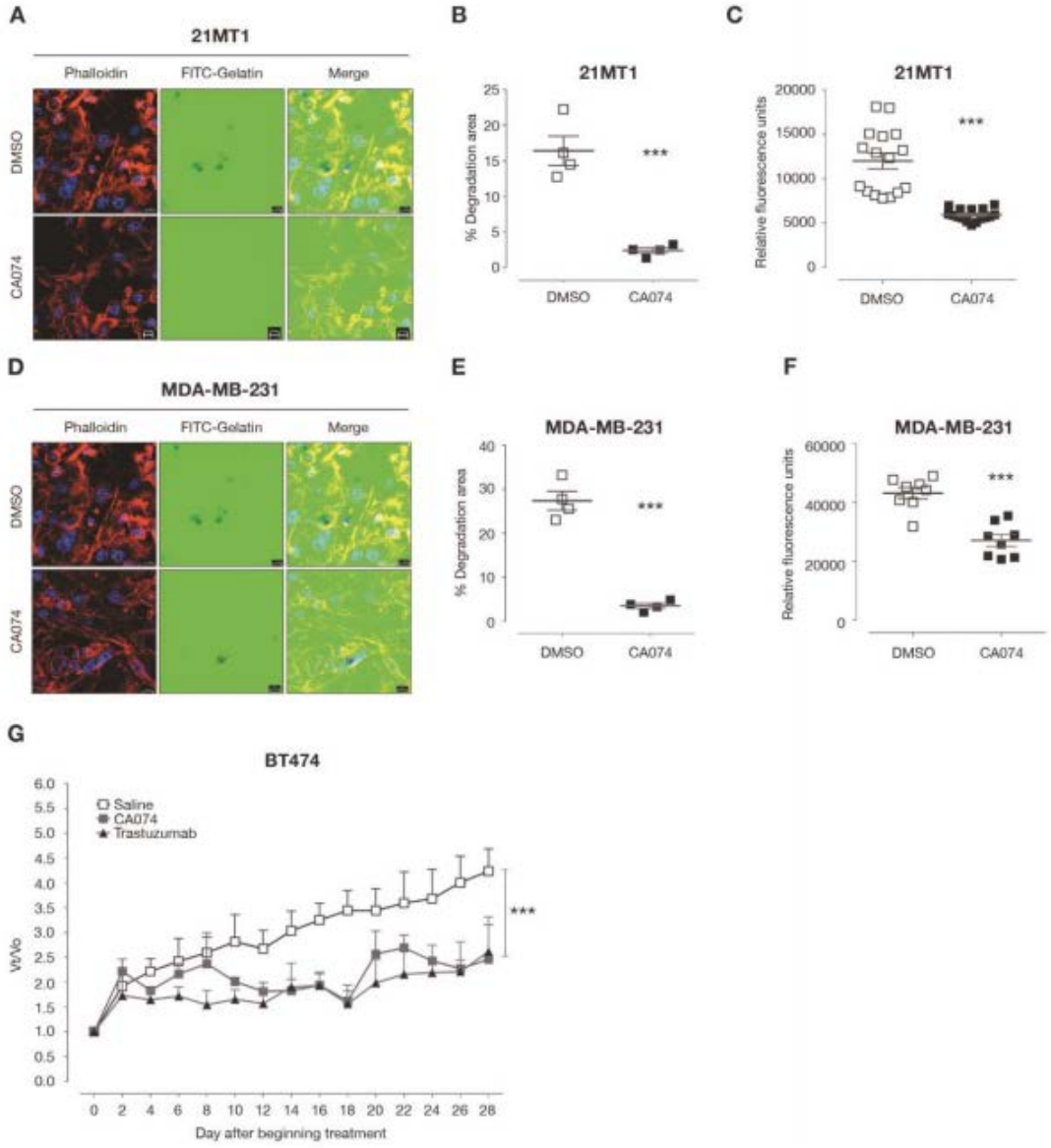
A
21MT1
Phalloidin
FITC-Gelatin
Merge
DMSO
CA074
B
21MT1
% Degradation area
***
DMSO
CA074
C
21MT1
Relative fluorescence units
***
DMSO
CA074
D
MDA-MB-231
Phalloidin
FITC-Gelatin
Merge
DMSO
CA074
E
MDA-MB-231
% Degradation area
***
DMSO
CA074
F
MDA-MB-231
Relative fluorescence units
***
DMSO
CA074
G
BT474
Saline
CA074
Trastuzumab
Vt/Vo
***
Day after beginning treatment

Figure 7. CTSB inhibition reduces ErbB2+ breast cancer cell tumorigenesis. (A) 21MT1 cells cultured on FITC-gelatin were treated with DMSO or CTSB inhibitor (CA074; 25 □g/ml) for 48h and degradation analyzed as in Figure 5G. (B) Quantification of FITC-gelatin degradation shown in 7A. Mean ± S.D., n=4. (C) 21MT1 cells seeded on Matrigel-coated membranes were treated with DMSO (control) or CA074 (25 □g/ml) for 24h, invaded cells stained with a fluorescent dye and quantified using a fluorescence reader. Mean ± S.D., n=18. (D) FITC-gelatin degradation by MDA-MB-231 cells was analyzed after 48h culture in DMSO (control) or CTSB inhibitor (CA074; 25ug/ml) as in Figure 5G. (E) Quantification of FITC-gelatin degradation. Mean ± S.D., n=4. (F) Invasion of MDA-MB-231 cells incubated with DMSO (control) or CA074 (25 □/ml) as in Fig. 6C. Mean ± S.D., n=8. (G) Groups of nude mice carrying BT474 xenografts (average 0.5 cm^3 size) received Trastuzumab (via tail vein; 4 mg/kg every 4 days) CA074 (i.p., 25 mg/kg in saline daily) or saline (control), and tumor volumes were monitored every other day. Mean +/- SEM., n=9.

Tables:

Table 1: The association between Nuclear (N) CHIP and clinical-pathological variables in the whole patient cohort.

Clinicopathological variables	N-CHIP		
	Negative/ low expression, N (%)	High expression, N (%)	p-value
Age (years)			
<50	231(35.1%)	100(31.8%)	**0.316**
≥50	426(64.9%)	214(68.2%)	
Menopausal status			
Pre	248(37.8%)	121(38.7%)	**0.798**
Post	409(62.2%)	192(61.3%)	
Tumour Size			
<2 CM	89(44.5%)	168(53.5%)	**0.008**
≥2CM	361(55.5%)	146(46.5%)	
Tumour Grade			
1	66(10.2%)	72(22.9%)	**1×10^{-7}**
2	194(29.9%)	126(40.1%)	
3	388(59.9%)	116(36.9%)	
Tubule formation			
1	23(3.7%)	23(7.5%)	**4×10^{-4}**
2	187(29.8%)	117(38.1%)	
3	417(66.5%)	167(54.4%)	
Pleomorphism			
1	11(1.8%)	6(2.0%)	**1×10^{-7}**

2	196(31.4%)	155(50.5%)	
3	418(66.9%)	146(47.6%)	
Mitosis			
1	157(25.0%)	148(48.2%)	**1×10^{-7}**
2	117(18.7%)	63(20.5%)	
3	353(56.3%)	96(31.3%)	
Lymph Node Stage			
1	398(61.4%)	192(61.1%)	**0.558**
2	195(30.1%)	101(32.2%)	
3	55(8.5%)	21(6.7%)	
Lymphovascular invasion (LVI)			
No	418(64.5%)	202(64.5%)	**0.993**
Definite	230(35.5%)	111(35.5%)	
Nottingham Prognostic Index			
Mild	147(23.8%)	126(41.7%)	**1×10^{-7}**
Moderate	368(59.5%)	144(47.7%)	
High	103(16.7%)	32(10.6%0	

Table 2: The association between Nuclear (N) CHP and different proteins related to ER and HER2 pathways in the whole patient cohort.

	N-CHIP		
	Negative/low expression, N (%)	**High expression, N (%)**	**p-value**
Hormone receptors			
Oestrogen receptor (ER)			
Negative	207(31.7%)	44(14.2%)	**1×10^{-7}**
Positive	447(68.3%)	266(85.8%)	
Progesterone receptor (PgR)			
Negative	296(47.0%)	97(32.1%)	**1×10^{-5}**
Positive	334(53.0%)	205(67.9%)	
Androgen receptor (AR)			
Negative	272(6.5%)	65(23.7%)	**1×10^{-7}**
Positive	313(53.5%)	209(76.3%)	
Triple negative (TN) status			**1×10^{-5}**
Non-TN	497(78.1%)	276(89.9%)	
TN	139(21.9%)	31(10.1%)	
Basal phenotype			**5×10^{-5}**
Negative	528(82.8%)	285(92.5%)	
Positive	110(17.2%)	23(7.5%)	
Other ER related proteins			
CK7/8			

Negative	12(1.9%)	3(1.0%)	**0.310**
Positive	621(98.1%)	297(99.0%)	
CK18			
Negative	2(16.2%)	22(7.9%)	**0.001**
Positive	476(83.8%)	258(92.1%)	
CK19			
Negative	63(10.2%)	16(5.4%)	**0.014**
Positive	554(89.8%)	283(94.6%)	
E-Cadherin			
Negative	235(38.1%)	104(35.0%)	**0.368**
Positive	382(61.9%)	193(65.0%)	
p-Cadherin			
Negative	229(43.8%	144(56.9%)	**0.001**
Positive	294(56.2%)	109(43.1%)	
N-Cadherin			
Negative	107(22.3%)	78(34.7%)	**0.001**
Positive	372(77.7%)	147(65.3%)	
Tumour suppressor proteins			
p53			
Negative/low	423(67.9%)	228(77.3%)	**0.003**
Positive	200(32.1%)	67(22.7%)	
BRCA1			
Negative/low	266(52.3%)	87(34.0%)	**2×10^{-6}**
High	243(47.7%0	169(66.0%)	
Proliferation markers			

KI67-LI			
Negative/low	171(33.5%)	138(54.8%)	**1×10^{-7}**
High	339(66.5%)	114(45.2%)	
Apoptosis related markers			
BCL2	219(44.6%)	71(32.7%)	**0.003**
Negative/low	272(55.4%)	146(67.3%)	
High			
HER family proteins			
HER1			
Negative	482(76.0%)	254(83.6%)	**0.009**
Positive	152(24.0%)	50(16.4%)	
HER2			
Negative	521(82.6%)	273(90.7%)	**0.001**
Positive	110(17.4%)	28(9.3%)	
HER3			
Negative	44(7.5%)	30(10.8%)	**0.112**
Positive	539(92.5%)	248(89.2%)	
HER4			
Negative	65(10.4%)	50(16.4%)	**0.009**
Positive	560(89.6%)	254(83.6%)	

Supplemental Table 1: The list of transcription factors whose DNA-binding activities were downregulated by CHIP overexpression in ErbB2+ BT474 cells.

ACPBP	E12/E47	L-lll BP	NF-E6/CP1
ADD-1	E2	Lactoferrin-BP	NF-Y
ADR-1	EGR-1	LF-A1	NFkB
ALF-1	EKLF	LSF	p-53
alpha-PAL	ETF	LXRF-1	PAX-2
AML-1	Freac-2	MEF-1	PAX-4
ARP	Freac-4	MRE	PAX-5
ATF	GAG	MT-box	PAX-6
ATF adelta	GBF-1/2/3/HY5	MTF	PBGD BP
ATF-a	H4TF-1	MUSF-1	Pbx1
c-Rel	HFH-1	MyoD	PCF
CACC	HFH-3	MZF1	PEBP-2
CCAAT	HFH-8	NF-1	PPUR
CEBP	HIF-1	NF-1/2	PPUR
CEF-2	HNF-3	NF-4FA	PRDll-BF1
COUP-TF	HNF-4a	NF-Atx	PUR
CTCF	ISGF	NF-E1/YY1	RAR/DR-5
E12	Isl-1	NF-E2	RB

Supplemental Table 2: The list of transcription factors whose DNA-binding activities were downregulated by CHIP overexpression in MDA-MB-231 cells.

alpha-PAL	Ets	LF-A2	PTF-1b
ACPBP	Fast-1	LXRE-1	PU1
AF-1	Fra-1/JUN	LyF	PUR
AFP-1	GAG	MAZ	RIPE3a1
AhR/Amt	GATA-3	MDBP	RORE
ALF-1	GBF-1/2/3	MHC W box	RREB
AIC/CBF	GKLF	MEF-2a	Skn
AP-4	HEN-1	Myo D	Sp-1
ARP	HFH-1	MZF1	SPERM-1
ATF	HFH-8/3/LUN	NF-1	SRF
ATF adelta	HFH-11B/11a	NF-4FA	Stat-1/3
CACC	HOX4C	NFAT-1	Tat
CBF	HIF-1	NF-Y	Tax/CREB
CCAC	HiNF-A	OCT	TFE3
Cdx-2	HiNF-B	ORE	TF-LF
CEBP	HNF-1A	P53	TGT-3
c-myb BP	ICSBP	P55	TIF-1
CP-1	Ikoros	PAX-2	TREF-1/2
CSBP	IRF-1/2	PAX-5	URE
CYBP1A1	ISGF	PEBF	WT1
DE-1	KKLF	PEPCK PR	YB-1
E2	Lacto-ferrin BP	PO-B	ZNF174
EKLF	LCR-F1	PPAR	
EGR-2	LH2/Lim-1	PPUR	

Supplementary Fig. S1

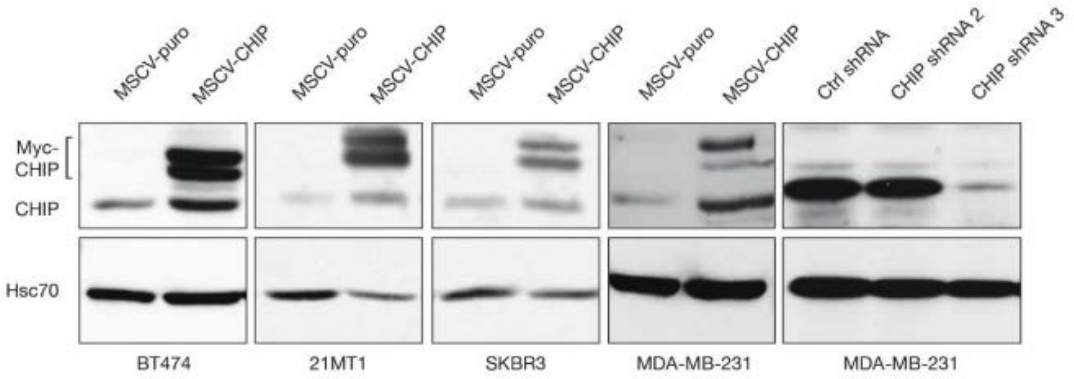

B

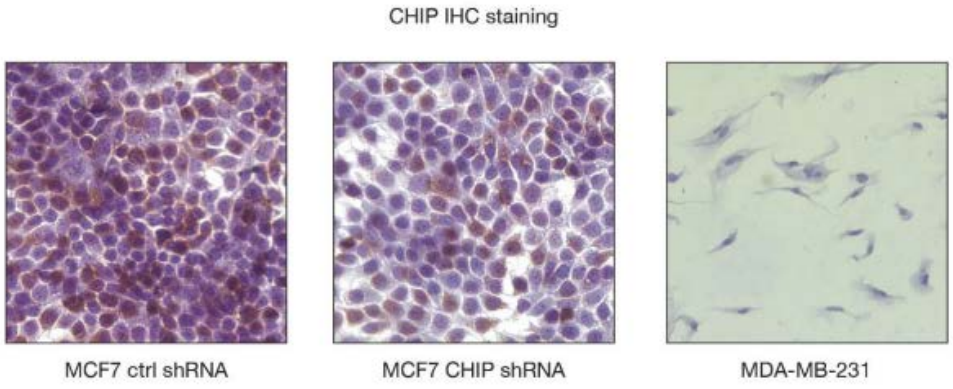

Supplementary Figure S1. Validate the antibody-based CHIP staining in vitro and in vivo. (A) Western blotting showed endogenous and exogenous CHIP expression in breast cancer cell lines. Hsc70 was used as loading control. (B) CHIP IHC staining in MCF7 CHIP-hi (control shRNA), CHIP-low (CHIP shRNA) and MDA-MB-231cells.

Supplementary Fig. S2

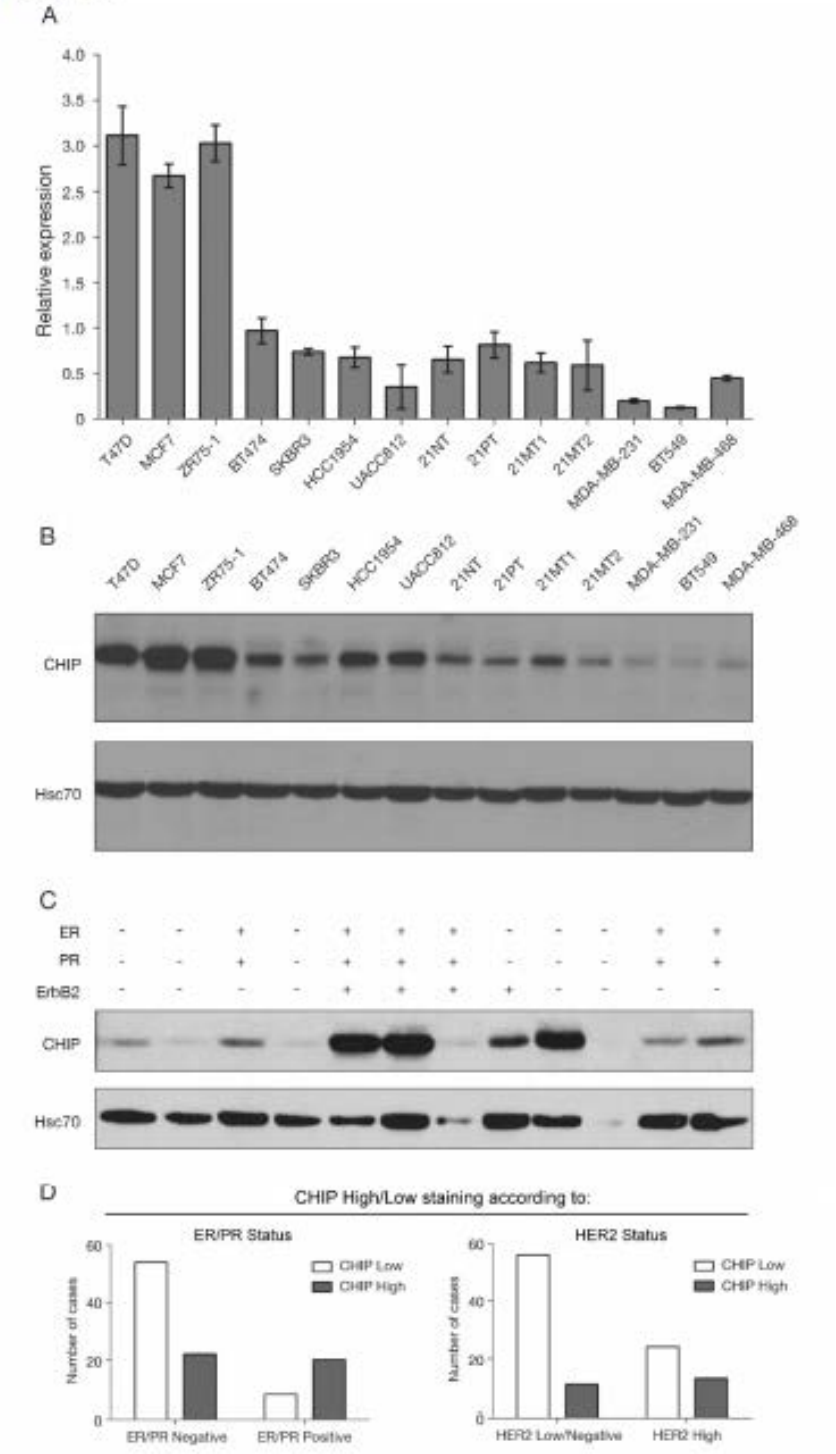

Supplementary Figure S2. CHIP expression level in breast cancer cell lines. (A) Real-time QPCR analysis shows reduced CHIP mRNA expression in ErbB2+ and triple negative breast cancer cell lines comparing with ER+ breast cancer cell lines. GAPDH was used as control. (B) Western blotting showed reduced CHIP protein expression in ErbB2+ and triple negative breast cancer cell lines comparing with ER+ breast cancer cell lines. Hsc70 was used as loading control. C) Western blotting showed reduced CHIP protein expression in most ErbB2+ and triple negative PDX samples. Hsc70 was used as loading control. (D) Analyses of CHIP, ErbB2, TN status in commercial TMA (BR20837, from US Biomax)

Supplementary Fig. S3

A

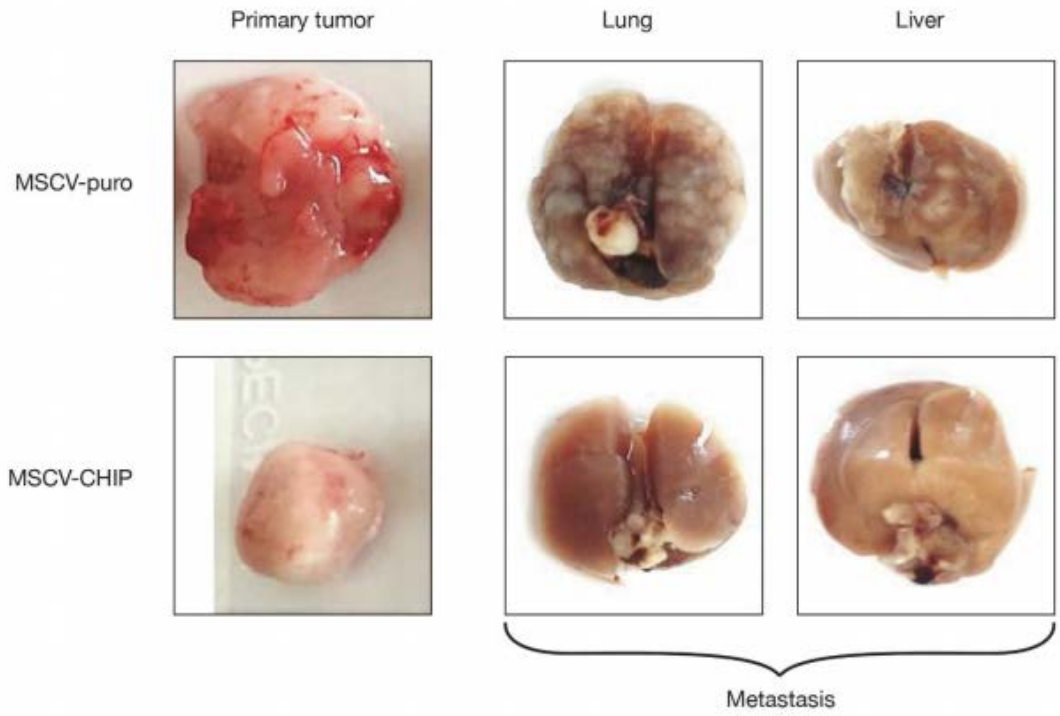

MDA-MB-231	Lung metastasis	Liver metastasis
Puro	5/5	3/5
CHIP	1/8	0/8

Supplementary Figure S3. CHIP-dependent reduction of tumor volume and metastasis in MDA-MB-231 xenograft model. (A) Representative tumor, liver and lung organs from MDAMB-231 CHIP-lo (MSCV-puro) and CHIP-hi (MSCV-CHIP) xenograft. (B) Live and lung metastasis from MDA-MB-231 CHIP-lo (MSCV-puro) and CHIP-hi (MSCV-CHIP) xenograft were summarized.

Supplementary Fig. S4

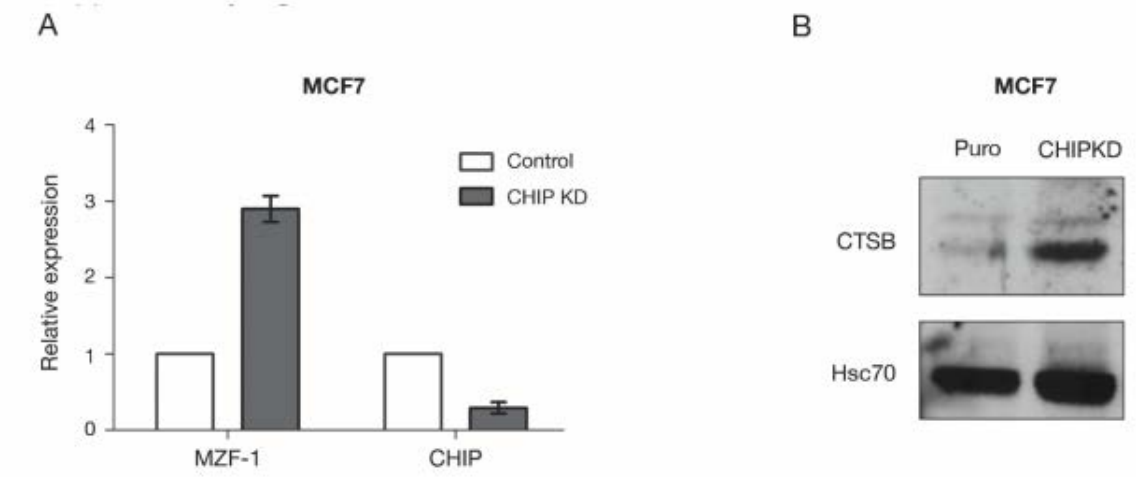

Supplementary Figure S4. MZF1/Cathepsin B expression is regulated by CHIP in MCF7. (A) Real-time QPCR analysis shows reduced MZF1 mRNA expression in MCF7 CHIP-hi (control shRNA) comparing with CHIP-lo (CHIP shRNA) cells. GAPDH was used as control. (B) Western blotting showed reduced cathepsin B protein expression in MCF7 CHIP-hi (control shRNA) comparing with CHIP-lo (CHIP shRNA) cells. Hsc70 was used as loading control.

Detailed Materials and Methods (Supplementary)

Antibodies and Reagents: Antibodies used for immunoblotting were as follows: Ubiquitin (mouse monoclonal P4D1; Cat. 3936S, Cell signaling, Denver, PA); ErbB2 (mouse monoclonal; Cat. 554299, BD-Pharmingen, San Jose, CA); MZF1 (mouse monoclonal; Cat. SAB1402398, Sigma Aldrich, St. Louis, MO); Cathepsin B (rabbit monoclonal; Cat. Ab125067, Abcam, Cambridge, MA); and HSC70 (B-6 antibody; Cat. sc-7298, Santa Cruz Biotechnology, Santa Cruz, CA). Rabbit anti-CHIP antibody used for blotting has been described (1).A second rabbit antibody (Cat. PA5-29024, Thermo Scientific, Waltham, MA) was used for IHC staining of CHIP. Secondary antibodies for immunoblotting included horseradish peroxidase (HRP)-conjugated Protein A or HRP-conjugated rabbit anti-mouse antibody (Invitrogen, Carlsbad, CA).

Cell Lysates: Cells were either lysed in RIPA lysis buffer (50 mM Tris pH 7.5, 150 mM NaCl, 1% Triton-X-100, 0.05% deoxycholate, 0.1% SDS, 1 mM phenylmethylsulfonyl fluoride (PMSF), 10 mM NaF, and 1 mM sodium orthovanadate) or Triton-X-100 lysis buffer (50 mM Tris pH 7.5, 150 mM NaCl, 0.5% Triton-X-100, 1 mM PMSF, 10 mM NaF, and 1 mM sodium orthovanadate)(2). Lysates were rocked at 4°C for at least 1 hour, centrifuged at 13,000 rpm for 20 minutes at 4°C and the supernatants assayed for protein concentration using the BCA assay kit (Thermo Fisher Scientific, Rockford, IL) or the Bradford assay (Bio-Rad Laboratories, Hercules, CA).

Immunoprecipitation: 1 mg of RIPA lysates and an optimized amount of the indicated antibody was rocked overnight at 4°C. 200 μl of 10% Protein A Sepharose (GE

Healthcare, Chalfont St. Giles, UK) beads (washed with RIPA buffer) were added to each IP sample and rocked at 4°C overnight. The beads were washed five times with RIPA buffer and bound proteins resolved by SDS-Polyacrylamide (Biorad) Gel Electrophoresis (PAGE), transferred to Polyvinylidene fluoride (PVDF) membrane (Bio-Rad Laboratories, Hercules, CA) and subjected to Western Blotting(1).

RNA extraction and real-time PCR: The total RNA was extracted using TRIzol reagent (Invitrogen), reverse transcribed using Quantitative real-time PCR kit (cat. 204141, Qiagen, Germantown, MD) was performed using the following primers: (a) MZF1 forward primer 5′-CGTAGAGAAGTGAGGAAA-3′ and reverse primer 5′-ATGATCAGGTCATACTCC-3′; (b) CTSB forward primer 5′-AACCACAGGCTGGGATGTAG-3′ and reverse primer 5′-CACTGACTGGGGTGACAATG-3′; (c) CTSL forward primer 5′-GATGGAGGAGAGCAGTGTGG-3′and reverse primer 5′-GCACTAAAAGCCCAACAAGAAC-3′; (d) GAPDH forward primer 5′-CCACTCCTCCACCTTTGAC-3′ and reverse primer 5′-ACCCTGTTGCTGTAGCCA-3′.

Transfection Reagents and Plasmids: XtremeGENE 9 transfection reagent was from Roche Applied Science (Indianapolis, IN). A pMSCV expression construct encoding the Myc- epitope-tagged full-length CHIP protein (amino acids 1–303) was generated as described preciously(3).

Cumulative proliferation assay: Cells were seeded in 6-well plates at 5,000 cells per well, counted after seven-day culture and re-plated in fresh 6-well plates at the original

plating density for a total of five serial passages. The cumulative cell numbers were calculated based on the fractions of each harvest used for replating and plotted as a function of the overall time in culture.

Anchorage-independent growth assay: 2,500 cells were seeded in 0.35% soft agar on top of 0.6% soft agar layer in 6-well plates. After two weeks, cells were stained with crystal violet and imaged under a phase contrast microscope. The colonies from the whole wells were enumerated using Image J (NIH, MD). All experiments were done in triplicates, and repeated three times.

Transwell migration and invasion assays: The cells were seeded in the top chamber of transwell chambers with 8 μm pore size nitrocellulose filters (Corning) in serum-free medium. Medium containing 10% FBS served as a chemoattractant in the lower chamber. For the invasion assay, the membranes were coated with 1:2 diluted Matrigel (BD Biosciences) before seeding the cells. After 24 h, the cells on the upper side of the membrane were removed by scraping with cotton swabs, while those on the lower side were fixed with methanol, stained with crystal violet and cells were counted. Experiments were run in triplicates and repeated thrice. For invasion assay in Figure 7, cells were seeded in top chambers of 96-well invasion chambers coated with Matrigel (CytoSelect™ 96-well Cell Invasion Assay Kit; Cat. CBA112, Cell Biolabs, INC.) followed by analyses as in migration assays.

Extracellular matrix degradation assay: This assay was carried out using QCM™ Gelatin Invadopodia kit (Cat. ECM670, EMD Millipore, Billerica, MA) according to the

manufacturer's protocol. FITC-labeled gelatin was coated onto glass chamber slides and crosslinked with 0.5% glutaraldehyde in PBS for 30 minutes. Slides were then washed three times each with PBS and 50 mM glycine in PBS. Cells were cultured for various time points to allow ECM degradation, seen as focal loss of fluorescent signal ("holes") in the labeled gelatin layer. Experiments were run in replicates and repeated thrice. Six fields per chamber were imaged and the fluorescence intensity was further analyzed using Image J (NIH).

In vivo xenograft experiment: 10 million cells mixed with 0.2 ml Matrigel (BD Biosciences) were implanted in the mammary fat pad of 4-6 week old non-pregnant female NSG mice (The Jackson Laboratory). Three days prior to cell implantation, the mice were primed with s/c estrogen pellet (0.72 mg/ 60 day pellets; Innovative Research of America, Sarasota, FL). Tumor growth was monitored weekly for 10 weeks. Tumor dimensions were measured with Vernier calipers and tumor volume calculated as length x width x depth/2. Mice were euthanized when control tumors reached 2 cm^3 in volume or showed signs of ill health, as per institutional IACUC guidelines. At the end of the experiment the tumor, as well as liver and lung, are resected, and formalin-fixed and paraffin-embedded for further analyses.

References

1. Zhou P, Fernandes N, Dodge IL, et al. ErbB2 degradation mediated by the co-chaperone protein CHIP. J Biol Chem 2003;278(16):13829-37.

2. Raja SM, Clubb RJ, Ortega-Cava C, et al. Anticancer activity of celastrol in combination with ErbB2-targeted therapeutics for treatment of ErbB2-overexpressing breast cancers. Cancer Biol Ther 2011;11(2):263-76.

3. Jan CI, Yu CC, Hung MC, et al. Tid1, CHIP and ErbB2 interactions and their prognostic implications for breast cancer patients. J Pathol 2011;225(3):424-37.